

12

AD-A177 590

David W. Taylor Naval Ship Research and Development Center

Bethesda, MD 20084-5000

DTNSRDC/SPD-1180-01 December 1986

Ship Performance Department

Departmental Report

MEASUREMENTS OF PROPELLER-INDUCED UNSTEADY
SURFACE FORCE AND PRESSURES

by

Michael B. Wilson

John McHugh

DTNSRDC/SPD-1180-01 MEASUREMENTS OF PROPELLER-INDUCED UNSTEADY SURFACE FORCE AND PRESSURES

DTIC FILE COPY

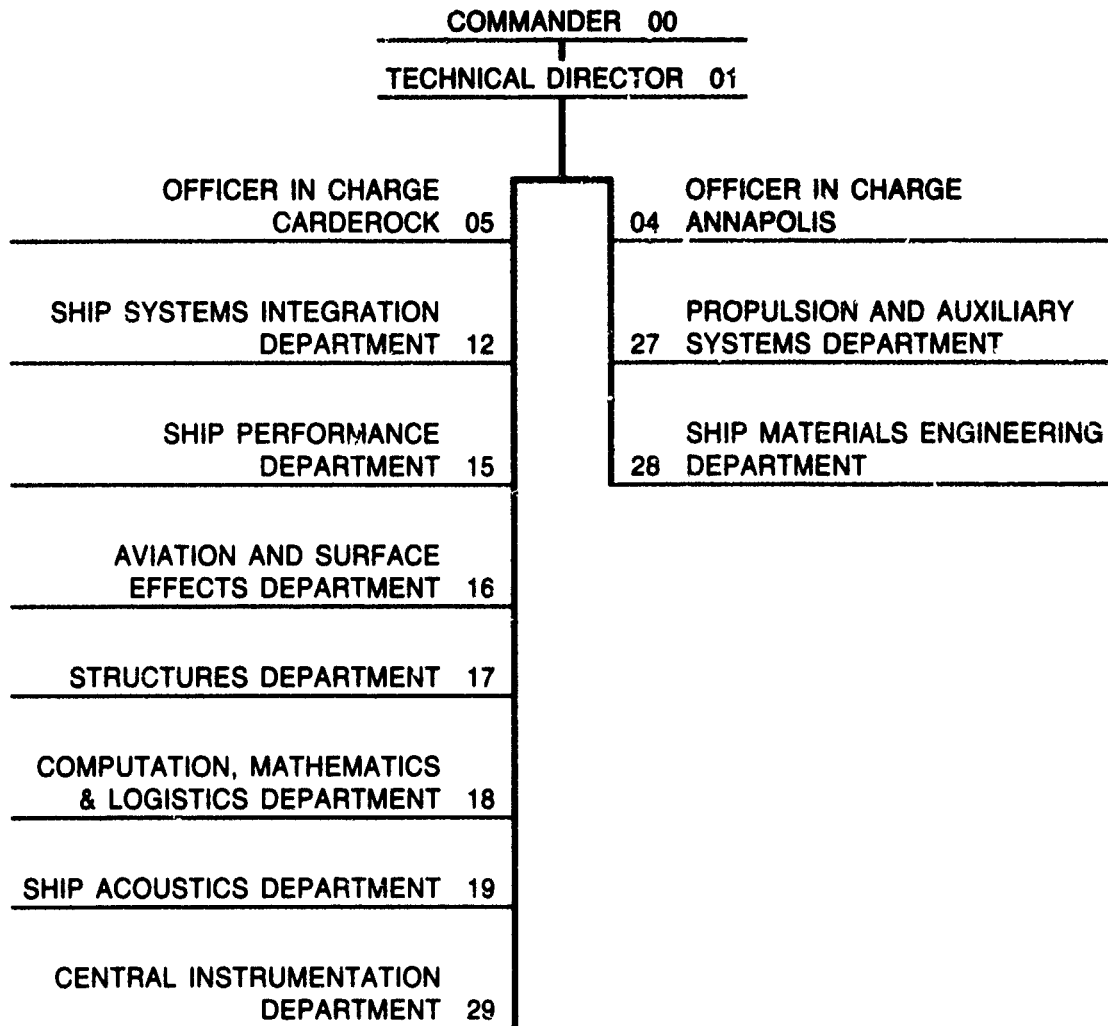
DTIC
SELECTED
MAR 04 1987
S
E
P

Approved for Public Release: Distribution Unlimited



87 3 2 027

MAJOR DTNSRDC TECHNICAL COMPONENTS



DESTRUCTION NOTICE — For **classified** documents, follow the procedures in DOD 5220.22M, Industrial Security Manual, Section II-9, or DOD 5200.1-R, Information Security Program Regulation, Chapter IX. For **unclassified**, limited documents, destroy by any method that will prevent disclosure of contents or reconstruction of the document.

ADA177 590

REPORT DOCUMENTATION PAGE

1a. REPORT SECURITY CLASSIFICATION UNCLASSIFIED		1b. RESTRICTIVE MARKINGS	
2a. SECURITY CLASSIFICATION AUTHORITY		3. DISTRIBUTION/AVAILABILITY OF REPORT	
2b. DECLASSIFICATION/DOWNGRADING SCHEDULE NA			
4. PERFORMING ORGANIZATION REPORT NUMBER(S) DTNSRDC/SPD-1180-01		5. MONITORING ORGANIZATION REPORT NUMBER(S)	
6a. NAME OF PERFORMING ORGANIZATION David Taylor Naval Ship R&D Center	6b. OFFICE SYMBOL (if applicable) Code 1522	7a. NAME OF MONITORING ORGANIZATION	
6c. ADDRESS (City, State, and ZIP Code) Bethesda, Maryland 20084		7b. ADDRESS (City, State, and ZIP Code)	
8a. NAME OF FUNDING/SPONSORING ORGANIZATION Naval Sea Systems Command	8b. OFFICE SYMBOL (if applicable) SEA 05R	9. PROCUREMENT INSTRUMENT IDENTIFICATION NUMBER	
8c. ADDRESS (City, State, and ZIP Code) Washington, D.C. 20360		10. SOURCE OF FUNDING NUMBERS	
		PROGRAM ELEMENT NO. 62543N	PROJECT NO. SF43421
		TASK NO. SF43421	WORK UNIT ACCESSION NO. DN178067
11. TITLE (Include Security Classification) MEASUREMENTS OF PROPELLER-INDUCED UNSTEADY SURFACE FORCES AND PRESSURES			
12. PERSONAL AUTHOR(S) Michael B. Wilson and John McHugh			
13a. TYPE OF REPORT Final	13b. TIME COVERED FROM TO	14. DATE OF REPORT (Year, Month, Day) December 1986	15. PAGE COUNT ix+77
16. SUPPLEMENTARY NOTATION <i>cont from B)</i> <i>Keywords:</i>			
17. COSATI CODES		18. SUBJECT TERMS (Continue on reverse if necessary and identify by block number)	
FIELD	GROUP	SUB-GROUP	→ Pressure amplitude; Reciprocity experiment; Surface force; Cavity volume velocity; Propeller excitation) P&F (Propeller-induced unsteady forces)
19. ABSTRACT (Continue on reverse if necessary and identify by block number)			
<p>Results of an experimental investigation carried out in the 24-inch water tunnel at DTNSRDC are presented for the cavitating propeller-induced surface pressures and a reference-area surface force measured on a flat plate boundary representation of a nearby ship hull. Newly designed apparatus for the measurement of surface force on an instrumented disc is described in detail. It involves special dynamometry that can be used in a reverse mode so that the force disc can be driven as a mechanical shaker. Reciprocity calibration measurements were made with this equipment and the resulting pressure-to-acceleration transfer function was used to make estimates of cavity volume velocity. A model of a seven-bladed propeller was run in a screen-generated simulation of the steep axial wake velocity distribution for a single screw ship. Results are displayed for the longitudinal and transverse distribution of the first three blade rate harmonic components of the unsteady pressure amplitudes and the unsteady disc → pg 8</p>			
20. DISTRIBUTION/AVAILABILITY OF ABSTRACT <input type="checkbox"/> UNCLASSIFIED/UNLIMITED <input checked="" type="checkbox"/> SAME AS RPT <input type="checkbox"/> DTIC USERS		21. ABSTRACT SECURITY CLASSIFICATION UNCLASSIFIED	
22a. NAME OF RESPONSIBLE INDIVIDUAL Michael B. Wilson and John McHugh		22b. TELEPHONE (Include Area Code) (202) 227-1697	22c. OFFICE SYMBOL Code 1522

Block 19 (Continued)

(diameter)

force amplitudes at the blade tip clearances of $0.26D_A$ and $0.41D$, over a range of cavitation numbers. The unsteady pressure pulse amplitudes obtained in this work compare reasonably well with measured values obtained previously in a large water tunnel experiment using a complete scale model of the ship hull. The experimentally inferred blade rate harmonic component of cavity volume velocity from the reciprocity measurement agrees approximately with the prediction by the PUF-3 propeller analysis scheme.

cont pg A



TABLE OF CONTENTS

	Page
LIST OF FIGURES	111
LIST OF TABLES	vi
NOTATION	vii
ABSTRACT	1
ADMINISTRATIVE INFORMATION	1
INTRODUCTION	1
BACKGROUND	4
CHARACTERIZING EXCITATION	5
REVIEW OF EXPERIMENTS	9
APPARATUS AND INSTRUMENTATION	13
FACILITY	13
MOUNTING PLATE AND INSTRUMENTATION	14
CALIBRATIONS	15
EXCITATION EXPERIMENTS WITH MODEL PROPELLER	18
PROPELLER	18
EXPERIMENTAL PROCEDURE	18
RESULTS	23
DISCUSSION AND RECOMMENDATIONS	28
ACKNOWLEDGMENT	30
REFERENCES	31
APPENDIX A - RECIPROCITY CONCEPT AND APPLICATION	72
APPENDIX B - CAVITY VOLUME MEASUREMENTS AND COMPARISONS	75



Accession For	
NTIS GRA&I	<input checked="" type="checkbox"/>
DTIC TAB	<input type="checkbox"/>
Unannounced	<input type="checkbox"/>
Justification	
By _____	
Dist _____ / _____	
AV _____	
Dist _____	
A-1	

LIST OF FIGURES

	Page
1 - Definition Sketch of Rotating Pressure Field Near an Operating Propeller	37
2 - Schematic of Force Measuring Device Installed in the 24-Inch Water Tunnel Open Jet Test Section	38
3 - Flat Boundary Plate, Force Disc, and Pressure Gauge Locations	39
4 - Calibrated Dynamic Response Curve for Force Measuring Device	40
5 - Reciprocity Calibration for the Driven Force Disc: Pressure-to-Acceleration Transfer Function versus Frequency	41
6 - Drawings of Propeller Model 4677	42
7 - Open Water Characteristics of Propeller Model 4677	43
8 - Circumferential Distribution of Axial Wake Velocity Ratio, Comparison of Measurements in Water Tunnel and Towing Basin, at $r/R = 0.557$	44
9 - Circumferential Distribution of Axial Wake Velocity Ratio, Comparison of Measurements in Water Tunnel and Towing Basin at $r/R = 0.774$	45
10 - Circumferential Distribution of Axial Wake Velocity Ratio, Comparison of Measurements in Water Tunnel and Towing Basin at $r/R = 1.178$	46
11 - Three Blade Rate Harmonics of Measured Pressure Amplitude Coefficients Taken at the Disc Center with $a_z/D = 0.26$	47
12 - Three Blade Rate Harmonics of Measured Pressure Amplitude Coefficients Taken at the Disc Center with $a_z/D = 0.41$	48
13 - Blade Rate Harmonic of Measured Pressure Amplitude Coefficient versus Longitudinal Position for Five Cavitation Numbers, with $a_z/D = 0.26$...	49
14 - Twice Blade Rate Harmonic of Measured Pressure Amplitude Coefficient versus Longitudinal Position for Several Cavitation Numbers, with $a_z/D = 0.26$	50
15 - Thrice Blade Rate Harmonic of Measured Pressure Amplitude Coefficient versus Longitudinal Position for Five Cavitation Numbers, with $a_z/D = 0.26$	51
16 - Blade Rate Harmonic of Measured Pressure Amplitude Coefficient versus Longitudinal Position for Five Cavitation Numbers, with $a_z/D = 0.41$	52

17 - Twice Blade Rate Harmonic of Measured Pressure Amplitude Coefficient versus Longitudinal Position for Five Cavitation Numbers, with $a_z/D = 0.41$	53
18 - Thrice Blade Rate Harmonic of Measured Pressure Amplitude Coefficient versus Longitudinal Position for Five Cavitation Numbers, with $a_z/D = 0.41$	54
19 - Blade Rate Harmonic of Measured Pressure Amplitude Coefficient versus Transverse Position for Five Cavitation Numbers, with $a_z/D = 0.26$	55
20 - Twice Blade Rate Harmonic of Measured Pressure Amplitude Coefficient versus Transverse Position for Several Cavitation Numbers, with $a_z/D = 0.26$	56
21 - Thrice Blade Rate Harmonic of Measured Pressure Amplitude Coefficient versus Transverse Position for Five Cavitation Numbers, with $a_z/D = 0.26$	57
22 - Blade Rate Harmonic of Measured Pressure Amplitude Coefficient versus Transverse Position for Five Cavitation Numbers, with $a_z/D = 0.41$	58
23 - Twice Blade Rate Harmonic of Measured Pressure Amplitude Coefficient versus Transverse Position for Five Cavitation Numbers, with $a_z/D = 0.41$	59
24 - Thrice Blade Rate Harmonic of Measured Pressure Amplitude Coefficient versus Transverse Position for Five Cavitation Numbers, with $a_z/D = 0.41$	60
25 - Three Blade Rate Harmonics of Measured Disc Force Coefficient with $a_z/D = 0.26$	61
26 - Three Blade Rate Harmonics of Measured Disc Force Coefficient with $a_z/D = 0.41$	62
27 - Blade Rate Harmonics of Disc Force Coefficient versus Cavitation Number, Comparison Between Measured Force and Integrated Pressure, with $a_z/D = 0.26$	63
28 - Blade Rate Harmonic of Disc Force Coefficient versus Cavitation Number, Comparison Between Measured Force and Integrated Pressure, with $a_z/D = 0.41$	64
29 - Twice Blade Rate Harmonic of Disc Force Coefficient versus Cavitation Number, with $a_z/D = 0.26$	65

	Page
30 - Twice Blade Rate Harmonic of Disc Force Coefficient versus Cavitation Number, with $a_z/D = 0.41$	65
31 - Thrice Blade Rate Harmonic of Disc Force Coefficient versus Cavitation Number, with $a_z/D = 0.26$	66
32 - Thrice Blade Rate Harmonic of Disc Force Coefficient versus Cavitation Number, with $a_z/D = 0.41$	66
33 - Comparison of Measured Blade Rate Pressure Amplitude Longitudinal Distribution	67
34 - Comparison of Blade Rate Pressure Amplitude Coefficient Over the Propeller versus Cavitation Number	68
35 - Schematic of the Measurement of Cavity Volume Velocity by Reciprocal Method	69
B.1- Comparison of Measured and Calculated Blade Rate Cavity Volume Velocity versus Cavitation Number	77

LIST OF TABLES

	Page
1 - Summary of Instrumentation Characteristics	70
2 - Geometric Characteristics of AO-177 Class Auxiliary Oiler Highly Skewed Propeller Design	71
B.1- Estimate of Blade Rate Cavity Volume Velocity Using Reciprocal Measurements	76

NOTATION

		<u>Units*</u>
A_m	Fourier cosine coefficient of the mth harmonic	-
a	Measured level of acceleration	L/T^2
a_z	Vertical clearance between blade tip and nearby surface	L
B_m	Fourier sine coefficient of the mth harmonic	-
C_{th}	Thrust loading coefficient; $8K_T/\pi J^2$	-
D	Propeller diameter	L
\tilde{F}_S	Unsteady force amplitude on hull or boundary element	ML/T^2
$(F_S)_m$	Unsteady surface normal force amplitude on disc, mth harmonic component	ML/T^2
i	Complex number, $\sqrt{-1}$	-
J	Advance coefficient; V_A/nD	-
$(K_p)_m$	Pressure amplitude coefficient of mth harmonic; $(\Delta p)_m/\rho n^2 D^2$	-
$(K_F)_m$	Disc force amplitude coefficient of mth harmonic; $(F_S)_m/\rho n^2 D^4$	-
K_T	Propeller thrust coefficient; $T/\rho n^2 D^4$	-
m	Index for harmonic component, $m = \mu Z$	-
N	Propeller rate of revolution (RPM)	rev/T
n	Propeller rate of revolution (rps)	rev/T
P_m	Total amplitude of mth harmonic of unsteady pressure	F/L^2
\tilde{p}	Unsteady fluid pressure	F/L^2
p_0	Fluid static pressure at propeller center	F/L^2
p_v	Vapor pressure of water	F/L^2
$T(\text{and } \bar{T})$	Propeller mean thrust force	F
t	Time	T

*M = mass, L = Length, T = time, F = force = ML/T^2

		<u>Units</u>
t_m	Blade section maximum thickness	L
\dot{V}	Time rate of change of volume (volume velocity), general	L^3/T
\dot{V}_c	Time rate of change of blade cavity volume	L^3/T
V	Free stream velocity	L/T
V_A	Speed of advance; $V(1-w_T)$	L/T
V_X	Axial component of nominal wake velocity into propeller plane	L/T
w_T	Wake fraction based on thrust identity	-
x_{PC}	Longitudinal coordinate measured from propeller center, positive upstream	L
y	Transverse coordinate measured from propeller center, positive to starboard, looking upstream	L
Z	Number of propeller blades	-
β_m	Harmonic phase angle of the mth harmonic component of disc force	deg
γ_m	Harmonic phase angle of the mth harmonic component of unsteady pressure	deg
Δp	Unsteady pressure amplitude, general	F/L^2
$(\Delta p)_m$	Unsteady pressure amplitude, mth harmonic component	F/L^2
θ	Circumferential position angle for wake velocity, measured positive counterclockwise from 12 o'clock, looking upstream	deg
μ	Index for harmonic component of blade rate, $\mu = m/Z$	-
ρ	Fluid mass density	M/L^3
σ_n	Cavitation number; $(p_o - p_v)/1/2\rho n^2 D^2$	-
σ_{VA}	Cavitation number; $(p_o - p_v)/1/2\rho V_A^2$	-
ϕ_m	Spatial phase angle of mth harmonic component of pressure	deg
ϕ	Position angle measured clockwise from 12 o'clock looking upstream; ωt	deg

Units

ω Shaft circular frequency; $2\pi n$

rad/T

ABBREVIATIONS

DTNSRDC David Taylor Naval Ship Research and Development Center

SSPA (Statens Skeppsprovninganstalt) Maritime Research and Consulting, Goteborg Sweden

BR Blade rate frequency

MARIN Maritime Research Institute Netherlands

PUF-3 Propeller Unsteady Force Computer Code Developed at MIT

MIT Massachusetts Institute of Technology

ABSTRACT

Results of an experimental investigation carried out in the 24-inch water tunnel at DTNSRDC are presented for the cavitating propeller-induced surface pressures and a reference-area surface force measured on a flat plate boundary representation of a nearby ship hull. Newly designed apparatus for the measurement of surface force on an instrumented disc is described in detail. It involves special dynamometry that can be used in a reverse mode so that the force disc can be driven as a mechanical shaker. Reciprocity calibration measurements were made with this equipment and the resulting pressure-to-acceleration transfer function was used to make estimates of cavity volume velocity. A model of a seven-bladed propeller was run in a screen-generated simulation of the steep axial wake velocity distribution for a single screw ship. Results are displayed for the longitudinal and transverse distribution of the first three blade rate harmonic components of the unsteady pressure amplitudes and the unsteady disc force amplitudes at the blade tip clearances of $0.26D$ and $0.41D$, over a range of cavitation numbers. The unsteady pressure pulse amplitudes obtained in this work compare reasonably well with measured values obtained previously in a large water tunnel experiment using a complete scale model of the ship hull. The experimentally inferred blade rate harmonic component of cavity volume velocity from the reciprocity measurement agrees approximately with the prediction by the PUF-3 propeller analysis scheme.

ADMINISTRATIVE INFORMATION

This work was funded by the Naval Sea Systems Command under the Ships, Subs, and Boats Program, Program Element 62543N, Task Area SF43421, and was carried out by the Ship Performance Department under Work Units 1506-102 and 1506-103.

INTRODUCTION

Propeller-excitation has long been known as a major source of vibration and noise on ships. Problems arise in the form of excessive hull girder vibrations in the stern area and at the upper levels of deckhouses; unacceptable localized vibrations in important aft end spaces; fatigue damage to hull plating, internal stiffeners, appendages, or other structures near the propeller; high levels of inboard airborne noise; and general crew nuisance. Any one or all of these symptoms could lead to the imposition of speed restrictions, limitations on certain maneuvers, or avoidance of certain propeller RPM regimes. Understanding the hydrodynamic source of fluctuating forces and unsteady pressures is crucial for the eventual prediction of the magnitudes and spatial extent of the excitation. Thus an important aspect of the design of the propeller-hull

arrangement, in addition to satisfactory steady propulsive performance, is the proper accounting for the propeller-induced unsteady forces, moments, and periodic hull pressure fluctuations.

There are two main categories of propeller excitation. Both are concerned with the interaction of the propeller blade elements operating in the nonuniform velocity wake inflow conditions. (1) Unsteady shaft-transmitted loads (bearing loads) are forces and moments developed on the propeller and transmitted to the hull through the thrust bearing foundation and reduction gearing system and the aftermost shaft bearing. The most important class of problems involving unsteady bearing loads are those associated with the longitudinal shafting vibration excited by the unsteady thrust and torque. (2) Unsteady hull surface loads or pressure-transmitted loads are forces and moments that arise from the spatially integrated effect of the fluctuating pressure field induced by the propeller blades passing through a varying inflow velocity pattern. The presence of intermittent blade cavitation causes further magnified pressure fluctuations due to a monopole behavior of the unsteady cavity volume. Under the worst conditions, periodic pressure pulses having nearly constant phase angle may act over a wide expanse of hull surface and on nearby appendages. In this situation, integrated surface forces of very substantial magnitude can be delivered to the hull.

Presently, methods for prediction of the exciting loads are different for each of the categories. In the area of unsteady bearing loads, prediction capability has been available for some time and it has been well integrated into the propeller design process in the U.S. Navy. Notable examples of analysis and design methods and verification of the prediction accuracy are provided by Boswell and Cox^{1*}, Valentine and Dashnaw², Boswell, et al³, and Boswell, et al⁴, and in the numerous fundamental references listed in these works. A Z-bladed propeller acts as effective mechanical filter that picks out only certain wake velocity harmonic components and their radial distributions for the excitation of the various unsteady bearing load components (Z th harmonic for fluctuating thrust and torque, and the Z-1, Z+1 harmonics for the transverse components of fluctuating forces and moments). The application of bearing load analyses to design has been rather successful because of the development of specific design modifications such as blade skew, warp, etc for reducing excessive unsteady blade loads.

*A complete listing of references is given on page 31.

Capability for the analytical prediction of unsteady pressure pulses and distributed surface forces, on the other hand, has just emerged. There is a vast and growing literature on this subject by now, largely stemming from work in the early 1970's after it became clear that unsteady variations of cavity volume in conjunction with large wake velocity gradients could significantly magnify the blade fanning pressures caused by a propeller operating near a boundary. A sampling of important references concerned with prediction of unsteady surface forces and/or periodic hull pressure amplitudes includes Huse⁵, Noordzij,⁶ Vorus, et al⁷ Fitzsimmons,⁸ Kaplan et al⁹, Hoshino,¹⁰ Kaplan, et al,¹¹ Breslin, et al¹², and Huse and Guoqiang.¹³

The U.S. Navy has been fortunate over many years to have relatively few experiences with the severe vibration and noise problems that can be attributed to surface force excitation. Typically, the merchant ship designs displaying problems (tankers, product carriers, Ro-Ro, ferries, LNG ships) have tended to exacerbate the difficulties because of high installed power (increasing dramatically through the late 1960's and 1970's) and restrictive propeller-hull arrangements, giving rise to steep and deep wake patterns. In contrast, the open stern arrangements of most Naval combatants and many auxiliary ships have wake distributions for which simple vertical tip clearance allowances, such as the values recommended by Navy customary practice, have generally been satisfactory.

Problems of excessive interior noise, early stage blade surface erosion, and heavy localized vibration encountered on the first of the class U.S. Navy Auxiliary Oiler AO-177 have been described by Wilson, et al,¹⁴ and illustrate a case where the neglect of surface force excitation in the original design consideration led to an unsatisfactory mismatch of propeller and hull shape (wake). In this case, intermittent blade cavitation resulted in excessive unsteady pressure pulses over a wide area of the stern near the propeller and unstable cavity flow behavior near the blade tips and trailing edge (cloud cavitation). Among the many lessons learned from the experimental and analytical investigations carried out for the AO-177 project was the observation of how such subtle changes of the blade cavitation extent and appearance could produce improvements in the excitation magnitude. An important result of the improved wake achieved by use of a fin on the AO 177 was a significant reduction of magnitudes of unsteady pressure pulse amplitudes distributed nearby and away from the propeller plane.

The hydrodynamics of the blade cavity behavior (thickness, total cavity volume variation, and interaction with tip vortex cavity) appeared to be crucial to understanding the magnitudes and character of these changes.

Experiments are essential for providing better understanding and as the source of empirical estimates of realistic excitation magnitudes, and will continue to be important because:

a) There is difficulty and uncertainty in predicting analytically detailed unsteady blade cavity flows. This is because of the complex three-dimensional tip flow around propeller blades involving boundary layer, turbulent and tip vortex flow effects coupled with the unsteady sheet cavity and its break-up into a bubbly wake flow.

b) There is a need to predict cavity volume velocity at all interesting harmonics, not only at the blade rate value.

c) There is a need for studying other important physical effects such as the influence of wake temporal velocity fluctuations on the cavity behavior and coincident propulsor-induced pressures and forces on nearby surfaces.

The purpose of the present project was to design and build an experimental system to be used in the existing water tunnels at DTNSRDC that could be of use in obtaining some of the basic information desired and provide a possible test-bed for design assessment. It was intended to include enough adaptability to cover standard propeller-excitation experiments, as well as new investigations. The set-up was also directed to provide some measure of interim capability and development of experimental skills for propeller-hull interaction studies, before the advent of a planned new large facility¹⁵. This report covers the background of model testing on propeller-excitation, the requirements and details of the experimental set up, and future plans for the system.

BACKGROUND

Model experiments are very important to the study of propeller-excitation characteristics that can give rise to ship vibration and inboard noise. Many of the significant milestones in our understanding of the phenomena involved and in the estimation of unsteady loadings for full scale designs of propellers and shafting systems have been achieved through model testing in a variety of

experimental facilities. It is anticipated that this will continue to be true as long as the large deficiencies persist in the reliability (or absence) of analytical predictions of such features as nominal and apparent wake velocity patterns, sheet cavity and tip vortex cavity geometry and volume dynamics, and interaction of hull-propulsor-wake-cavity flows.

Full scale experiments are also essential for correlations with model results, for observing flow features, and for crucial data on important measured ship responses such as localized and girder vibration and inboard noise.

CHARACTERIZING EXCITATION

If we confine our attention to the category of surface pressure/surface force and moment excitation, we can characterize the propeller exciting magnitudes by considering several main features.

1. Fluctuating pressure amplitudes. There is a rotating pressure field associated with the operation of a propeller. Figure 1 is a sketch of this pressure disturbance frozen at an instant in time and it shows a definition of the spatial phase angle ϕ_z measured to the reference line of the blade from the surface point just as the positive peak of the blade rate pressure signal passes (many other definitions are possible). When this free space pressure field interacts with a rigid nearby boundary, and when the pressure is observed from a stationary point on the boundary, the amplitude on the surface will fluctuate in time with the blade passing frequency and multiples of that frequency. The surface pressure pulse can reach up to twice the free space magnitude because of reflection effect from the boundary. Point pressure measurements on a nearby hull surface or on appendages of a ship or a model can be obtained experimentally with flush mounted pressure transducers, and provide some picture of the pressure loads delivered to the hull. A single point pressure measurement (over the tip of the propeller at the closest distance to the hull) is sometimes taken as the sole indicator of the magnitude of the surface force excitation. Such a value is certainly interesting for comparisons, but it is generally insufficient to characterize a representative surface force magnitude that would be useful to estimate, for instance, the hull girder vibration response. On the other hand, the distribution of point pressures over a region of hull surface may well be used for the loading excitation for structural vibration predictions.

In any case, point pressure pulses should be obtained at several locations forward and aft of the propeller plane and laterally off centerline to have an idea of the character and extent of the loading.

Some example of measured propeller-induced pressure pulse distributions are provided by Denny¹⁶ on the model scale and by Taniguchi and Ohtaka¹⁷ for a full scale destroyer.

2. Reference-area surface force amplitudes. The periodic surface force experienced by a patch of area of the nearby hull boundary represents a net or integrated effect of the distributed pressure pulses exerted on the surface. Such a quantity can be obtained experimentally with an instrumented surface segment (See for example, Kerwin, et al¹⁸) or by integrating measured point pressures over the desired area, accounting for the spatial and temporal (phase angle) variations. A manageable size of the reference area might be on the order of the propeller disc area.

3. Surface force density. The longitudinal distribution of the induced surface force-per-unit length is called force density. It is a convenient way to represent the fluctuating loading imposed on the hull girder, especially in relation to excitation of overall girder vibration. It cannot be determined by direct measurement, but can be approximated by performing girthwise integration of measured point pressures resolved as vertical or other force components at each section down the length of the hull shape. It is noted here because it is especially useful for displaying the rate of change of exciting surface force as a function of distance in the vicinity of the propeller, and away from it as well.

4. Net surface force amplitude. In principle, the total integrated or net surface force amplitudes induced by the propeller can be determined approximately from area integrations of measured point pressure amplitudes. There has never been a direct model experimental measurement made of the total induced vertical surface force (separated from any moment effects), and none accomplished on a full scale ship. The net force magnitude, at various blade rate harmonics, would represent the most condensed parameter for measuring excitation level important to girder vibration, although of less importance to inboard noise. The net vertical force is not likely to act exactly at the propeller plane location because of asymmetries in the longitudinal distribution of force density.

Example discussions of vertical surface force values obtained either from distribution of measured pressure amplitudes or by calculation using computed distributions of pressure pulses can be found in references by Hylarides,¹⁹ Skaar and Raestad²⁰, and Huse.¹³ Recommendations on the levels of vertical force ratio (total surface force-to-mean propeller thrust) that could cause hull girder vibration problems could be inferred from each of these references, but there is no agreement among them. Recommended ratios for the critical value of surface force-to-thrust ratio for the onset of unacceptable vibration excitation seem to range from about 7 percent to 30 percent. Occasionally values well above 100 percent have been predicted with no report of excessive ship vibration on the ship itself. There is considerable need for improvement on how to interpret and use estimated values of net surface force amplitude.

5. Cavity volume pulsation strength. For a propeller operating with intermittent blade cavitation in a nonuniform flow, the resultant pressure amplitudes are typically increased noticeably over noncavitating levels. The increase is relatively even greater for the corresponding amplitudes of, say, the vertical surface force density or the total surface force because they are area-integrated quantities of pressure fluctuations having nearly constant phase angles everywhere. The dominating feature is the monopole-like pressure source behavior of the fluctuating cavity volume of each blade sheet cavity. Although the primary characteristic of a typical sheet cavity volume variation is similar to that of a pulsating spherical bubble,¹² there are contributions from cavitating tip vortices²¹ and possibly significant contributions from bulging tip vortices.²² The term cavity volume variation refers to the total volume within the blade cavities plotted as a function of the circumferential position angle.

A useful representation of the main physical mechanism involved with exciting pressures from cavity pulsation is given in a simple expression for the pressure fluctuation produced at a distance r from the center of a pulsating spherical bubble

$$\Delta p = \frac{\rho}{4\pi r} \frac{d^2 V_c}{dt^2} \quad (1)$$

where the cavity volume variation is given by $\dot{V}_c(t)$. This shows that the spatial rate of decay of the induced pressure amplitude is r^{-1} and that the pulsation strength is proportional to the cavity volume acceleration \ddot{V}_c (or $\omega\dot{V}_c$ for harmonic variations). An important difficulty in making use of this type of relationship is obtaining accurate determination of the cavity volume variation, either by analytical prediction or by experiment.

It is possible to determine cavity volume pulsation strength experimentally by an indirect means involving the concept of reciprocal measurements. From the reciprocity principle for linear dynamic systems, a simplified expression is available (see Appendix) to cover the case of the unsteady force on a body or a body surface element fixed in position relative to a fluctuating point source. Then, in a water tunnel or full scale test environment, the "volume velocity" of a fluctuating blade sheet cavity can be approximated by

$$\dot{V}_c = \frac{F_2}{i\omega(p_1/a_2)} \quad (2)$$

where \dot{V}_c = time rate of change of cavity volume

F_2 = amplitude of measured unsteady force on a body or body element, harmonic component corresponding to the frequency ω

ω = circular frequency

(p_1/a_2) = transfer function, measured ratio of pressure amplitude at propeller location to the acceleration amplitude at the body

$i = (-1)^{1/2}$

All the quantities in this formula except ω are regarded as complex. A discussion of this expression and related forms is given in the Appendix.

To implement the reciprocity technique, there are two phases of measurements. During the calibration phase, the body element is forced to oscillate through a range of frequencies of interest. The transfer function ratio (p_1/a_2) is formed for each frequency from the simultaneous measurement of the pressure p_1 measured at a position in the fluid representing the approximate center of cavitation and the vertical acceleration a_2 of the forcing body element. The final measurement phase is run with excitation from the cavitating propeller.

Then once the cavitation-dependent component of the vertical surface force blade rate amplitude $(F_S)_Z$ on the body element is determined, the resulting blade rate component of volume velocity can be evaluated from the expression given above.

REVIEW OF EXPERIMENTS

It is useful to outline the scope of some example model experimental investigations that have been used to explore various features of propeller-induced surface pressure/surface force excitation.

Early Experiments on Exciting Loads and Induced Pressures.

The earliest work that showed an appreciation of the presence of propeller-induced surface forces in addition to the bearing loads was that of Lewis^{23,24}. An experimental scheme was devised for testing rigid ship models in a towing basin, where the model vibration response was used to determine the exciting forces under self-propelled conditions by comparing the response to that produced by a calibration vibration exciter located in the stern that delivered known oscillating force levels. Lewis was able to decide that the major contribution to the measured propeller-induced effective vertical force on the hull, for example, was due to the surface force. Similar measurements were made on a model of a cargo ship form and reported by Lewis and Tachmindji.²⁵ Continuing with an improved rigid model approach, but with smaller models, Lewis presented a summary of results of such experiments for several different examples.²⁶ Unsteady blade cavitation played no role in these model basin studies, and was not suspected as being important until many years later.

An experimental program to measure the aft end vibratory surface loads and inferred bearing loads was presented by Stuntz, et al²⁷. In this case, the stern end of the ship model was mounted on flexures and instrumented to measure the vertical, horizontal, and torsional unsteady loads induced by the operating propeller as tested in a towing basin. No conditions involving intermittent blade cavitation could be considered.

Early experiments conducted in water to measure the periodic pressure disturbances ahead of, behind, and beside an operating propeller have been presented in reports by Tachmindji and Dickerson^{28,29} on the free space pressure pulses near a propeller running in uniform flow and behind a strut; by

Pohl³⁰ on the fluctuating pressures induced on a flat plate surface mounted parallel to the propeller axis in a water channel and on the pressure pulses acting on the hull surface of a model ship in a towing basin; by Taniguchi³¹ on the pressures induced on a flat plate; and by Weitendorf³² on the variations of fluctuating pressures induced on flat and concave curved plates at various tip clearance ratios, on pressure pulses on flat plates with various elastic mountings, and on pressure pulses at locations near the propeller on the hull surface of surface ship models. All these early tests involved non-cavitating flow conditions. Experiments by Nelka³³ were also concerned with the induced pressure amplitudes on a flat plate boundary near a propeller and showed the effects of tip clearance ratio with a series of propellers with increasing blade skew angles and blade warp angles and the effect of nonuniform inflow velocity pattern.

Examples of complete ship model experimental results obtained in towing basin tests for propeller-induced vibratory pressure amplitudes on the hull surface near the propeller have been reported by Keil³⁴ for an oceanographic ship; by Huse³⁵ for a tanker form; by Weitendorf³² for semi-tunnel tunnel stern combatant form; and by Jacobs, et al³⁶ for a destroyer hull form. All these have been conducted under nonuniform inflows, but noncavitating conditions, so that crucial interaction between nonuniform inflow and intermittent cavity volume variation is missing in each of these investigations.

Experiments with Cavitating Propellers and Modelled Wake Inflow

Simple Boundary Arrangements. Early water tunnel experiments were carried out by Denny¹⁶, who made extensive measurements of the propeller-induced periodic pressure amplitudes on a flat plate boundary. A number of important effects were studied, including tip clearance ratio, propeller loading, nonuniform inflow, propeller geometry (expanded area ratio and blade skew angle), and cavitation in uniform flow. Extensive comparisons were made with theoretical predictions available at the time, and these were used to check the separate contributions of loading and thickness. It is interesting that Denny was the first to note that blade cavitation served to accentuate the magnitudes of the induced pressure pulses in the case of uniform inflow and extensive sheet cavitation. The increases of pressure pulse level in the steady cavitating flow were

comparable to the increases caused by noncavitating operation in certain of the wake patterns tested. However, the crucial combination of nonuniform flow with blade sheet cavitation was not included by Denny, so the important influence of intermittent blade cavitation was not revealed in these experiments.

The pivotal paper by Takahashi and Ueda³⁷ describes measurements of propeller-induced pressure amplitudes on a flat plate in both noncavitating and cavitating conditions and in both uniform and nonuniform wake flow. It is this work that is often credited with first providing the experimental motivation of the connection between intermittent blade cavitation and exaggerated pressure pulses that arise in operation in nonuniform flow.

Other water tunnel experiments concerned with distributions of fluctuating pressure amplitudes induced on a flat plate boundary by a cavitating model propeller in nonuniform flow have been carried out and reported by Weitendorf^{38,39} Takahashi,⁴⁰ Chiba and Hoshino,⁴¹ Sasajima,⁴² Takekuma,⁴³ and Weitendorf²¹ who provides a summary discussion of a number of different effects.

Water tunnel experiments involving measurement of the localized propeller-induced excitation levels on somewhat more complicated boundaries have been carried out, for example, by Nelka⁴⁴ on the pressure pulses produced on the inside surface of a duct of an ducted propeller system, and by Peck⁴⁵ on the pressure pulses at points on the centerline of a tunnel enclosing 65 percent of the diameter of two different propellers. Kerwin, et al¹⁸ presented results on the levels of propeller-excited unsteady normal surface force measured on a flat force disc imbedded flush with a flat boundary, for a series of propellers.

Partial Stern (Dummy Model) Experiments. The use of foreshortened ship hull models, often termed dummy models, in variable pressure water tunnel experiments with operating propellers has long provided a practical approach to the problem of attempting to model the proper three dimensional wake velocity patterns for model propeller cavitation tests. Since the early 1970's, dummy models have also been used in many laboratories around the world to try to survey the propeller-induced periodic pressures at points near the propeller, with approximate representation of the wake velocities, hull boundary shape, and cavitation number environment.

Some early published investigations using foreshortened hull models in the determination of cavitating propeller-induced pressure pulses include van Manen,⁴⁶ Huse,⁴⁷ van Oossanen and van der Kooij,⁴⁸ and van der Kooij and Jonk.⁴⁹ Examples of more recent publications that have either made use of results from dummy model tests or mention this test technique in some fashion are Hylarides,⁵⁰ Glover, et al,⁵¹ Glover and Patience,⁵² Lover and Wills,⁵³ Chiba, et al,⁵⁴ Reed, et al,⁵⁵ Lovik,⁵⁶ Munk, et al,⁵⁷ and Hadler, et al⁵⁸.

Useful and informative work on the test techniques and interpretive problems of dummy model testing in water tunnels has been reported on by English⁵⁹ and by Larsen.⁶⁰

Complete Model Experiments. Because of the importance of the wake velocity pattern to the correct modelling of the intermittent blade cavitation, the idea of using complete ship hull models for cavitation experiments is very appealing. The idea is that, at least on the model scale, the correct wake pattern is represented closely by using the geometrically scaled hull form. There are two prominent facilities actively used for research and engineering assessments of ship propulsion systems using complete ship hull models: the MARIN Depressurized Towing Tank in Wageningen Netherlands, which provides for the simultaneous satisfaction of the Froude number and the cavitation number; and the large cavitation tunnel (Tunnel No. 2) at SSPA in Sweden which provides no free surface boundary at the model waterline, but employs typical free stream velocities that lead to relatively high model blade Reynolds numbers. Good summaries of some experimental results and discussions of testing techniques, data analyses, and comparison studies are given by van der Kooij⁶¹ on the Depressurized Towing Tank, by Lindgren and Bjarne⁶² on the large cavitation tunnel at SSPA, and by Dyne and Hoekstra⁶³ on comparisons of results between the two.

Reciprocity Experiments. Application of a simplified form of the reciprocity principle to shipboard measurement of the propeller source strength (volume velocity) was developed in References 64 and 65, with particular reference to the problem of inboard noise transmitted by means of ship structure vibration excited by the propeller. The basic ideas for this approach are discussed in the Appendix. Gray⁶⁶ has also demonstrated the use of the reciprocity concept

in determining the source strength of cavity pulsation and the estimate of oscillating hull pressure amplitudes on full scale ships. Van der Kooij⁶¹ has indicated that the same ideas have been used to measure the model scale cavity source strength from model tests in the NSMB Depressurized Towing Basin.

Vorus in a discussion of a paper given by Kerwin, et al¹⁸ proposed an experimental/analytical method for estimating the unsteady force on a body (any shape) located near a fluctuating point source by exploiting the results of a reciprocity experiment conducted with very simple model geometry in a water tunnel. This suggestion was subsequently followed by experiments carried out with the instrumented force disc described in Reference 18, using a model of a destroyer propeller. The calibration experiment to determine the acceleration-to-pressure transfer function is described by Whalen, et al.⁶⁷ Description of the wake simulation tests and results of the measurement of the disc force amplitude leading to the determination of cavity volume velocity are presented by Whalen, et al⁶⁸. Application of these results to determine the effect of blade tip clearance on the propeller-induced vertical hull surface force for the DD 963 has been summarized by Vorus.⁶⁹

An attempt to exploit a more complete statement of the reciprocity principle has been carried out by des Moutis⁷⁰ in the M.I.T. water tunnel for the experimental determination of cavity volume velocity as well as the six unsteady propeller bearing force and moment amplitudes.

APPARATUS AND INSTRUMENTATION

FACILITY

The particular experimental equipment developed for this work was designed for use in the 24-inch Variable Pressure Water Tunnel at DTNSRDC. This facility provides the basic propeller dynamometry, adjustable ambient tunnel pressure to simulate cavitating flow conditions, and an access chamber on the top side of the open jet section which provides space for the force measuring apparatus.

MOUNTING PLATE AND INSTRUMENTATION

A one-inch thick, aluminum flat plate insert was positioned horizontally and parallel to the axis of the open jet test section of the water tunnel. This functioned as the representative boundary surface for the initial experiments.

With the propeller installed along the tunnel centerline on the downstream shaft, the vertical position of the plate can be varied from 7.5 in. (19.1 cm) to 9.0 in (22.9 cm) from the centerline to provide vertical tip clearances in the range of $a_z/D = 0.25$ to 0.4 for a nominal 10-inch (25.4 cm) diameter model propeller. The upstream end of the plate was faired into the tunnel convergence with a flexible nylon sheet joining the plate to a nose piece fastened to the tunnel wall. This allowed a simple adjustment of the vertical position of the plate boundary.

Force Measuring Apparatus

The surface force measuring device is shown in the sketch of Figure 2. It consists of an instrumented force disc connected to a robust inner plate and backup support structure. The entire support system is connected to the water tunnel structure through the flexures of two block gauges.

The force disc itself is a circular aluminum plate with a diameter of 10 in. (25.4 cm) and thickness of 1 in. (2.54 cm) mounted flush with the flat plate boundary. An O-ring was fitted in the gap between the disc and the hole in the mounting plate. The disc is attached to the inner support plate by a tripod arrangement of three piezoelectric force gauges. The particular force gauge (Wilcoxon Model L10) was chosen because it satisfies several important requirements: (a) accurate measurement of oscillatory force levels with amplitudes expected in the range of 5×10^{-2} to 5 lbf (0.22 to 22 N) in a frequency range possibly up to 1500 Hz, (b) large value of effective spring stiffness constant, and (c) capability of being driven electrically in a reverse mode in order to be used as a force excitor by placing an oscillatory voltage signal at the input.

Various masses and support stiffnesses of the elements of the force measuring device were chosen to obtain a flat dynamic response characteristic of the force disc in the range of frequency covering the first three harmonics of the blade rate. The force disc mass plus its added mass is about 1 slug (14.6 kg) mounted on the force gauges having a combined spring stiffness of 15×10^6 lb/in. (26.3×10^6 N/cm). The massive support structure includes two stacks of weights and was sized to provide a large inertial mass of about 550 lb (17.1 slug or 249 kg) suspended on the flexures having an effective stiffness of 1×10^5 lb/in (1.75×10^5 N/cm). The system was designed to accommodate the exciting fre-

quency range of 50 Hz to 650Hz which brackets the range of the first three blade rate harmonics for any model propellers of interest, operating at the necessary rates of rotation (14 $\leq n \leq$ 25 rps).

The force disc could be instrumented with as many as three accelerometers mounted on the top side in order to measure the vertical vibration levels of the disc either during various calibrations or during an excitation experiment with a propeller running in the tunnel. Waterproofing of the accelerometers and all the force gauges was provided by coating them with standard potting material. Some details of instrumentation characteristics are given in Table 1.

Surface Pressures

Mounting holes for flush-mounted pressure gauges were arranged in the pattern shown in Figure 3 in the flat mounting plate and the force disc. There are 52 positions on the flat plate and 13 on the force disc. These provide the possibility of obtaining a comprehensive picture of the distribution of surface pressure amplitudes at points within a rectangle of dimension 1.1D by 2D in the vicinity of the propeller, for a normal 10-inch (25.4 cm) diameter. Special threaded adaptor fittings permitted the use of either of the two different types of pressure gauges available for the experiments. The expected range of maximum fluctuating pressure amplitude at points closest to the tip at the blade rate frequency or any of its higher multiples was on the order of ± 1 psi (6.9 kPa). The two types of gauges used were the Kulite XTM-190 and the CEC 4-312, with nominal operating ranges of ± 10 psi (69 kPa) and ± 25 psi (172 kPa), respectively. Both gauges are of the strain gauged diaphragm type. Some further details on the pressure gauges are given in Table 1.

CALIBRATIONS

The pressure gauges were calibrated in a static pressure test stand to determine the sensitivity (slope = pressure/volt) for each gauge. These slopes were also checked at intervals throughout the experimental program, using tunnel pressure.

Extensive calibrations were performed on the surface force measuring device in order to establish its characteristics as an unsteady dynamometer and for its application in a reciprocity experiment.

It was necessary to establish the correct force slope factors for the three force gauges and to determine the frequency response characteristic for the force disc. An unsteady force was applied to the disc by means of an electrodynamic shaker. The force applied to the disc was measured independently with a pre-calibrated piezoelectric force gauge. For the case of the tunnel full of water and with the O-ring in place around the edge of the disc, the measured dynamic response is shown in Figure 4, displaying the ratio force output-to-force input plotted versus frequency of excitation. The frequency response curve is essentially flat to around 650 Hz where it begins to rise toward a natural resonance frequency at 930 Hz. This indicates that the desired level response characteristic holds satisfactorily out to frequencies well beyond the third blade rate harmonic for model propellers with as many as seven blades. The flat force response also permitted the final determination of the calibration slopes for the three piezoelectric force gauges with the fully assembled dynamometer.

The second major function of the force disc apparatus is to provide the possibility of determining the characteristic cavity volume variation of a cavitating propeller in nonuniform inflow by means of the indirect method exploiting the reciprocity principle. To make this type of measurement it is necessary first to perform a reciprocity calibration which determines the transfer function relating the fluid pressure response at a field point to the magnitude of vertical vibration of the surface area element (force disc). The reciprocity calibration was carried out by oscillating the force disc vertically along its axis (normal to the surface) by means of a sinusoidally varying voltage placed across the three piezoelectric force gauges which support the disc. This effectively drove the force gauges in a reverse mode so that the disc was itself the electrodynamic shaker for the calibration phase. Excitation frequency covered a wide range from about 70 Hz to 1000 Hz in order to include the frequency variation up to the third harmonic of blade rate. The vertical acceleration of the disc was measured with accelerometers mounted on the back side of the disc. Pressure response in the fluid was measured in the absence of the propeller using a hydrophone located at a point in the 12 o'clock position at a distance $0.9 R$ from the axis. This location corresponds roughly to the expected center of the largest blade cavity volume determined from visual observation.

The resulting calibrated transfer function is shown in Figure 5 as the curve of the logarithm of the ratio of pressure amplitude-to-vertical acceleration

(p/a) plotted versus frequency. There is a variation with frequency apparent in this empirical function, with a local peak occurring at around 500 Hz, and a relative flattening beyond 800 Hz.

For frequencies below 300 Hz the measured values of the transfer function for (p/a) were found to display a temporal variation. Since the reciprocity calibration was obtained from a long analog tape record of the simultaneous measurement of fluid pressure and disc acceleration taken during the same calibration session, several values of (p/a) at a given frequency could be calculated from several different segments of the tape. For the data displayed, each segment consisted of a frequency sweep through the range of interest. This provides a check on repeatability and shows that the values of (p/a) were reliably repeatable for the frequency regime higher than 300 Hz. Below 300 Hz, however, there was a range of values computed for (p/a) at any one frequency, indicating that the transfer function varied with time. In Figure 5, the shaded region shows the range of values of the transfer function computed from several different segments of the measured record.

At this time, there is no conclusive explanation for the variability of the measured transfer function in the low frequency range. One possibility is that under unsteady excitation, there are pressure reflections from structural elements inside the tunnel and test section, such as the nozzles or the installed flat plate. There could be interfering unsteady pressures set up by induced vibrations of the tunnel walls and model structure. A likely contributor to the problem could be poor signal-to-noise ratio for the pressure response to the disc oscillation. This is expected to be worse at the low frequencies because of the very small acceleration levels being produced by the mechanical system in the frequency range involved. It is not likely that the variability of the (p/a) ratio is attributable to changing local properties such as temperature or ambient pressure, because the time scales of these changes are much longer than characteristic time involved with the changes of the transfer function magnitude. This problem requires further study.

For the model propeller experiments reported on here, the blade rate frequency at the convenient operating speed was 98 Hz. At this frequency, the variability of the (p/a) involves a range of about +34 percent.

EXCITATION EXPERIMENTS WITH MODEL PROPELLER

PROPELLER

For comparison purposes, it was decided to use the 9.812-in. (24.92 cm) diameter DTNSRDC model propeller number 4677 which represents the 21-ft, seven-bladed, skewed propeller for the single screw Naval Auxiliary Oiler AO-177 with the scale ratio 25.682. The wake adapted design of this propeller is described by Valentine and Chase.⁷¹ Table 2 is a summary of the particulars of the propeller geometry. Drawings of the blade shape are given in Figure 6. Figure 7 shows the propeller open water characteristics presented by Hendrican and Remmers⁷². Appropriate operating conditions for the propeller were selected on the basis of the model powering experiments reported in Reference 72.

EXPERIMENTAL PROCEDURE

Wake Simulation

All the experiments shown here were carried out in a non-uniform flow in the tunnel produced by a wake screen which provides for control of the axial velocity component only. The wake screen was designed to simulate the nominal wake distribution V_X/V produced by the AO-177 as determined from a towing basin wake survey with a scaled model of the ship hull. Wake surveys were conducted in the tunnel with the screen-generated flow using a rake of five, 5-hole spherically-headed pitot tubes. The flat plate boundary was set at two locations corresponding to propeller tip clearances of $a_z/D = 0.26$ and 0.41 . Figures 8, 9, and 10 are example comparisons of the measured axial velocity ratio V_X/V versus θ for $r/R = 0.557$, 0.774 , and 1.178 respectively, showing data obtained from a towing basin wake survey^{73,74} and the tunnel wake surveys. Definition of the position angle θ is given in the figures. These comparisons show that the V_X/V flow patterns behind the wake screen for the two different plate locations are generally similar to the target nominal velocity distributions, but are not identical. One noticeable feature is that there are differences in the level of the V_X/V values when the position angle θ is outside the main velocity defect region (which is contained inside $-90 \text{ deg} < \theta < 90 \text{ deg}$). The relatively higher values for the case $a_z/D = 0.26$ are attributable to relatively increased average flow velocity caused by the smaller flow cross section area. This speed-up influence is less pronounced for the case of $a_z/D = 0.41$, because the flow area

blockage is less. The narrow velocity defect from the lower skeg region, centered about the position angle $\theta = 180$ deg, and seen clearly in the towing basin velocity distribution, was not reproduced in the wake screen velocity pattern. The skeg wake velocity feature in this case is much less important than the main hull wake characteristic because there is no known blade cavitation that occurs in that region. For this reason, dense screen material was not applied along the centerline of the lower disc area of the wake screen used for the present experiments.

There are important similarities between the wake screen velocity patterns and the towing basin velocity distributions (the target wake). The values of the minimum V_X/V ratio in the vicinity of $\theta = 0$ are nearly the same in the two wake screen distributions as in the target wake, although the precise angular positions may be offset somewhat for the wake screen cases. More importantly, the relative slopes of the main velocity defect with respect to the circumferential angle, denoted by $d(V_X/V)/d\theta$, are approximately the same for the target distribution and the wake screen distributions along the rays, say $\theta = 40$ deg and $\theta = 320$ deg. These similarities are concerned with features of the wake that are most important to the production of unsteady pressures due to cavity volume variation, as noted, for instance in Reference 75. It is concluded that propeller blade cavities should reach approximately the same size at about the same circumferential position, and should grow and diminish at about the same rate in either of the two wake screen velocity patterns as in the towing basin velocity distribution. Since the dominant contribution to the propeller unsteady pressures and surface force comes from the unsteady cavity volume variation, experiments in the wake screen velocity patterns described above could be expected to provide excitation characteristics generally meaningful to the case of the A0-177 propeller and wake combination.

Unsteady Pressures and Disc Surface Force

Measurements have been carried out in the 24-inch water tunnel using the newly developed apparatus and propeller Model 4677. The propeller was mounted on the downstream shaft, with the boundary plate arranged parallel to the axis. Pressure gauge measurements were taken at 11 of the locations on the disc and at many locations on the surrounding boundary plane, concentrating on the points

along the longitudinal and transverse centerlines (x_{PC} and y axes, respectively) as depicted in Figure 3. The propeller reference center identified in Figure 6 was placed at the longitudinal position of the transverse axis, $x_{PC} = 0$. Thus, the location of a plane through the blade tips was at a distance $0.115D$ downstream of the $x_{PC} = 0$ position.

Unsteady disc force measurements were made with the three piezoelectric force gauges in place, and in some cases, simultaneously with pressure gauge measurements.

All the experiments conducted for this work were performed at the loading condition corresponding to the advance coefficient $J = 0.79$ and thrust coefficient $K_T = 0.295$, producing a thrust coefficient of $C_{Th} = 1.2$. Test section velocity was set for the target J by using the thrust identity method from the open-water characteristics. This was accomplished by setting the shaft rotation speed for the desired advance coefficient and adjusting the tunnel water speed until the thrust coefficient matched the open-water thrust coefficient. The velocity calibrated in this way was held constant and the tunnel pressure varied to change the cavitation number. Shaft rotation speed was maintained at 14 rps for all the conditions tested. The Reynolds number based on chordlength at the $0.7R$ and the approximate total velocity was 0.51×10^6 .

The range of cavitation numbers included $\sigma_n = 17.86$ to 8.36 ($\sigma_{VA} = 28.6$ to 13.4) which covered non-cavitating reference conditions as well as conditions with mixed tip vortex and sheet cavitation characteristic for this propeller. The minimum cavitation number used here was limited by a tunnel flow speed that would not damage the wake screen. With the loading conditions held the same throughout the range of σ_n , the effects of different blade cavitation patterns on the unsteady pressures and disc force could be studied independent of the propeller loading condition.

Total air content of the tunnel water, measured with a Van Slyke apparatus, was held in the range of 24 to 35 percent of saturation at atmospheric pressure, mainly to provide clear visibility. Water temperature varied from 69° to 74° F (20.6° to 23.3° C).

Measurements of both the pressure fluctuations and disc unsteady force were obtained with the flat plate boundary positioned at two different locations corresponding to propeller tip clearance ratios $a_z/D = 0.26$ and 0.41 . The vertical tip clearance ratio on the AO-177 ship is $a_z/D = 0.292$.

The test procedure consisted of recording the pressure and force transducer signals for several minutes at a particular cavitation number, with the simultaneous recording of the data onto magnetic tape. Throughout most of the test conditions, the pressure and force signals were checked online with a time series analyzer to review the character of the pressure and force spectra and the relative contributions at the blade rate frequency and its higher harmonics. Taped pressure and force gauge records consisted of a recorded digitized signal at 256 points around each shaft rotation as triggered from a shaft encoder attached to the propeller shaft. A timing channel, recorded simultaneously with the pressure and force signals, provided a single pulse per shaft rotation that was arranged to indicate the passage of a blade reference line past the 12 o'clock position (point of closest approach to the flat boundary). It was used for the measured phase analysis.

After the recording sessions, the data were analyzed using a Model 70 Interdata computer to provide the Fourier Series harmonic components over a convenient specified time interval, usually 10 seconds. Thus a typical analysis record for these experiments covered 140 propeller revolutions.

It was clear from the harmonic analysis and from the time series analyzer spectra that the signals of the surface pressures and disc force were dominated by the blade rate frequency. Amplitudes of higher multiples of blade rate were always smaller than the blade rate itself, but not necessarily with magnitude decreasing strictly with increasing harmonic order.

Data Analysis

The unsteady behavior of the pressure measured at any location is a periodic fluctuation $p(t)$ and can be represented by the Fourier series.

$$\tilde{p}(t) = \sum_{m=1}^{\infty} (A_m \cos m\omega t + B_m \sin m\omega t) \quad (3)$$

rewritten in a form to display total amplitude and phase angle as

$$\tilde{p}(t) = \sum_{m=1}^{\infty} P_m \sin(m\phi - \gamma_m) \quad (4)$$

where $\phi = \omega t$ is the position angle taken positive clockwise from 12 o'clock, looking upstream

$\omega = 2\pi n$ = shaft circular frequency

$P_m = (A_m^2 + B_m^2)^{1/2}$ = total amplitude of the mth harmonic component of the pressure fluctuation

$\gamma_m = \tan^{-1}(-A_m/B_m)$ = harmonic phase angle of the mth pressure harmonic

The positive peak (maximum positive value) of the mth harmonic component of pressure fluctuation occurs when

$$m\phi - \gamma_m = \frac{\pi}{2} \quad (5)$$

Thus the spatial phase angle at which, say, the Zth or blade rate harmonic of pressure reaches a maximum positive value is

$$\phi_Z = \left(\frac{\gamma_Z + \frac{\pi}{2}}{Z} \right) \quad (6)$$

This phase angle is the angular location of the blade reference line when the blade rate pressure positive peak occurs, measured clockwise looking upstream (see Figure 1).

The amplitude of the mth harmonic pressure component $(\Delta p)_m = P_m$ is made non-dimensional in the following definition

$$(K_p)_m = \frac{P_m}{\rho n^2 D^2} \quad (7)$$

In the present work, we confine our interest to the results for the first three blade rate harmonics, with $m = \mu Z$

$$m = Z, 2Z, 3Z$$

so that $\mu = 1, 2, 3$

Similarly, the unsteady reference area surface force on the disc can be expressed in terms of its Fourier series

$$\tilde{F}_S(t) = \sum_{m=1}^{\infty} (F_S)_m \sin(m\phi - \beta_m) \quad (8)$$

where $\phi = \omega t$ is the position angle

$(F_S)_m$ = total amplitude of the m th harmonic component of fluctuating disc force (obtained from the sum of the three force gauge signals)

β_m = harmonic phase angle of the m th disc force component

The nondimensional form of the disc force amplitude for the m th harmonic is

$$(K_F)_m = \frac{(F_S)_m}{\rho n^2 D^4} \quad (9)$$

Using this, the ratio of the unsteady force amplitude to propeller mean thrust, say at blade rate frequency, is the ratio of the coefficients

$$\frac{(F_S)_Z}{T} = \frac{(K_F)_Z}{K_T} \quad (10)$$

RESULTS

Propeller Cavitation

Visual observation of the propeller operated under the test conditions described earlier showed that tip vortex cavitation springing from the blade tips

appeared at around $\sigma_n = 13$. As the cavitation number was decreased from this value, the tip vortex increased in size. Sheet cavitation began forming on the suction side near the blade tips at σ_n near 12. At $\sigma_n = 10.5$ there was substantial sheet cavitation on each blade. For the cavitation number $\sigma_n = 8.36$, the lowest value achieved in this test series, the sheet cavity on each blade covered a portion of the outer 25 percent of the propeller radius. The circumferential extent of the blade sheet cavitation was from about 90° before 12 o'clock around to 60° beyond the top-dead-center position.

Unsteady Pressures

Figures 11 and 12 show the variation of pressure coefficient values K_p versus cavitation number for the amplitudes of fluctuating pressure acting at the center of the disc (directly over the propeller center) for the first three harmonics of blade rate. Figure 11 shows data for the tip clearance ratio $a_z/D = 0.26$, with Figure 12 applicable to the larger tip clearance $a_z/D = 0.41$. The pressure amplitude curves are flat in the non-cavitating regime of large σ_n . For values of $\sigma_n < 12$, the pressure amplitude characteristics start to rise with decreasing cavitation number. The noticeable increase in the levels of all the $(K_p)_m$ values coincides with the appearance and growth in size of blade sheet cavities, a fact that confirms our general understanding of the importance of unsteady cavity volume variation to the pressure excitation.

For both tip clearances, the blade rate harmonic component is typically larger than the second and third blade rate contributions. The differences are clearly dependent on the tip clearance ratio. At the smallest tip clearance of $a_z/D = 0.26$ the blade rate amplitudes exceed the higher harmonics by a factor of more than 2.5. For the larger $a_z/D = 0.41$, the higher harmonic amplitude values are comparable to the fundamental blade rate amplitude.

In a comparison of the results of magnitudes of the blade rate component for the two tip clearance ratios, there appears to be a large influence of tip clearance. The smaller tip clearance produces the larger $(K_p)_z$ levels in both the non-cavitating and cavitating regimes. This is certainly consistent with previous experimental findings. Some of the difference in pressure amplitudes between the two tip clearance cases may be attributed to differences in the screen-generated nominal wakes for the two tip clearance ratios, as seen in

Figures 8 through 10. The extremes of the hydrodynamic advance angle away from the mean value are different for the two wakes, and this could influence the variation of blade cavitation. However, visual observation of the blade cavitation for the two tip clearance cases revealed no significant differences. It is plausible that for the gauge location over the propeller center, the measured differences of pressure amplitude are due mainly to the tip clearance variation.

The longitudinal distributions of the first three blade rate harmonics of fluctuating pressure amplitude coefficient along the centerline of the plate (the x_{PC} -axis shown in Figure 3) are displayed, respectively, in Figures 13, 14, and 15 for tip clearance ratio $a_z/D = 0.26$. The comparable distributions of $(K_p)_z$ versus x_{PC}/D for the tip clearance case $a_z/D = 0.41$ are given in Figure 16 through 18. Here, positive values of x_{PC}/D are upstream of the propeller center. The contours in these groups of figures are for five different values of cavitation number. These plots show the expected fall-off of pressure amplitude both upstream and downstream of the location of the propeller center.

The transverse distributions of the first three blade rate harmonics of pressure coefficient are plotted versus the nondimensional distance y/D (along the lateral axis in line with propeller center) in Figures 19 through 21 for $a_z/D = 0.26$; and in Figures 22 through 24 for $a_z/D = 0.41$. Here the positive values of y/D are taken to starboard, looking upstream. Generally, the largest blade rate pressure amplitudes occur near the propeller centerline and fall off to either side. It has been observed from published experimental work with a variety of propeller types, that the transverse distributions of blade rate pressure amplitudes are not necessarily expected to be symmetric about the propeller centerline or about a line passing through the location of the peak pressure. Propeller blade skew will tend to accentuate the non-symmetry, particularly for the lower range of σ_n where transient cavitation begins to dominate excitation pressures. The propeller used in the present experiments has 45 deg skew at the tip radius. With blades having positive skew ("skew back"), even with a symmetrical wake, the region of greatest cavitation extent is displaced around to the right hand side of the disc area for a right-handed propeller (see for instance, Reference 14). For very low cavitation numbers, the largest unsteady pressures are associated with the cavity-collapse portion of the cavity volume variation, which

occurs over in the right-hand quadrant of the propeller disc rather than at the 12 o'clock position where the tip clearance is smallest. The displacement and distortion of cavity volume due to effects of skew can influence the higher harmonics of the surface pressure in non-trivial ways as well. In the present experiments, carried out at intermediate values of cavitation number, the location of the peak blade rate pressure amplitude is apparently influenced most by the effect of tip proximity, and occurs at or near the position of closest approach of the blade tip.

For higher harmonics of blade rate, the curves of pressure amplitudes at constant σ_n - values are sometimes skewed to one side, or may show some slightly mixed trend with respect to cavitation number on one side of the centerline that differs from the opposite side. (See, for instance, Figures 17, 20, 21, 23, and 24). These are the manifestations of a combination of higher harmonic distortion by a skewed cavitation extent (noted above) and scatter and inaccuracy associated with the relatively low levels of pressure magnitude of the higher harmonic components compared with the blade rate contributions.

Unsteady Disc Force

The measured fluctuating disc force amplitude coefficients for the first three blade rate harmonics are shown plotted versus cavitation number for $a_z/D = 0.26$ in Figure 25, and for $a_z/D = 0.41$ in Figure 26. The symbols plotted in these graphs represent the average values for two or three data spots at each of the tested cavitation numbers. Similar to the trends of the pressure amplitudes, the disc force amplitude curves are flat for σ_n larger than about 12, then there are noticeable increases as the cavitation number is decreased. This characteristic is linked to the appearance and growth of blade sheet cavities.

When comparing the first blade rate harmonic of disc force for the two different tip clearance cases, the force amplitude for $a_z/D = 0.26$ is about 20 percent larger than the force amplitude for $a_z/D = 0.41$. This relative difference of force amplitude is considerably less than that for the pressure amplitude at the disc center for the same tip clearance ratios. For instance, from data displayed in Figures 11 and 12, at $\sigma_n = 8.36$, the blade rate pressure amplitude for the smaller tip clearance ratio is 170 percent larger than that for $a_z/D = 0.41$. Thus, the variation of pressure pulse amplitude versus cavitation number

measured at one surface point location is not necessarily indicative of the magnitude of force amplitude variation acting on a surrounding reference area for this propeller and wake.

Simultaneously with the disc force measurements, pressure amplitude and phase angle measurements were obtained at 11 locations on the disc. For the first three blade rate harmonic components, the measured pressure values were integrated over the surface of the flat disc to determine a net normal force estimate on the disc area. Proper account was made for the variation of phase angle for each transducer location, so that the presence of transverse asymmetries of pressure amplitude distributions should not affect the accuracy of the integrated pressure results. The results provide interesting comparisons with the measured force amplitudes at various cavitation numbers at the two different tip clearances.

Figures 27 and 28 compare the blade rate harmonic force coefficient values of measured force and integrated pressure force for the tip clearance ratios $a_2/D = 0.26$ and 0.41 , respectively. The comparisons of twice blade rate harmonic force coefficients for the two tip clearances are given in Figures 29 and 30; and the three times blade rate amplitude coefficients are displayed in Figures 31 and 32, for $a_2/D = 0.26$ and 0.41 , respectively. In each of the comparisons, for all the harmonic components, the integrated pressure force amplitudes exceed the actual measured disc force amplitudes. The discrepancy is larger for the blade rate harmonic components than for the higher harmonics. This serves as another indication that a single point surface pressure amplitude is not necessarily an accurate representation of the net force acting over a reference area surrounding the point.

Comparison with Previous Results

Experimental results for the pressure pulse excitation were obtained previously for propeller model 4677 in the large cavitation tunnel at SSPA,⁷⁶ where a complete scale model of the A0-177 hull with appendages was installed in order to produce the desired model wake. Unsteady pressure amplitude measurements were recorded at several locations on the hull surface near the propeller. The nominal wake in the water tunnel flow behind the A0-177 model was not measured, but was assumed to match sufficiently well the nominal wake measured in a towing basin behind a model having the same scale.

Figure 33 shows a comparison of the longitudinal distribution of the blade rate pressure amplitude coefficients along the flat surface from the present 24-inch water tunnel results and along the hull surface from the complete model hull tests in the SSPA tunnel. Although this is not completely consistent because of the difference between the flat plate boundary and the actual hull shape and the mismatch of pressure gauge locations, it does provide an approximate comparison of the general trend of the longitudinal distribution of pressure pulse amplitudes. Measurements taken on the flat plate boundary positioned with tip clearance ratios $a_z/D = 0.26$ and 0.41 are shown in Figure 33 together with measurements obtained with the model hull shape with the vertical tip clearance of $a_z/D = 0.292$, all with the same cavitation number $\sigma_n = 8.36$. The values from the actual hull shape with $a_z/D = 0.292$ fall generally between the values obtained with the flat plate at the two different tip clearances. This indicates that the measurements on a flat plate represent a good order of magnitude approximation for the measurements along the hull. However, the shape of the curve of the $(K_p)_z$ values versus x_{pC}/D is not the same for the flat plate cases and the hull, and the details of differences are attributable to the difference in wake and boundary geometry (hull shape).

The variations with respect to cavitation number of the blade rate component of pressure amplitudes at or near the tip plane are shown in Figure 34. The values measured on the complete hull shape model were taken over the propeller tip and the values measured on the flat plate boundary were obtained in line with the propeller center. The curves compare favorably in an approximate way, considering the differences in boundary shape and tip clearances.

DISCUSSION

Useful measurements are described for three blade rate harmonics of the unsteady exciting force and pressures on a reference-area disc mounted in a flat boundary above a cavitating propeller operating in a screen-generated wake in the 24-inch variable pressure water tunnel at DTNSRDC. The inflow velocity distribution was intended to simulate the axial velocity pattern of a very severe single-screw ship type of wake, similar to that of the A0-177. Results of measurements are presented for a range of cavitation numbers covering

non-cavitating and cavitating conditions and for two different tip clearances. Comparisons are provided between the measured disc force and the force obtained by integrating the pressures over the disc area. The integrated pressure force values are always somewhat larger than the measured force values, principally because of the lack of sufficient detail in defining the variation of phase angles for the pressures over the disc.

Measured results from the complete array of pressure transducers over the flat plate boundary show the longitudinal and transverse centerline distributions of pressure pulse amplitudes in the region around the propeller. In general these show that the largest pressure excitation amplitudes occur near the propeller center.

All the computed harmonics of unsteady disc force and pressures show a noticeable increase with decreasing cavitation number, particularly below the onset of visible blade sheet cavitation at around $\sigma_n \approx 12$. Unsteady force and pressure amplitudes are largest for the smaller of the two tip clearance values.

A reciprocity experiment was performed to measure the pressure-to-acceleration transfer function (p/a), needed to estimate the time rate of change of cavity volume. The transfer function was found to have a noticeable variability at frequencies below about 300 Hz, and this was judged to represent an uncertainty in the capability to approximate the value of cavity volume velocity. As seen in Appendix B, the estimated blade rate cavity volume velocity inferred from reciprocity measurements and the calculated values agree in order of magnitude and trend with σ_n -variation. The experimental values are higher than the theory, and this could be due to the role of unsteady tip vortex cavitation, which is not accounted for. It is not possible at this time to sort out the magnitude of this effect on the discrepancy, which includes the combined uncertainty of the experimental calibrations and the sensitivity of computed cavity volume to the propeller inflow.

Comparisons between the present measured unsteady pressure amplitudes produced with the A0-177 model propeller on a flat plate boundary and those obtained previously on a complete scale model hull at SSPA show reasonable correlation with respect to the effect of tip clearance at comparable cavitation numbers. The differences between the results in terms of spatial distribution and variation with cavitation number are associated with the detailed differences in wake and boundary geometry.

It should be noted that with the capability developed here, propeller excitation experiments could be carried out with partial stern or dummy model representations of the near-propeller hull geometry that include characterizations of the reference-area unsteady vertical surface force as well as surface pressures. The disc force measuring system described here could be used to measure the vertical surface force amplitudes on a shaped element imbedded in the surface of a foreshortened hull model. Pressure gauges could be installed flush with the shaped surface as usual. The use of a partial body would provide some help with the simulation of a desired wake configuration, and it could be made less subject to low tunnel speed restrictions imposed by the use of wake screens alone.

ACKNOWLEDGMENTS

The authors gratefully acknowledge the work of Mr. George Gilbert for the careful design of the disc force measuring apparatus and Mr. Steve McQuigan for the computer system used in the data acquisition and analysis.

REFERENCES

1. Boswell, R.J. and G. G. Cox, "Design and Model Evaluation of a Highly-Skewed Propeller for a Cargo Ship," *Marine Technology*, Vol. 11, No. 1, pp. 73-89 (Jan 1974).
2. Valentine, D.T. and F.J. Dashnaw, "Highly Skewed Propeller for San Clemente Class Ore/Bulk/Oil Carrier Design Considerations, Model and Full Scale Evaluation," *First Ship Technology and Research (STAR) Symposium*, SNAME (1975).
3. Boswell, R.J., S. D. Jessup, and K-H Kim, "Periodic Blade Loads on Propellers in Tangential and Longitudinal Wakes," *SNAME Propellers '81 Symposium*, Virginia Beach (May 1981); also Report DTNSRDC-81/054 (June 1981).
4. Boswell, R.J., K.H. Kim, S. Jessup, and G.F. Lin, "Practical Methods for Predicting Periodic Propeller Loads," *Second Intern. Symp on Practical Design in Shipbuilding (PRADS 83)*, Tokyo and Seoul (Oct. 1983).
5. Huse, E., "Pressure Fluctuations on the Hull Induced by Cavitating Propellers," *Norwegian Ship Model Experimental Tank Publ. No. 111* (March 1972).
6. Noordzij, L., "Pressure Field Induced by a Cavitating Propeller," *International Shipbuilding Progress*, Vol. 23, No. 260 (April 1976).
7. Vorus, W.S., J.P. Breslin, and Y.S. Tein, "Calculation and Comparison of Propeller Unsteady Pressure Forces on Ships," *Ship Vibration Symposium*, SNAME (Oct 1978).
8. Fitzsimmons, P.A., "Cavitation Induced Hull Pressures: A Comparison of Analytical Results, Ship and Model Measurements," *RINA Symposium on Propeller Induced Ship Vibration*, London (Dec 1979).
9. Kaplan, P., J. Bentson, and J.P. Breslin, "Theoretical Analysis of Propeller Radiated Pressure and Blade Forces due to Cavitation," *RINA Symposium on Propeller Induced Ship Vibration*, London (Dec 1979).
10. Hoshino, T., "A Method to Predict Fluctuating Pressures Induced by a Cavitating Propeller," *Mitsubishi Technical Bulletin No. 150* (May 1982).
11. Kaplan, P., J. Bentson, and M. Benatar, "Analytical Prediction of Pressures and Forces on a Ship Hull Due to Cavitating Propellers," *14th CNR Symposium on Naval Hydrodynamics*, The University of Michigan (Aug 1982).
12. Breslin, J.P., et al, "Theoretical and Experimental Propeller-Induced Hull Pressures Arising from Intermittent Blade Cavitation, Loading, and Thickness," *Trans. SNAME*, Vol. 90 (1982).
13. Huse, E. and W. Guoqiang, "Cavitation-Induced Excitation Forces on the Hull," *Trans. SNAME*, Vol. 90 (1982).

14. Wilson, M.B. et al., "Causes and Corrections for Propeller-Excited Airborne Noise on a Naval Auxiliary Oiler," Trans. SNAME, Vol. 90 (1982).
15. Rothblum, R.S. and J.H. Pattison, "A New Large Cavitation Channel for Integrated Hull-Propulsor-Appendage Research Development Test and Evaluation," NAVSEA Association for Senior Engineers Conference (Mach 1983).
16. Denny, S., "Comparisons of Experimentally Determined and Theoretically Predicted Pressures in the Vicinity of a Marine Propeller," NSRDC Report 2349 (May 1967).
17. Taniguchi, K. and K. Ohtaka, "Measurements of the Propeller-Induced Vibratory Forces on a Destroyer," Journ. of Society of Naval Architects of Japan, Vol. 114, pp. 138-147 (1963).
18. Kerwin, J., S. Lewis, and S. Kobayashi, "Systematic Experiments to Determine the Influence of Skew and Rake on Hull Vibratory Excitation Due to Transient Cavitation," Ship Vibration Symposium, Arlington Va., SNAME (1978).
19. Hylarides, S, "Some Hydrodynamic Considerations of Propeller-Induced Ship Vibrations," Ship Vibration Symposium, Arlington Va, SNAME (1978).
20. Skaar, K. and A. Raestad, "The Relative Importance of Ship Vibration Excitation Forces," RINA Symposium on Propeller Induced Ship Vibration, London (Dec 1979).
21. Weitendorf, E., "Cavitation and Its Influence on Induced Hull Pressure Amplitudes," Symposium on Hydrodynamics of Ship and Offshore Propulsion Systems, Oslo Norway (Mach 1977)
22. English, J., "Cavitation Induced Hull Surface Pressures--Measurements in Water Tunnels," RINA Symposium on Propeller Induced Ship Vibration, London (Dec 1979).
23. Lewis, F.M., "Propeller Vibration," Trans SNAME, Vol. 43, pp. 252-285 (1935)
24. Lewis, F.M., "Propeller Vibration," Trans SNAME, Vol. 44, pp. 501-519 (1936).
25. Lewis, F.M. and A.J. Tachmindji, "Propeller Forces Exciting Hull Vibration," Trans. SNAME Vol. 62 (1954).
26. Lewis, F.M., "Propeller Vibration Forces in Single Screw Ships," Trans. SNAME, Vol. 77 (1969).
27. Stuntz, G.R, et al., "Series 60 - The effect of Variations in the Afterbody Shape Upon Resistance, Power, Wake Distribution, and Propeller Excited Vibratory Forces," Trans SNAME, Vol. 68 (1960).
28. Tachmindji, A.J. and M.C. Dickerson, "The Measurement of Oscillating Pressures in the Vicinity of Propellers," DTNSRDC Report No. 1130 (Apr 1957).

29. Tachmindji, A.J. and M.C. Dickerson, "The Measurement of Thrust Fluctuation and Free Space Oscillating Pressures for a Propeller," DTNSRDC Report No. 1107 (Jan 1957).
30. Pohl, K., "Die durch eine Schiffschraube auf benachbarten Platten erzeugten periodischen hydrodynamischen Drucke," (in German) Schiffstechnik Vol. 7, No. 35, pp 5-18 (1960).
31. Taniguchi, K., "On the Pressure Fluctuation in the Vicinity of Propellers," (in Japanese), Journ of Society of Naval Architects of West-Japan, No. 16 (1958).
32. Weitendorf, E-A., "Experimental Investigations of the Periodic Pressure Variations Produced by Propellers on the Outer Skin," Schiff und Hafen, Vol. 22, No. 1 pp. 11-22 (1970).
33. Nelka, J., "Experimental Evaluation of a Series of Skewed Propellers with Forward Rake: Open-Water Performance, Cavitation Performance, Field-Point Pressures, and Unsteady Propeller Loading," NSRDC Report 4113 (Jul 1974).
34. Keil, H., "Messung der vom Propeller induzierten Druckschwankungen um Forschungsschiff 'Meteor' und Vergleich mit dem Modellversuch," Vol. 59 pp. 368-377 (1965).
35. Huse, E., "The Magnitude and Distributon of Propeller-Induced Surface Forces on a Single-Screw Ship Model," Norwegian Ship Model Experimental Tank Publication No. 100 (Dec 1968)
36. Jacob, W.R., J. Mercier, and S. Tsakonas, "Theory and Measurements of the Propeller-Induced Vibratory Pressure Field," Journal of Ship Research, Vol. 16, No. 2 (1972).
37. Takahashi, H. and T. Ueda, "An Experimental Investigation into the Effect of Cavitation on Fluctuating Pressures Around a Marine Propeller," Proceedings 12th I.T.T.C., Rome (1969).
38. Weitendorf, E-A., "Vergleich von propellererregten Druckschwankungen fur Modell and Grossausfuhrung am Beispiel des Frachtschiffes MS 'Hornmeer'," Schiff und Hafen, Vol. 25, Part 5, pp. 423-428 (May 1973).
39. Weitendorf, E-A., "Experimentalle Untersuchungen der durch kavitierende Propeller erzeugten Druckschwankungen," (Experimental investigations on the pressure fluctuations caused by cavitating propeller), Schiff und Hafen, Vol. 25, Part 11 (Nov 1973).
40. Takahashi, H., "A Consideration on the Effect of the Propeller Cavitation upon the Surface Force," (in Japanese), Trans. of West-Japan Society of Naval Architects, No. 49 (1975).
41. Chiba, N, and T. Hoshino, "Effect of Unsteady Cavity on Propeller-Induced Hydrodynamic Pressure," Journal of Society of Naval Architects of Japan, Vol. 139 (1976).

42. Sasajima, T., "Application of Noise Measurements for Studying Unsteady Cavitation in Cavitation Tunnel," Proc. ASME Symposium on Cavitation Noise, Phoenix (1982).
43. Takekuma, K., "Effect of Air Bubbles Entrained from Bow on Propeller-Induced Pressure fluctuation," Mitsubishi Technical Bulletin No. 140 (June 1980); (see also RINA Symposium on Propeller Induced Ship Vibration, London 1979).
44. Nelka, J.J., "Induced Field-Point Pressures of a Ducted Propeller System," Naval Ship Research and Development Center Report 4270 (Oct 1974)
45. Peck, J.G., "Tunnel Hull Cavitation and Propeller Induced Pressure Investigation," Naval Ship Research and Development Center Departmental Report SPD-597-01 (Nov 1974).
46. van Manen, J.D., "The Effect of Cavitation on the Interaction Between Propeller and Ship's Hull," International Shipbuilding Progress, Vol. 19, No. 209 (Jan 1972).
47. Huse, E., "Trykkimpulser fra kaviterende propell," paper presented at Nordisk Skipsteknisk Mote, Åbo Finland (1971)
48. van Cossanen, P. and J. van der Kooij, "Vibratory Hull Forces Induced by Cavitating Propellers," Trans. RINA (1973)
49. van der Kooij, J. and A. Jonk, "Propeller-Induced Hydrodynamic Hull Forces on a Great Lakes Bulk Carrier. Results of Model Tests and Full Scale Measurements," Symposium on High Powered Propulsion of Large Ships, NSMB Publication No. 490, Part 2 (Dec 1974).
50. Hylarides, S., "Some Hydrodynamic Considerations of Propeller-Induced Ship Vibrations," Ship Vibration Symposium, SNAME (Oct 1978).
51. Glover, E.J., J.F. Thorn, and L. Hawdon, "Propeller Design or Minimum Hull Excitation," The Naval Architect, pp. 267-275 (Nov 1979).
52. Glover, E.J. and G. Patience, "Aspects of the Design and Application of Off-Loaded Tip Propellers," RINA Symposium on Propeller Induced Ship Vibration, London (Dec 1979).
53. Lover, E.P. and C.B. Wills, "Cavitation Tunnel Testing for the Royal Navy," Stone Manganese Marine/Newcastle University Conference (1979).
54. Chiba, N., T. Sasajima, and T. Hoshino, "Prediction of Propeller-Induced Fluctuating Pressures and Correlation with Full Scale Data," 13th Symposium on Naval Hydrodynamics, Tokyo (Oct 1980).
55. Reed, F.E., N.L. Bassett, and J.A. Norton, "Effects of Hull and Propeller Design Changes on the Vibration of a Lakes Freighter," Trans. SNAME, Vol. 89 (1981).

56. Lovik, A., "Scaling of Propeller Cavitation Noise," Paper D in Noise Sources in Ships I: Propellers, Edited by A. Nilsson and N. Tyvland, Nordforsk (1981).
57. Munk, T., J. Romeling, S. Spangenberg, and C. Aage, "Noise and Pressure Impulses form Cavitating Propellers. A comparative Study on Two Ships in Full Scale and Model Scale," Danish Ship Research Laboratory, Bulletin No. 47 (April 1982).
58. Hadler, J.B., J.W. English, and S.K. Gupta, "Program to Minimize Propeller-Induced Vibration on Converted Maersk 'E' Class Ships, " Trans. SNAME, Vol. 92 (1984).
59. English, J. "Cavitation Induced Hull Surface Pressures--- Measurements in a Water Tunnel, "RINA Symposium on Propeller Induced Ship Vibration, London (Dec 1979).
60. Larsen, A., "Prediction of Propeller Induced Hull Pressures by Means of a Medium-Size Cavitation Tunnel," Danish Ship Research Laboratory Report (April 1982).
61. van der Kooij, J., "Experimental Determination of Propeller-Induced Hydrodynamic Hull Forces in the NSMB Depressurized Towing Tank," RINA Syposium on Propeller Induced Ship Vibration, London (Dec 1979).
62. Lindgren, H. and E. Bjärne, "Ten Years of Research in the SSPA Large Cavitation Tunnel," Stone Manganese Marine/Newcastle University Conference (1979); also SSPA Publication No. 86 (1980).
63. Dyne, G. and M. Hoekstra, "Propulsion, Cavitation and Propeller-induced Pressure Fluctuations of a Tanker," SNAME Spring Meeting Transactions (June 1976).,
64. Steenhoek, H.F. and T. Ten Wolde, "The Reciprocal Measurement of Mechanical-Acoustical Transfer Functions," ACUSTICA, Vol. 23, No. 5, pp. 301-305 (Nov 1970).
65. Ten Wolde, T. and A. de Bruijn, " A New Method for Measurement of the Acoustical Source Strength of Cavitating Ship Propellers," International Shipbuilding Progress, Vol. 22, No. 25 (Nov 1975).
66. Gray, L.M., "Investigation into Modelling and Measurement of Propeller Cavitation Source Strength at Blade Rate on Merchant Ships," SNAME Propellers'81 Symposium Virginia Beach (May 1981).
67. Whalen, M., R.J. Van Houten, and J.E. Kerwin, "A Calibration Procedure to Enable the Derivation of Propeller Cavity Volume from Water Tunnel Measurements," Draft of M.I.T. Ocean Engineering Report to SNAME Purchase Order 6317 (May 1982).
68. Whalen, M., J.E. Kerwin, and R.J. Van Houten, "Experimental Determination of the Influence of Tip Clearance on Unsteady Propeller Cavitation," M.I.T. Department of Ocean Engineering Report 82-6 (May 1982).

69. Vorus, W.S., "An Analysis of the Vibratory Excitation of a Naval Ship with Variation of Blade Tip to Hull Clearance," Vorus and Associates Inc. Report No. 84-004 (Sept 1984).
70. des Moutis, E., "Reciprocity Measurements of Dynamic Source Characteristics of Cavitating Propellers Including the Effect of Air Content," M.I.T. Report No. 87620-1 (July 1981).
71. Valentine, D.T. and A. Chase, "Highly Skewed Propeller Design for a Naval Auxiliary Oiler (AO 177)," DTNSRDC Departmental Report SPD-544-12 (Sept 1976).
72. Hendrican, A. and K. Remmers, "Powering and Cavitation Performance for a Naval Fleet Oiler, AO-177 Class (Model 5326 and Propeller 4677)," DTNSRDC Departmental Report SPD-544-14 (Jan 1976).
73. Hampton, G., "Analysis of Wake Survey for Tunnel-Fin and Accelerating Fin Configurations for the Naval Auxiliary Oiler (AO 177) Represented by Model 5326-1," DTNSRDC Departmental Report SPD-0544-18 (April 1981).
74. Wilson, M.B. and G.A. Hampton, "Measurements of the Effect of Trim on the Nominal Wake of the Naval Auxiliary Oiler AO-177," DTNSRDC SPD-0544-19 (March 1981).
75. Odabasi, A.Y. and P.A. Fitzsimmons, "Alternate Methods for Wake Quality Assessment," International Shipbuilding Progress, Vol. 25, No. 282 (Feb 1978).
76. Bjärne, E., "US Navy Oiler AO 177 Class-Model Tests in SSPA Cavitation Tunnel No. 2," Swedish Maritime Research Centre (SSPA) Report No. 2564-1 (Nov 1980).
77. Chertock, G., "General Reciprocity Relation," Journal of Acoustical Society of America, Vol. 34, p. 989 (1962).
78. Lee, C-S., "Prediction of the Transient Cavitation on Marine Propellers by Numerical Lifting Surface Theory," Thirteenth Symposium on Naval Hydrodynamics, Tokyo (Oct 1980).
79. Kerwin, J., S. Kinnas, M.B. Wilson, and J. McHugh, "Experimental and Analytical Techniques for the Study of Unsteady Propeller Sheet Cavitation," Sixteenth Symposium on Naval Hydrodynamics, Berkeley (July 1986).

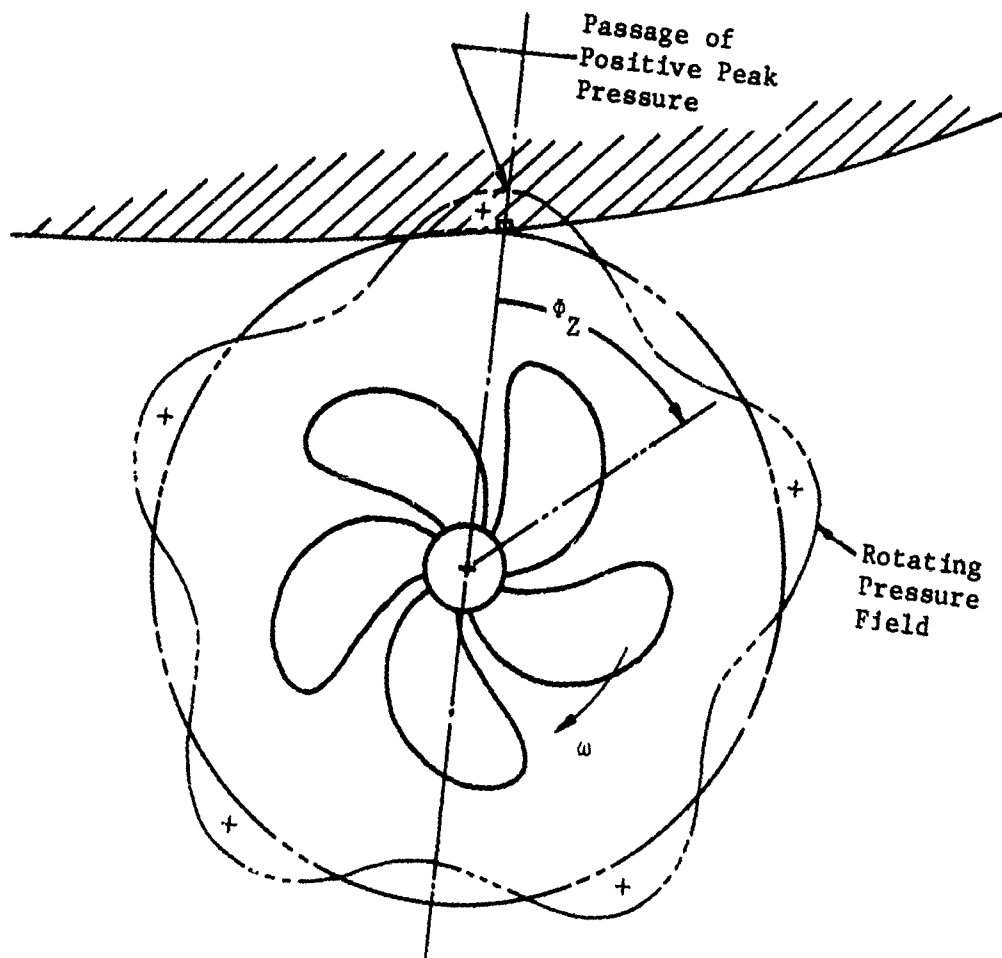


Figure 1 - Definition Sketch of Rotating Pressure Field Near an Operating Propeller

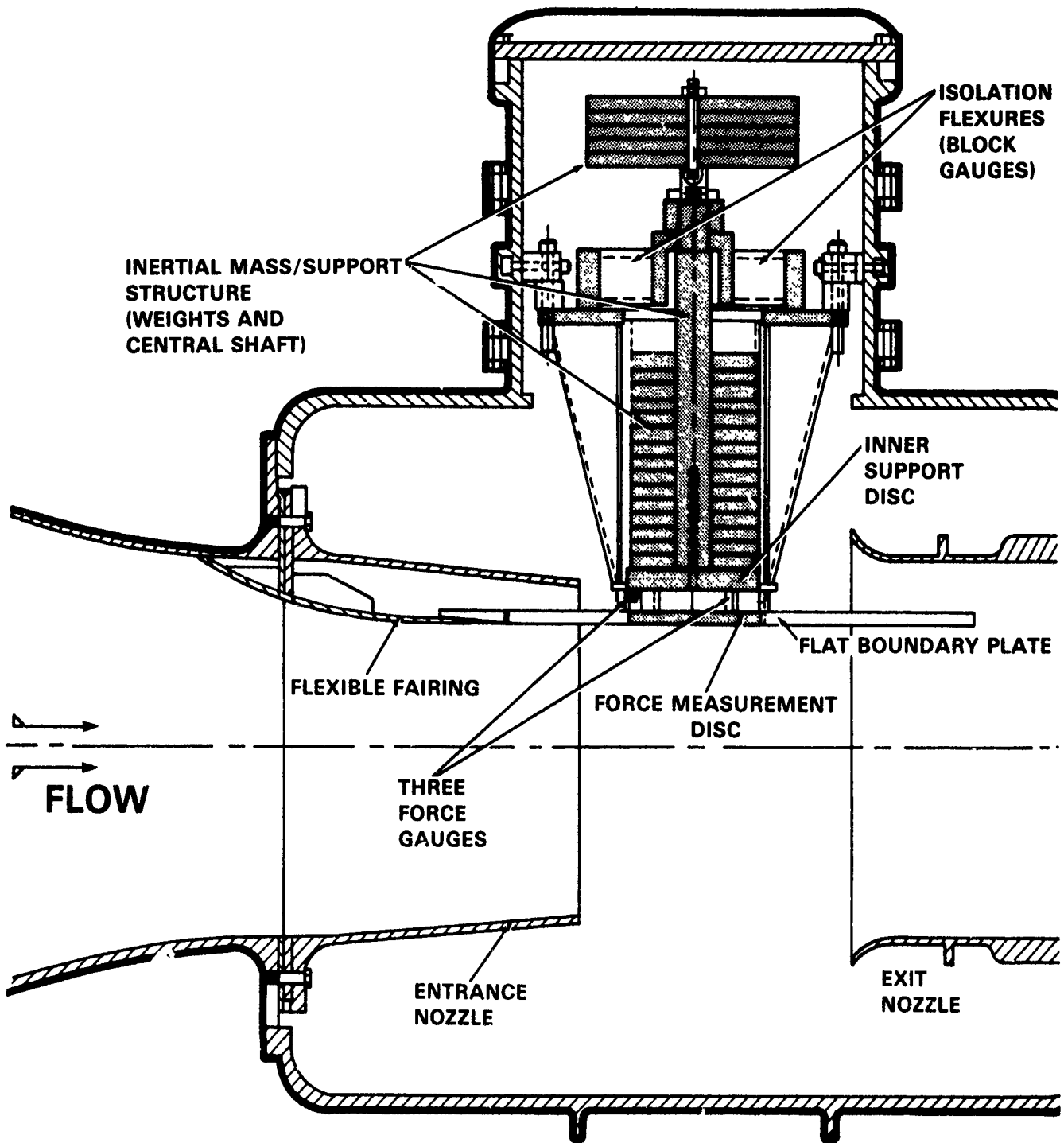


Figure 2 - Schematic of Force Measuring Device Installed in the 24-Inch Water Tunnel Open Jet Test Section

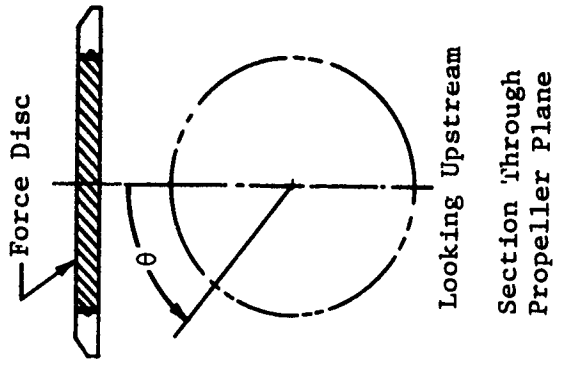
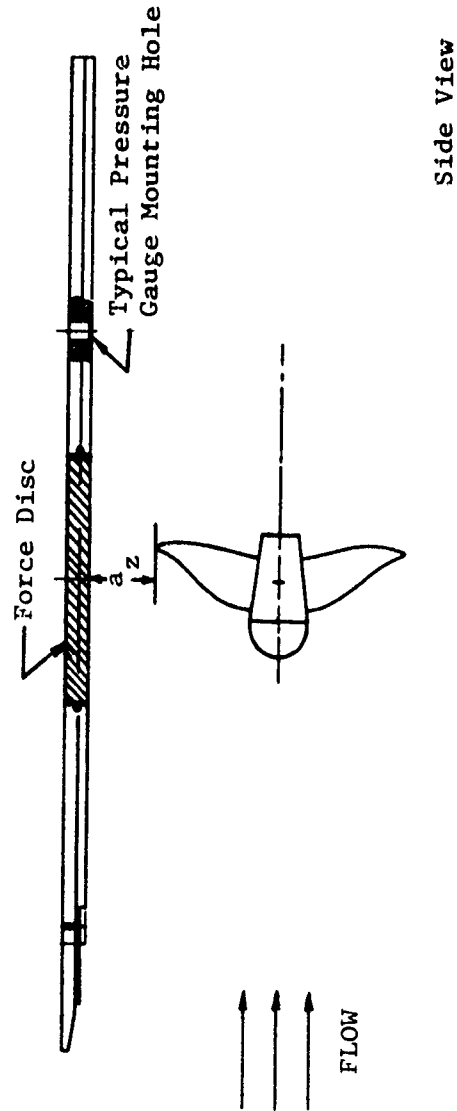
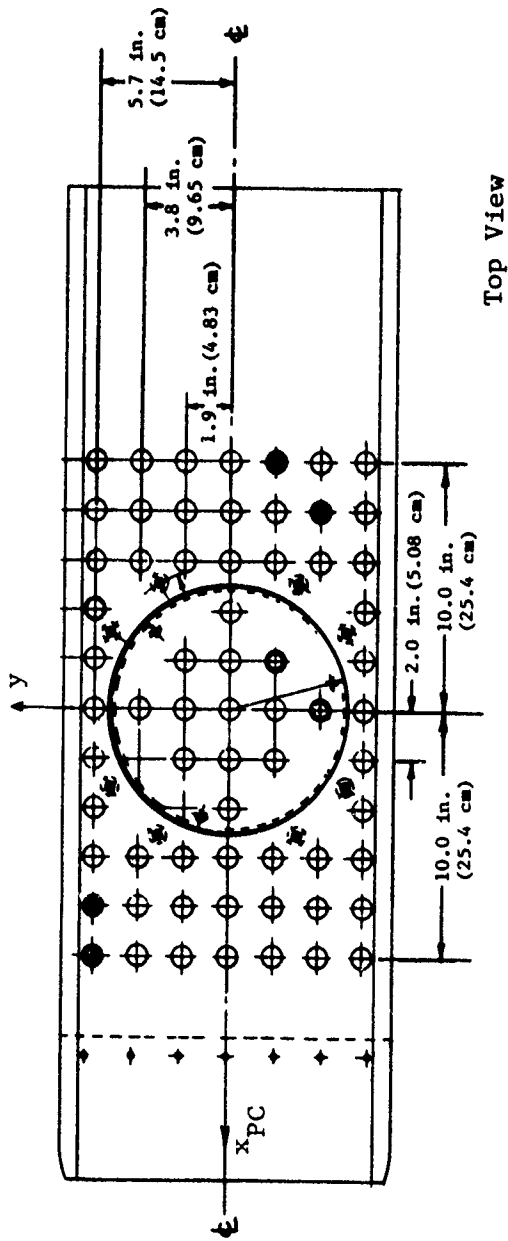


Figure 3 - Flat Plate Boundary, Force Disc, and Pressure Gauge Locations

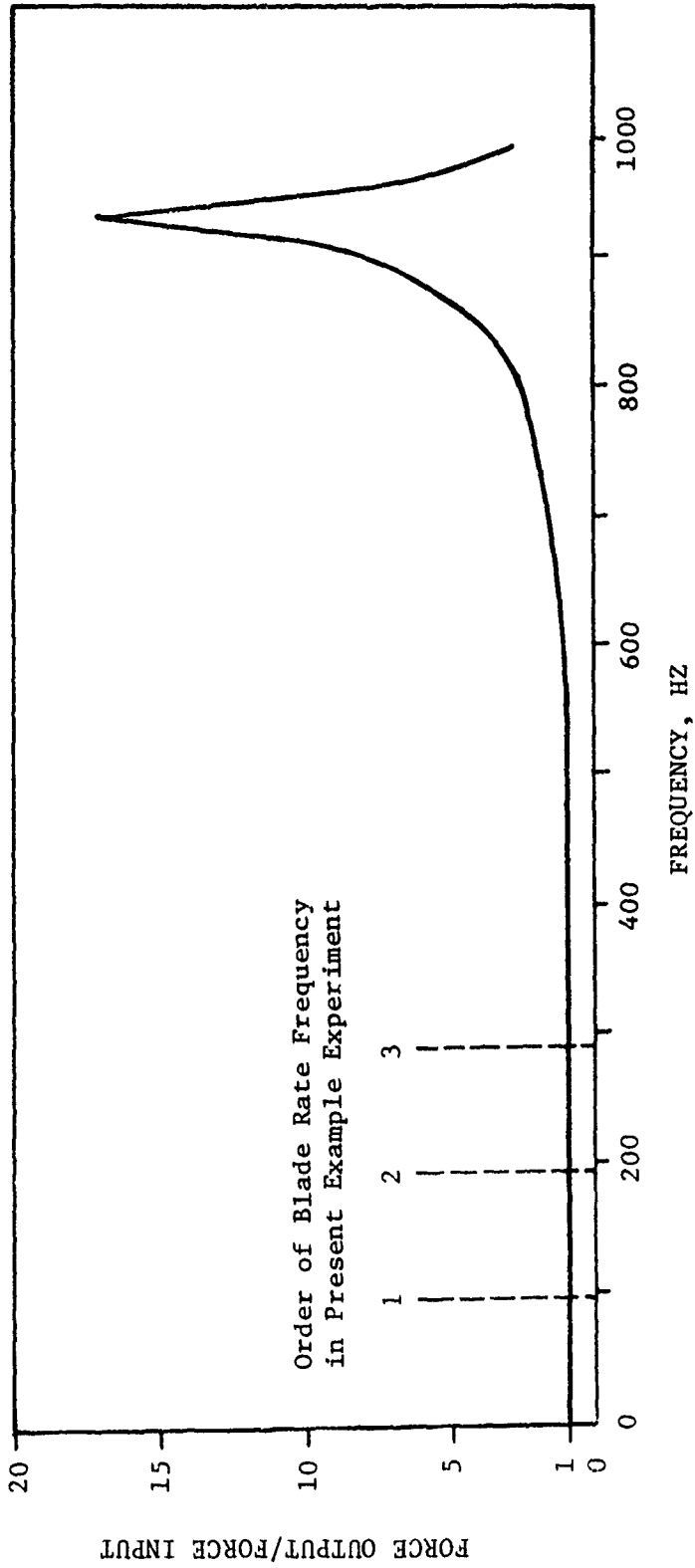


Figure 4 - Calibrated Dynamic Response Curve for Force Measuring Device

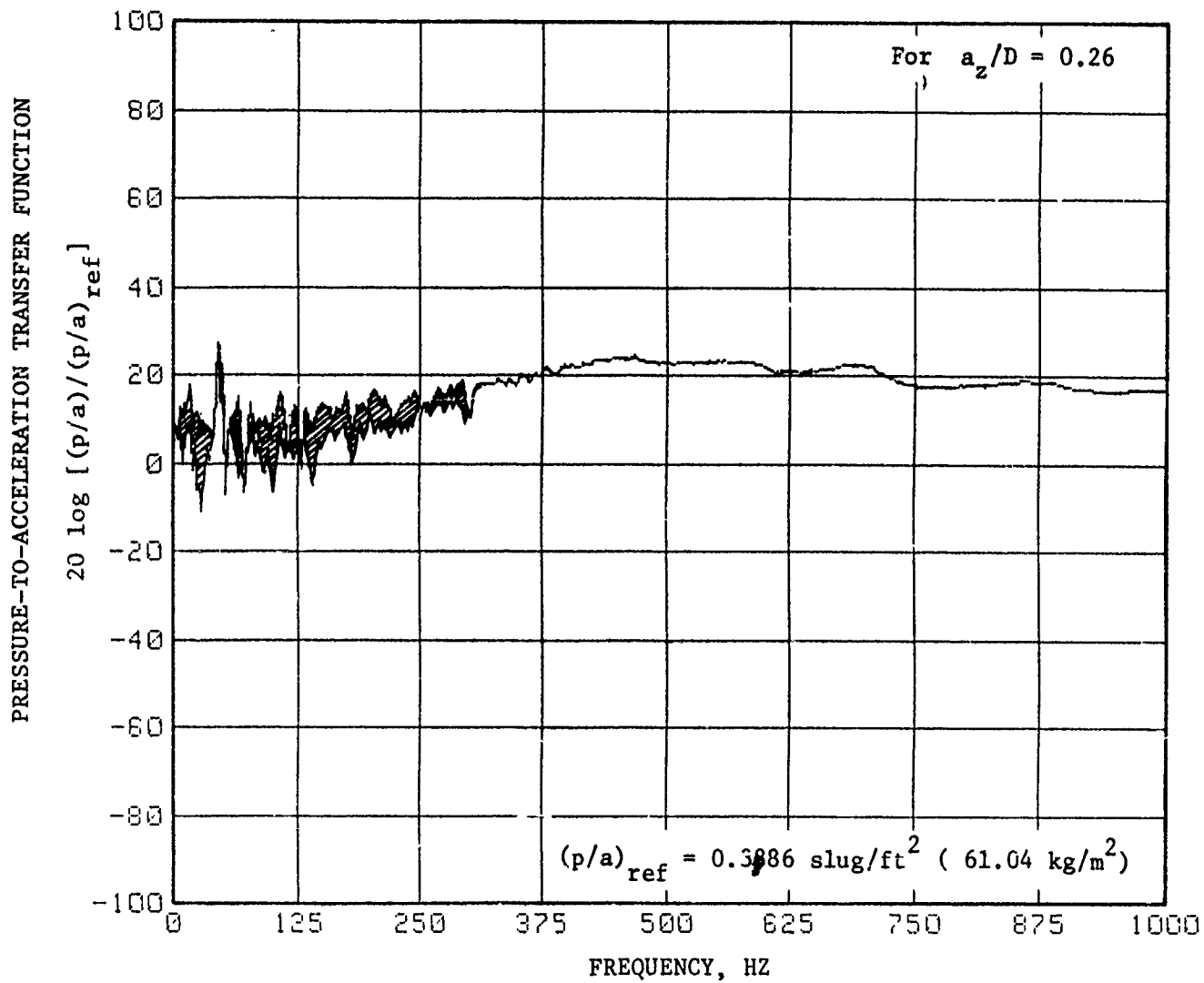


Figure 5 - Reciprocity Calibration for the Driven Force Disc:
 Pressure-to-Acceleration Transfer Function versus Frequency

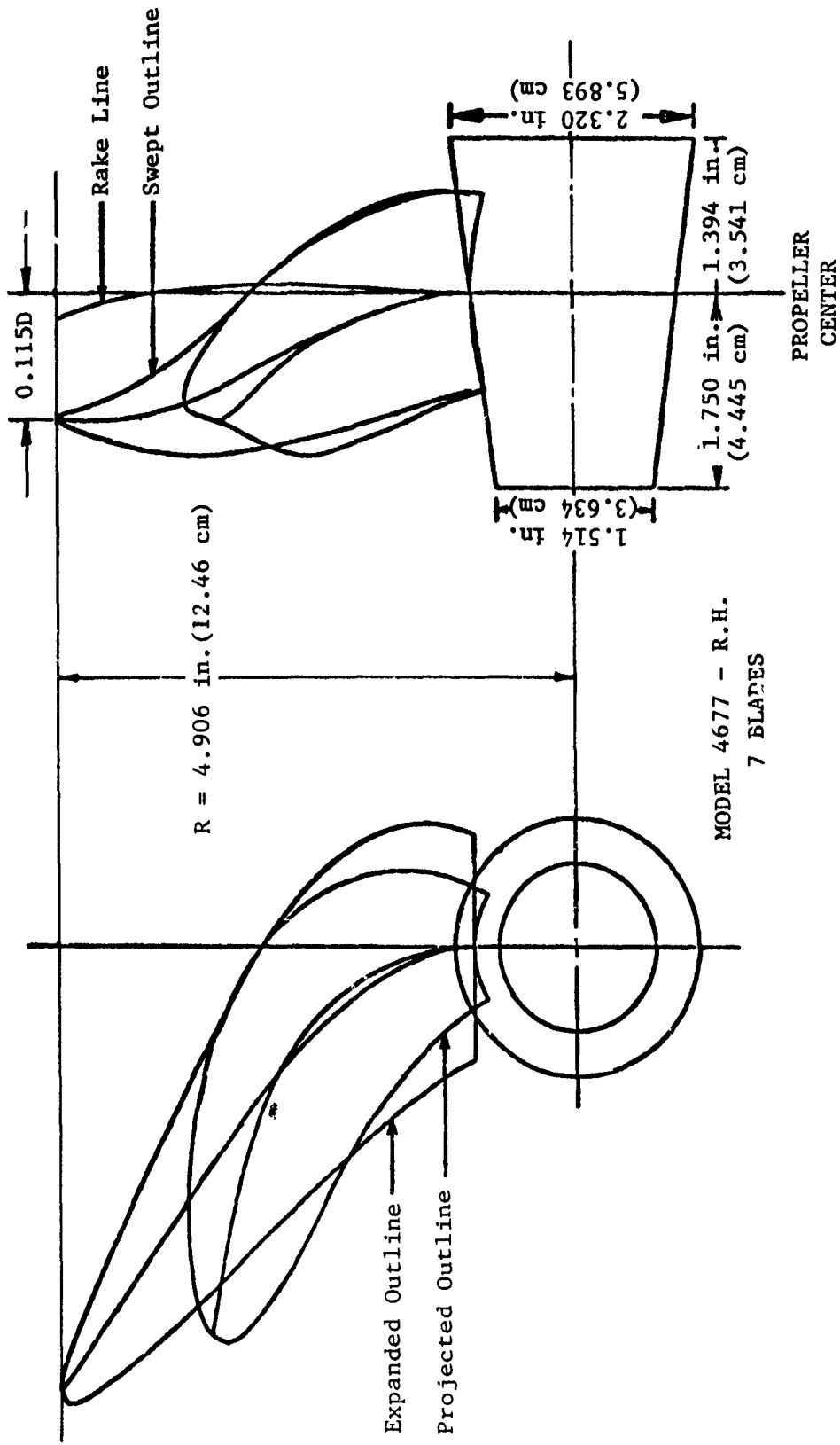


Figure 6 - Drawings of Propeller Model 4677

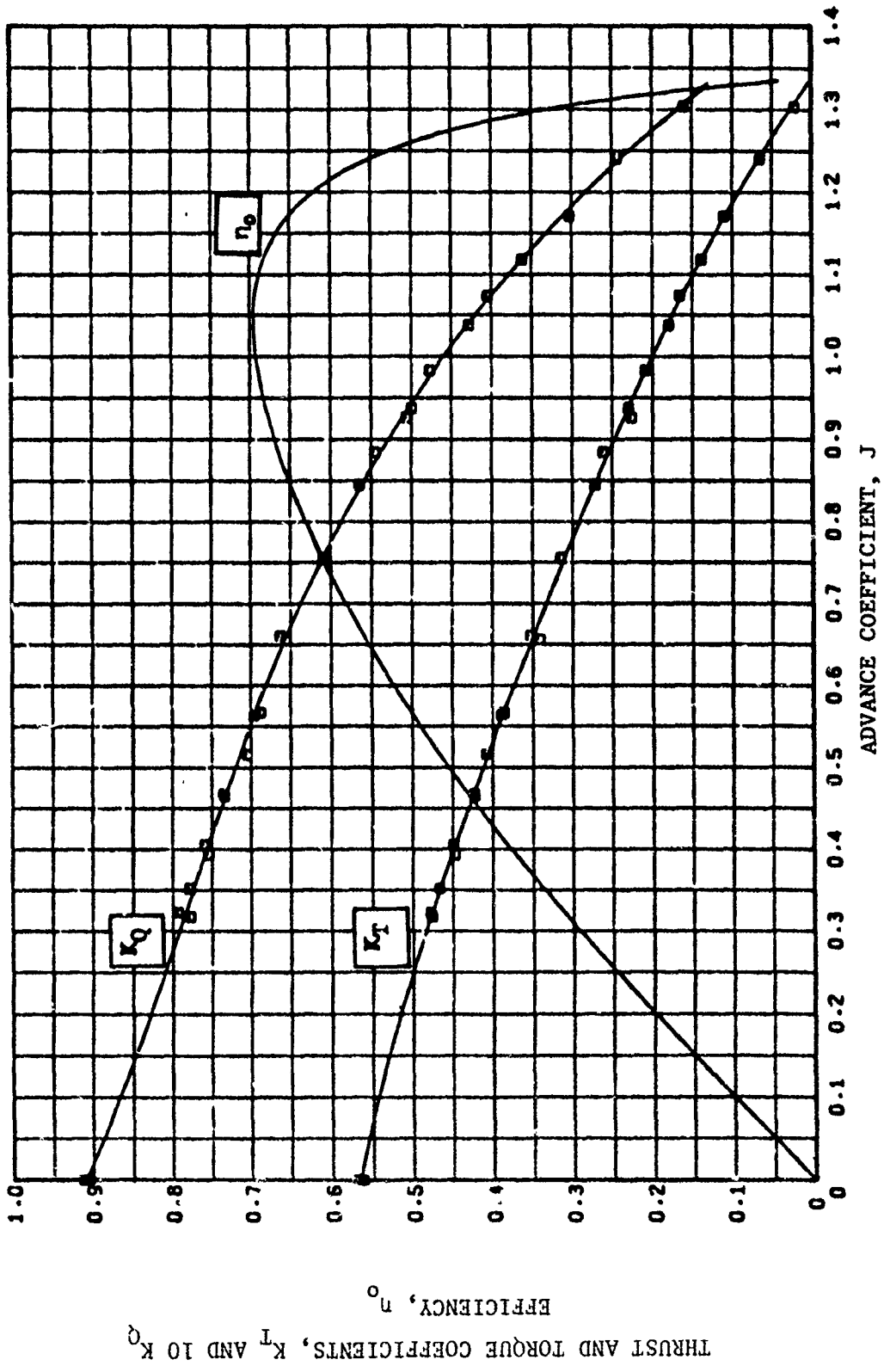


Figure 7 - Open Water Characteristics of Propeller Model 4677

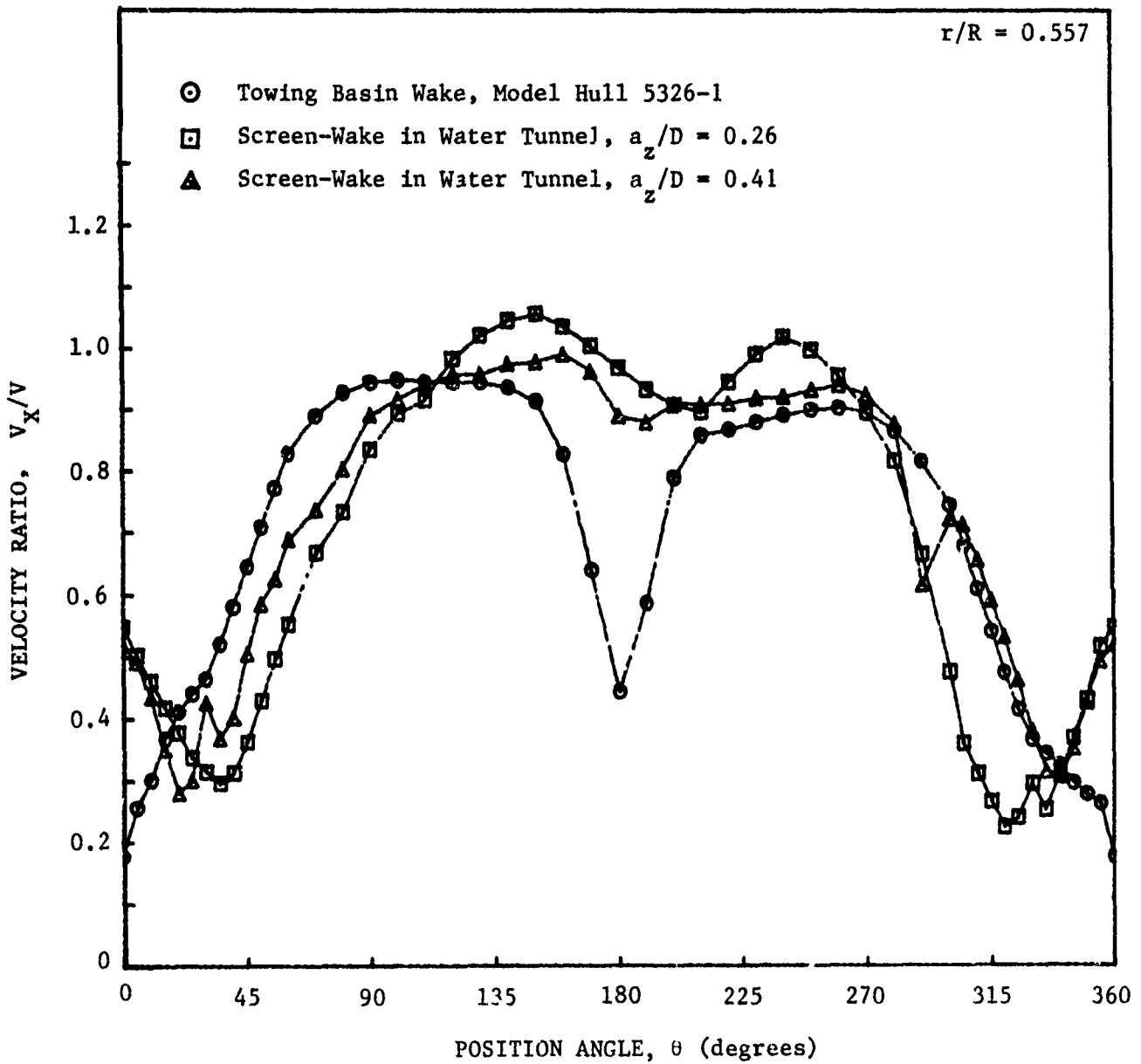


Figure 8 - Circumferential Distribution of Axial Wake Velocity Ratio, Comparison of Measurements in Water Tunnel and Towing Basin at $r/R = 0.557$

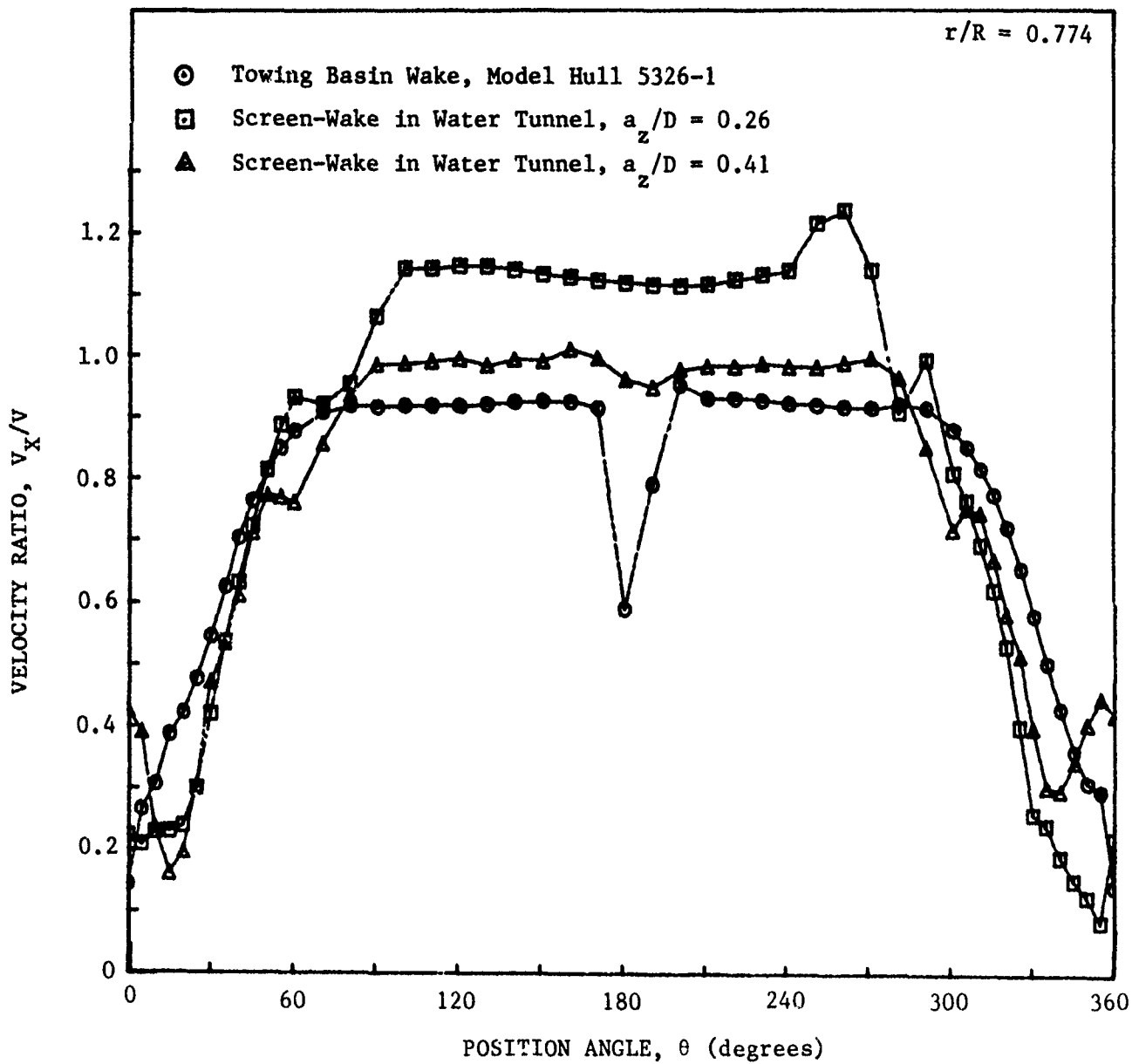


Figure 9 - Circumferential Distribution of Axial Wake Velocity Ratio, Comparison of Measurements in Water Tunnel and Towing Basin at $r/R = 0.774$

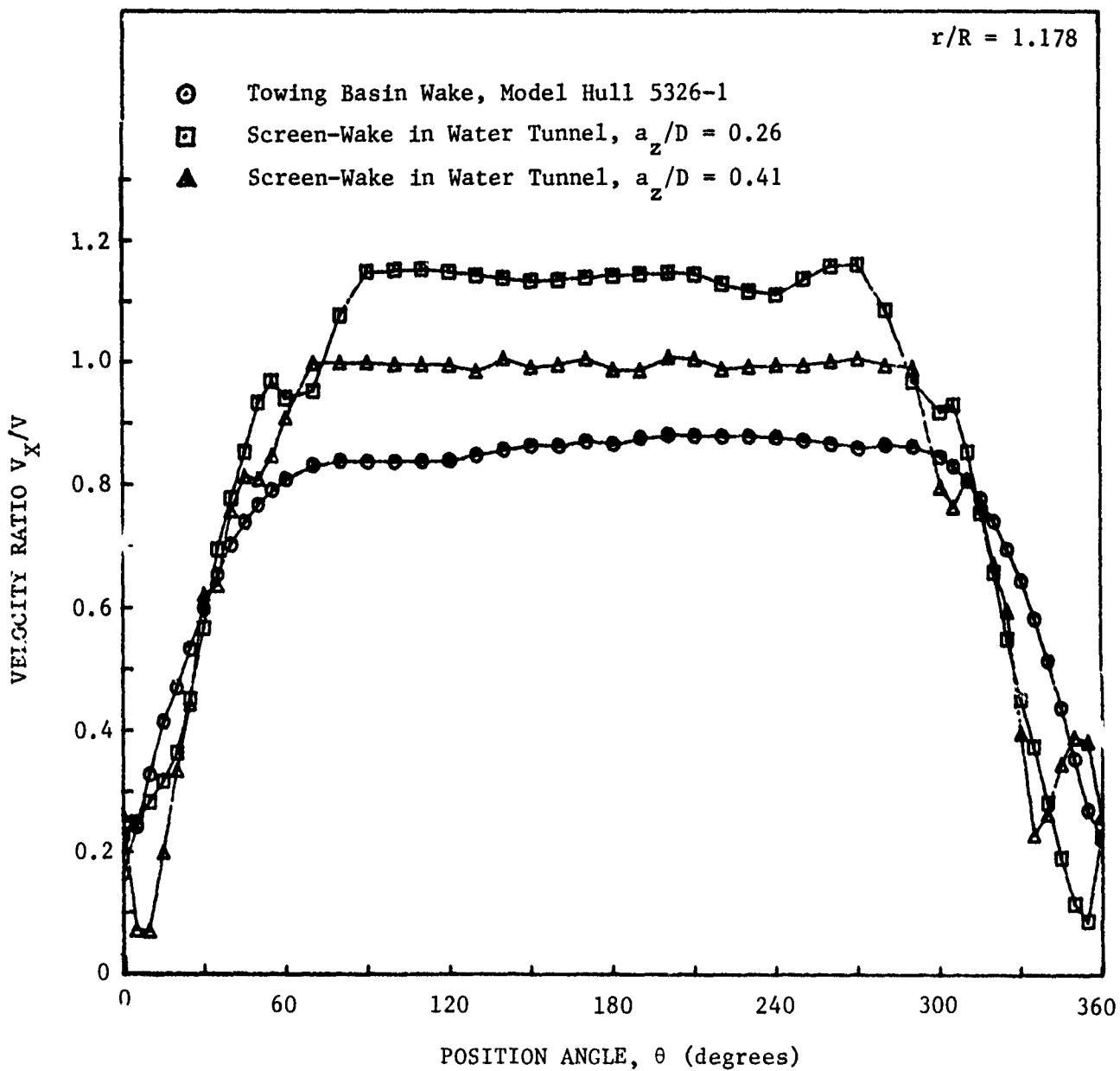


Figure 10 - Circumferential Distribution of Axial Wake Velocity Ratio, Comparison of Measurements in Water Tunnel and Towing Basin at $r/R = 1.178$

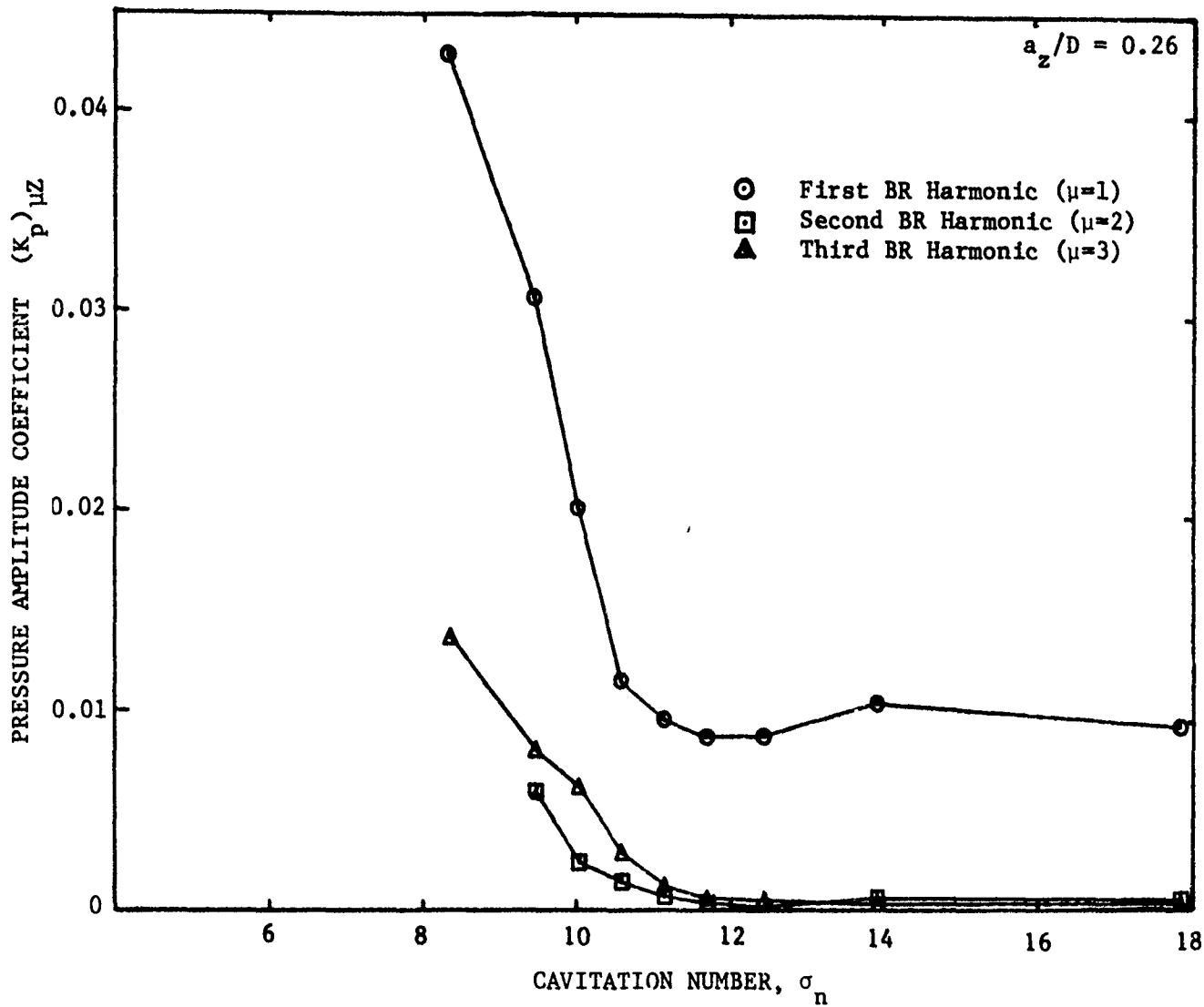


Figure 11 - Three Blade Rate Harmonics of Measured Pressure Amplitude Coefficients Taken at the Disc Center with $a_z/D = 0.26$

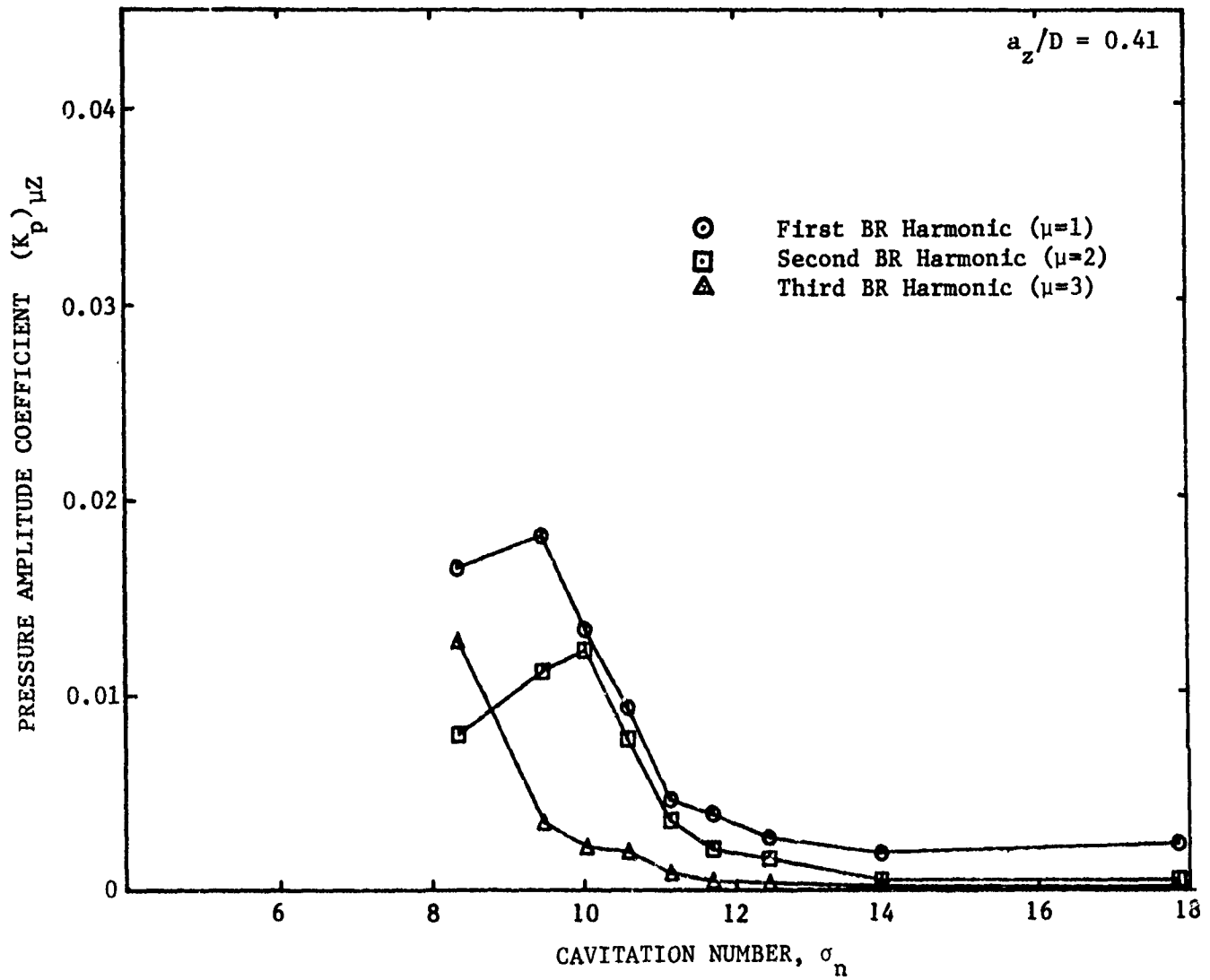


Figure 12 - Three Blade Rate Harmonics of Measured Pressure Amplitude Coefficients Taken at the Disc Center with $a_z/D = 0.41$

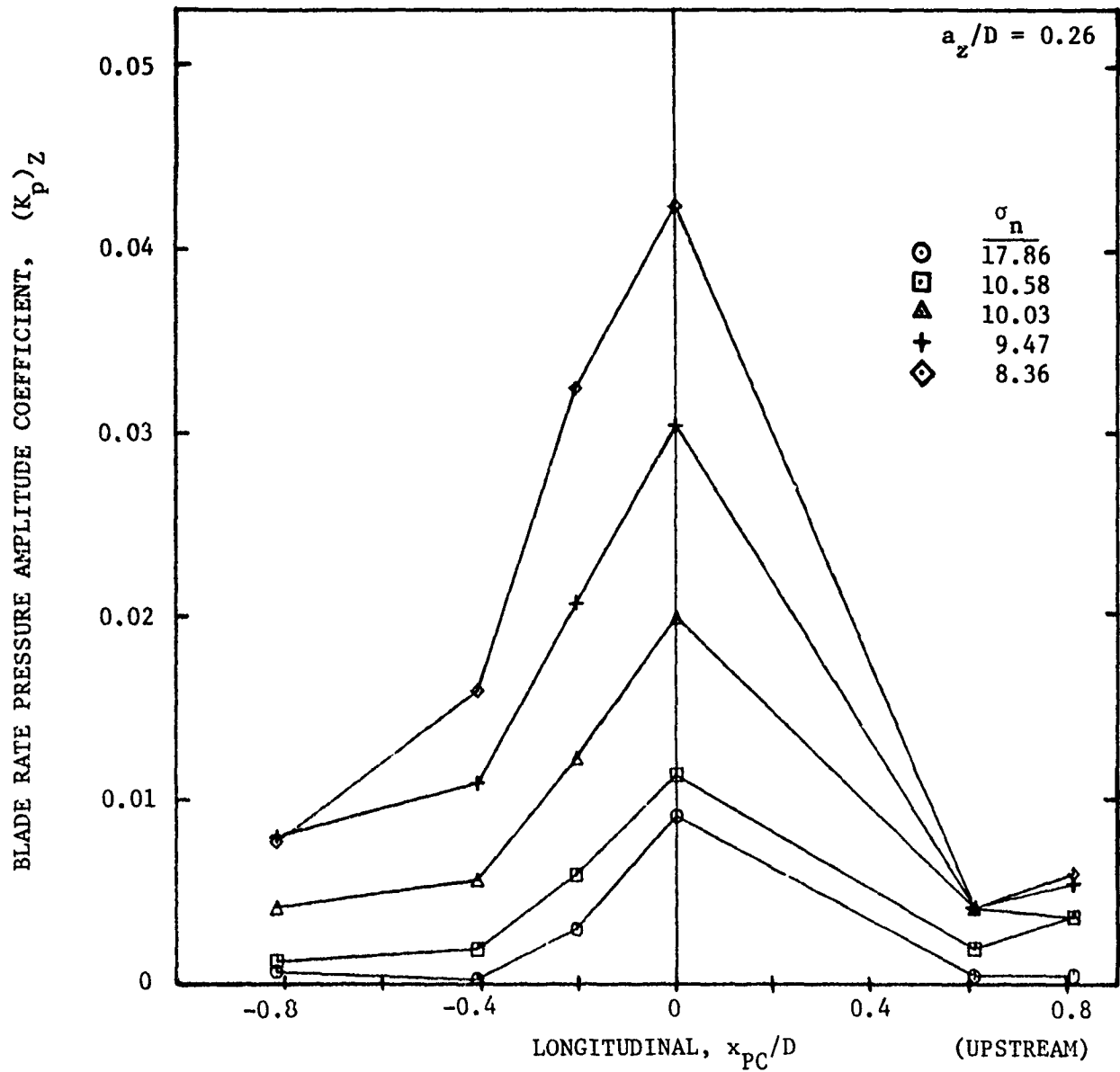


Figure 13 - Blade Rate Harmonic of Measured Pressure Amplitude Coefficient versus Longitudinal Position for Five Cavitation Numbers, with $a_z/D = 0.26$

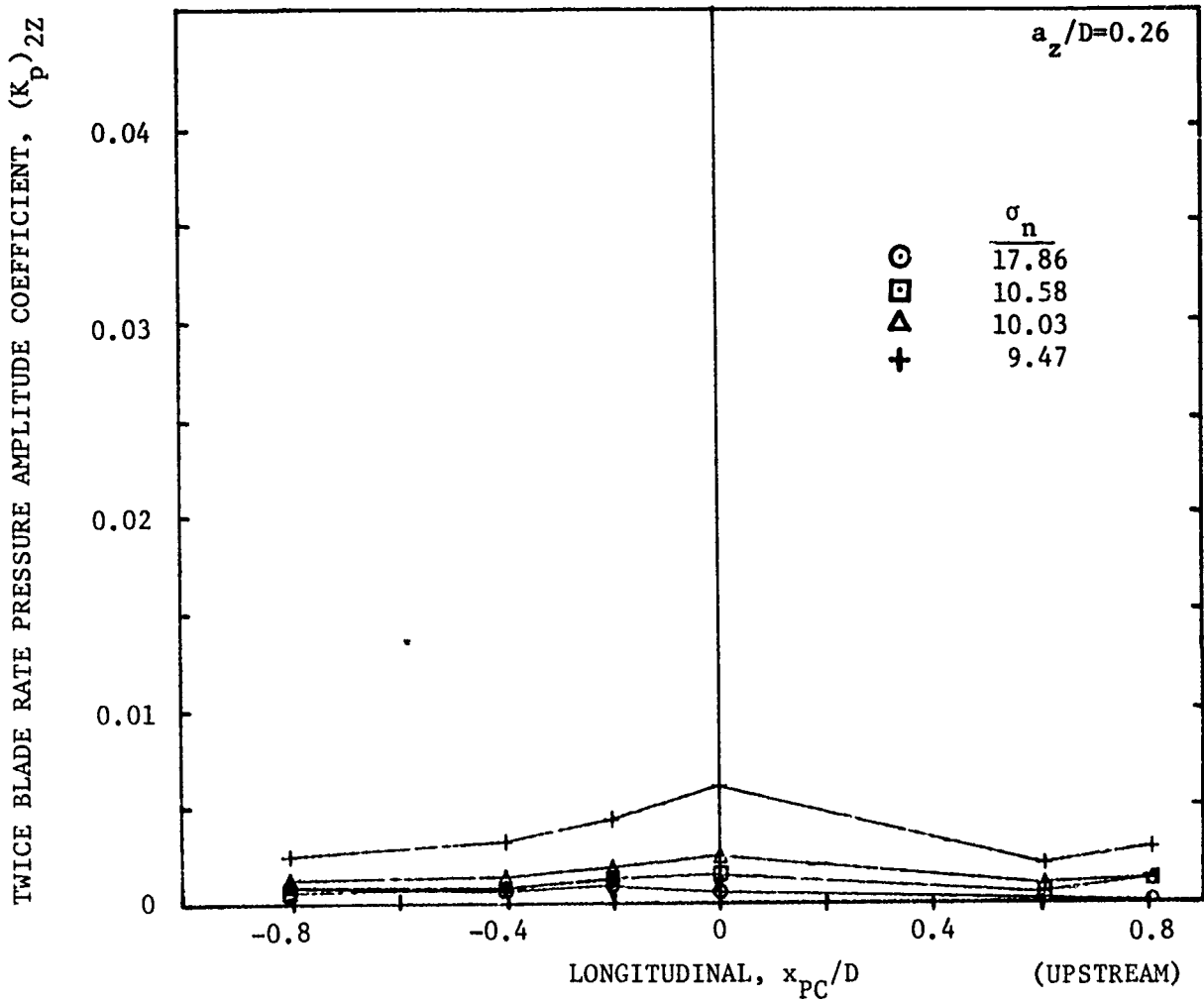


Figure 14 - Twice Blade Rate Harmonic of Measured Pressure Amplitude Coefficient versus Longitudinal Position for Several Cavitation Numbers, with $a_z/D = 0.26$

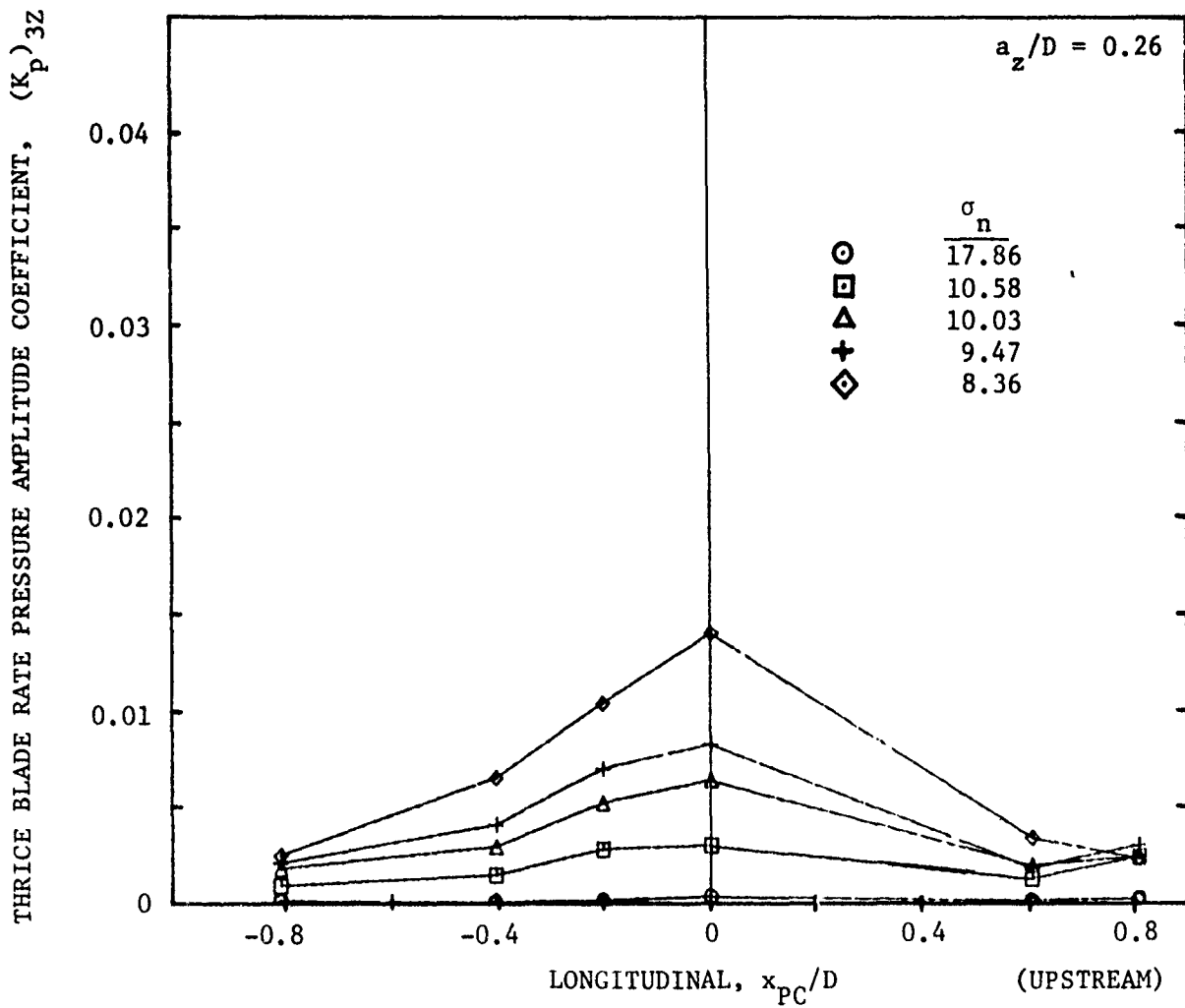


Figure 15 - Thrice Blade Rate Harmonic of Measured Pressure Amplitude Coefficient versus Longitudinal Position for Five Cavitation numbers, with $a_z/D = 0.26$

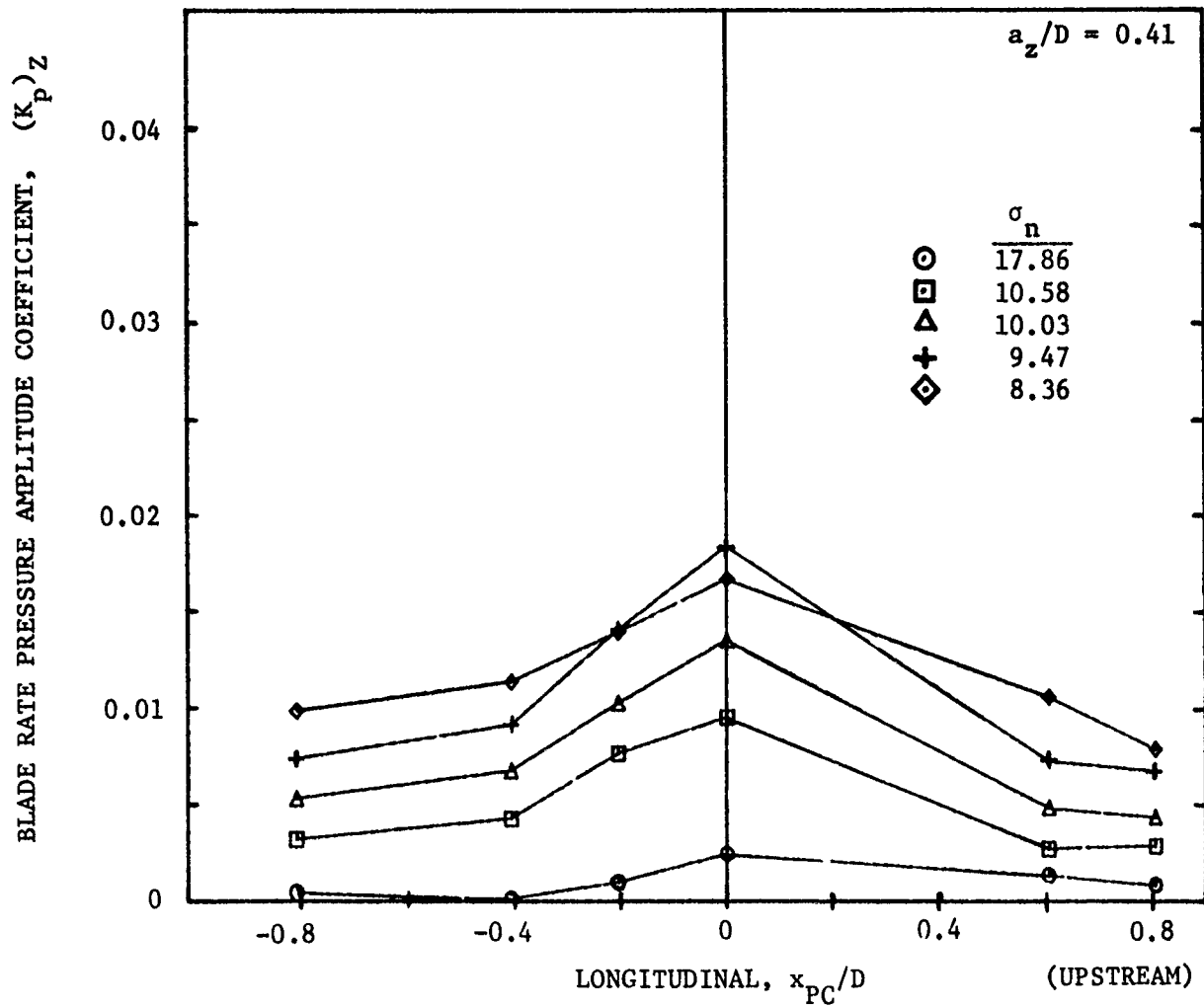


Figure 16 - Blade Rate Harmonic of Measured Pressure Amplitude Coefficient versus Longitudinal Position for Five Cavitation Numbers, with $a_z/D = 0.41$

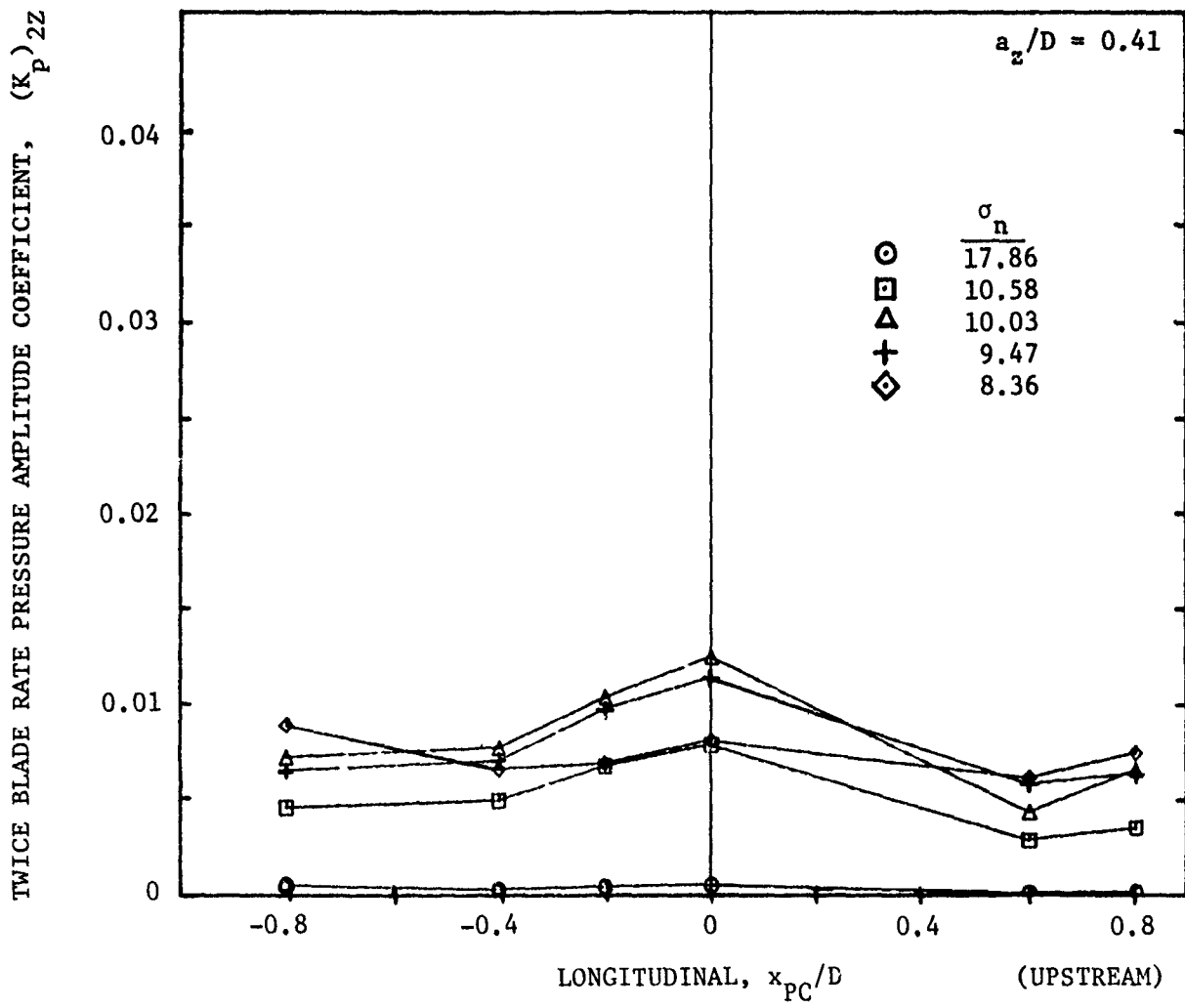


Figure 17 - Twice Blade Rate Harmonic of Measured Pressure Amplitude Coefficient versus Longitudinal Position for Five Cavitation Numbers, with $a_z/D = 0.41$

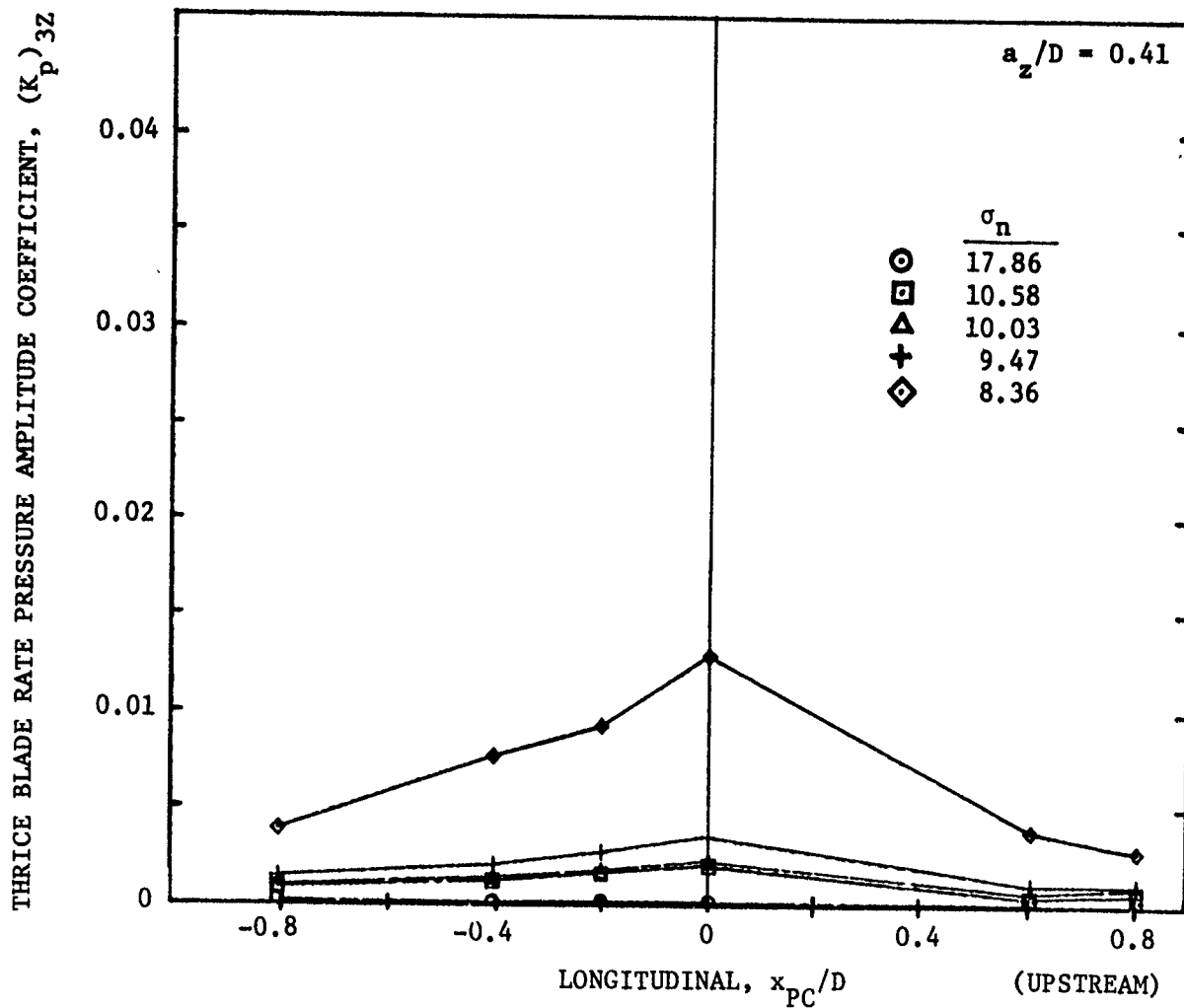


Figure 18 - Thrice Blade Rate Harmonic of Measured Pressure Amplitude Coefficient versus Longitudinal Position for Five Cavitation Numbers, with $a_z/D = 0.41$

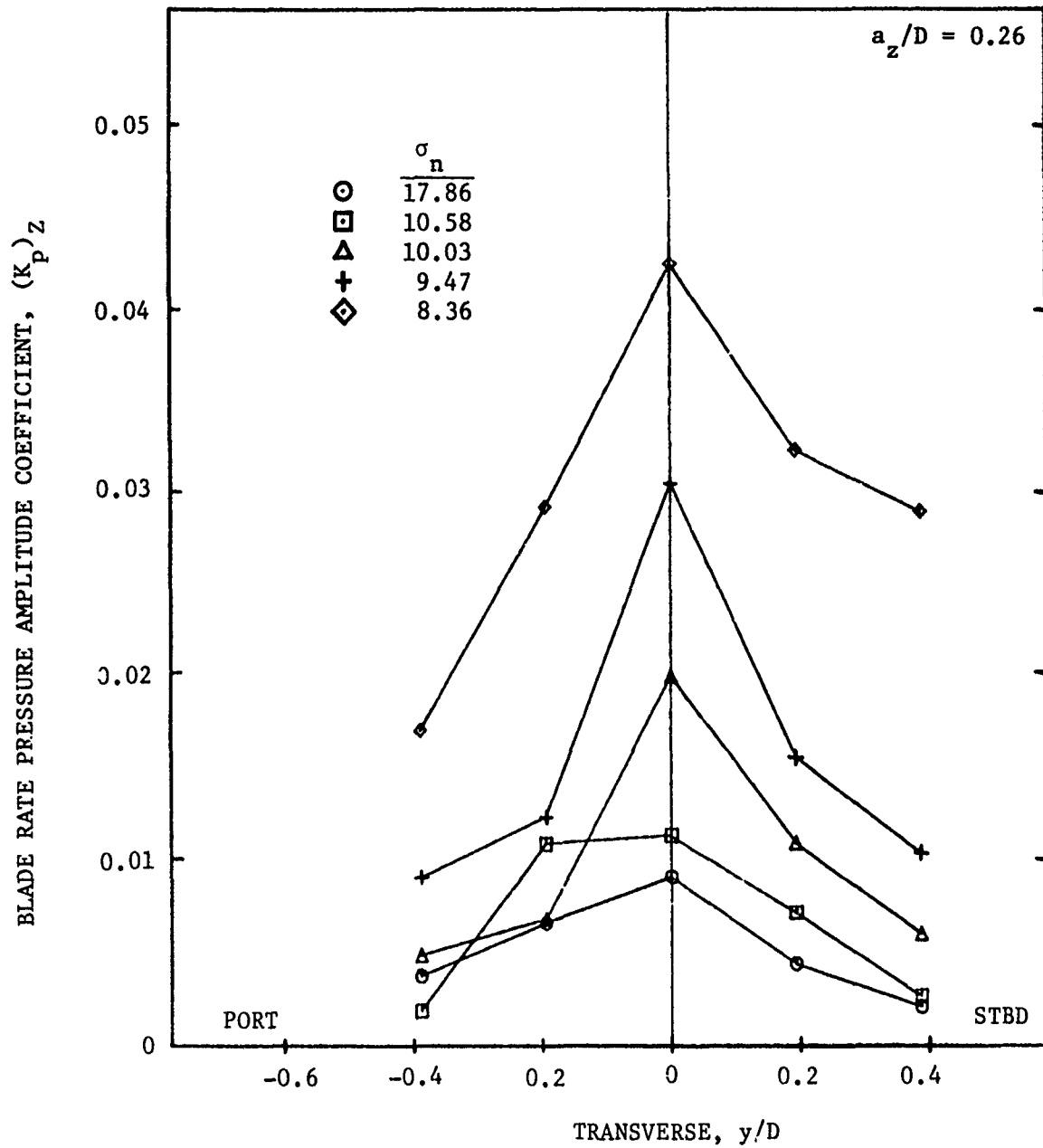


Figure 19 - Blade Rate Harmonic of Measured Pressure Amplitude Coefficient versus Transverse Position for Five Cavitation Numbers, with $a_z/D = 0.26$

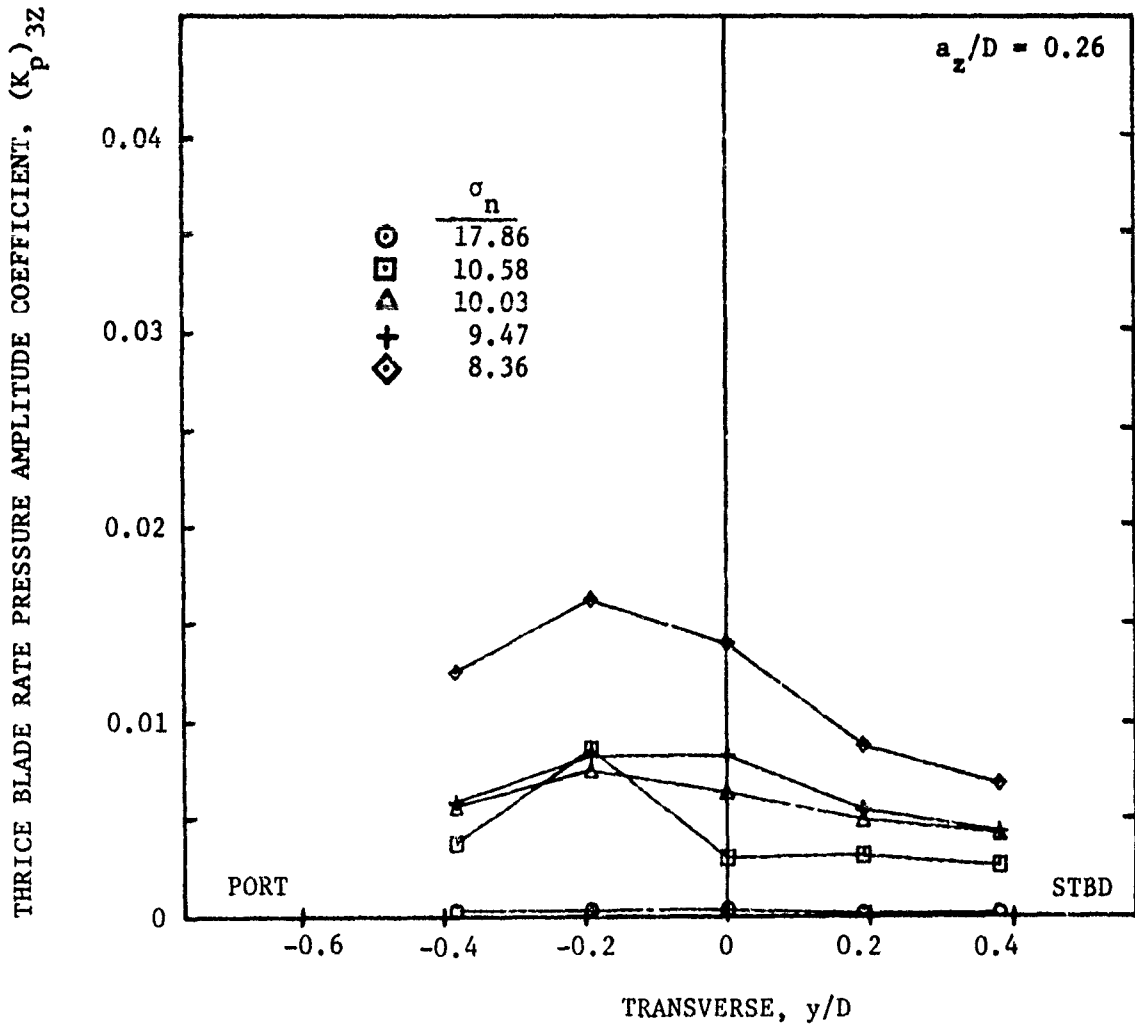


Figure 21 - Thrice Blade Rate Harmonic of Measured Pressure Amplitude Coefficient versus Transverse Position for Five Cavitation Numbers, with $a_z/D = 0.26$

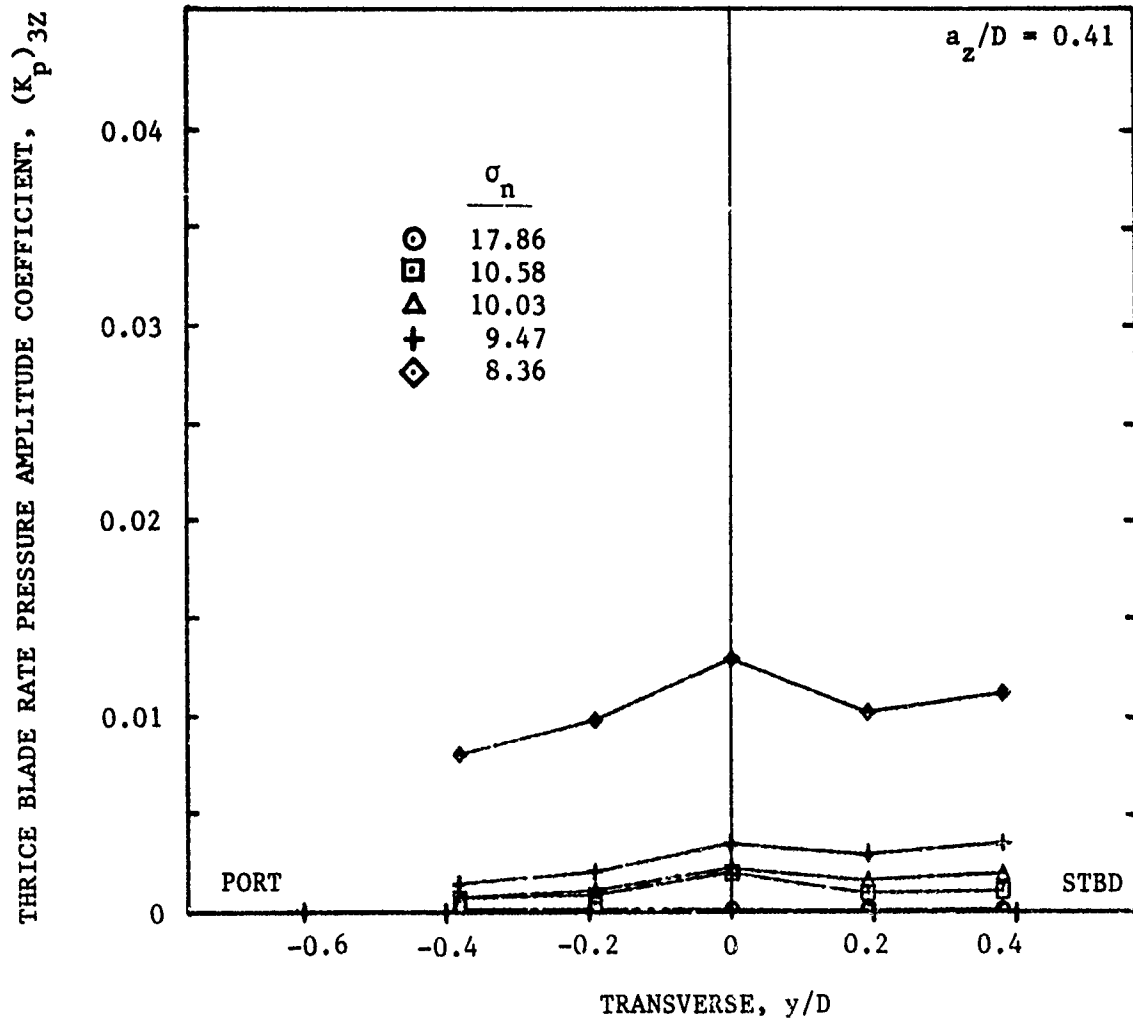


Figure 24 - Thrice Blade Rate Harmonic of Measured Pressure Amplitude Coefficient versus Transverse Position for Five Cavitation Numbers, with $a_z/D = 0.41$

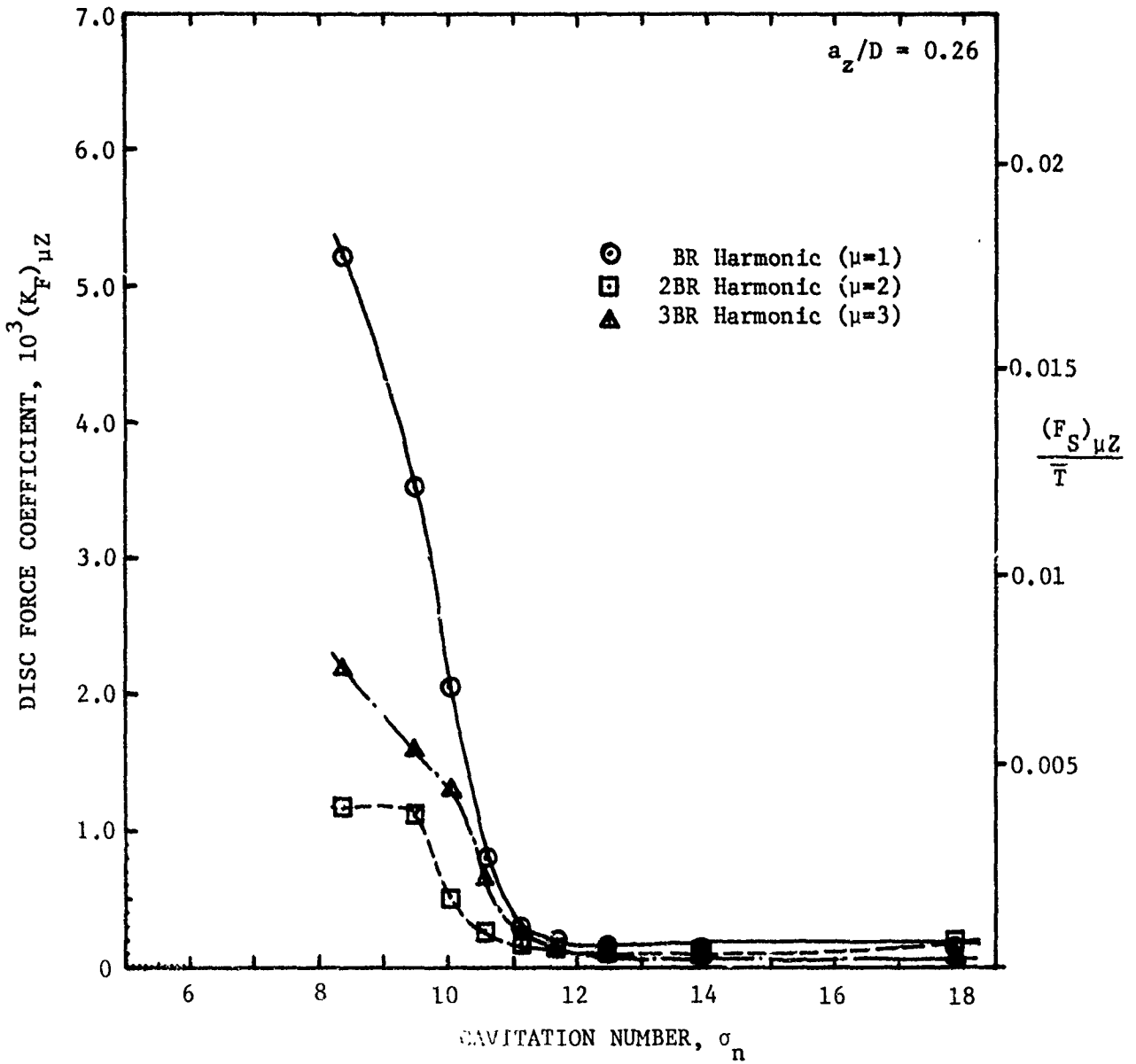


Figure 25 - Three Blade Rate Harmonics of Measured Disc Force Coefficient with $a_z/D = 0.26$

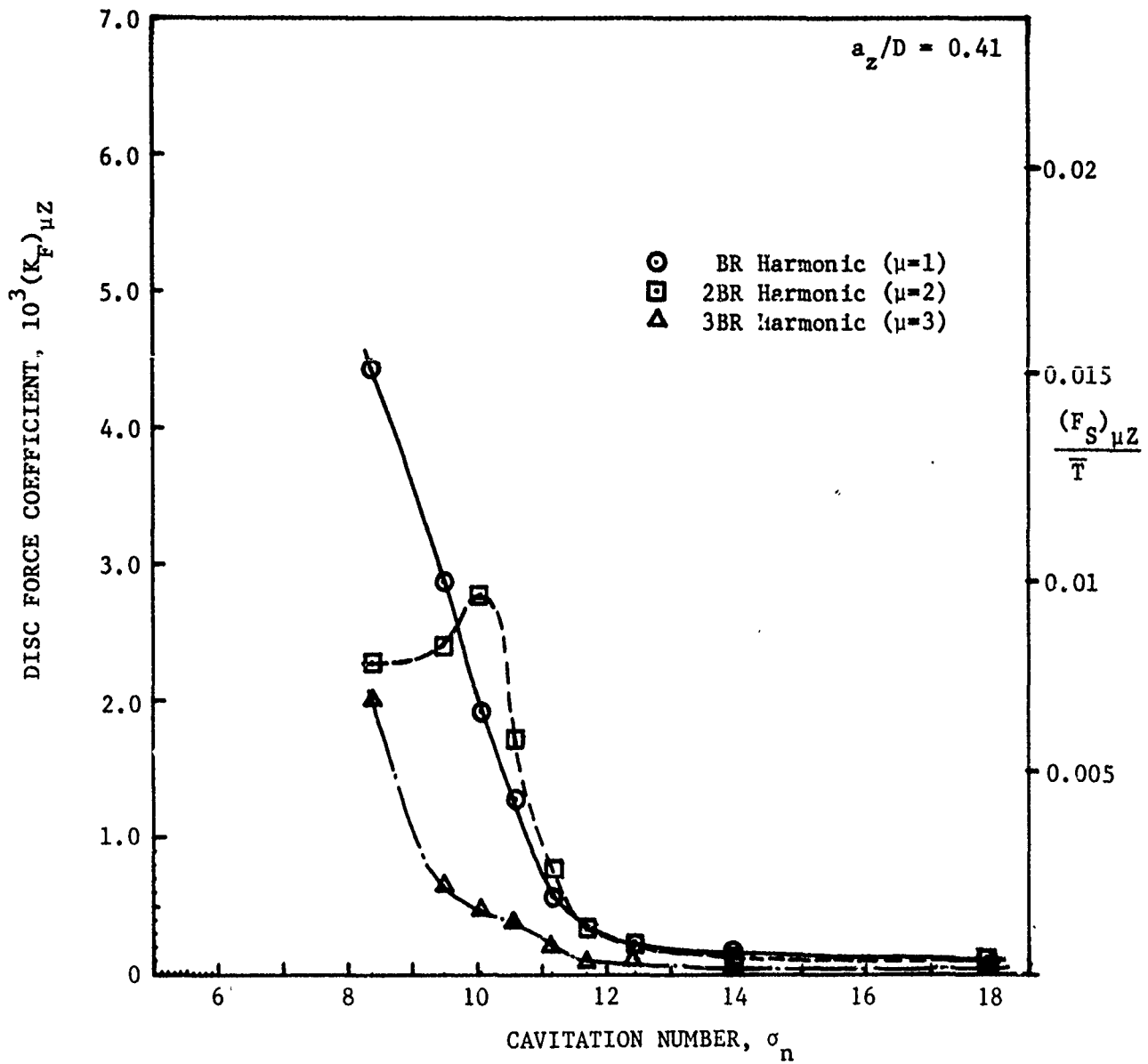


Figure 26 - Three Blade Rate Harmonics of Measured Disc Force Coefficient with $a_z/D = 0.41$

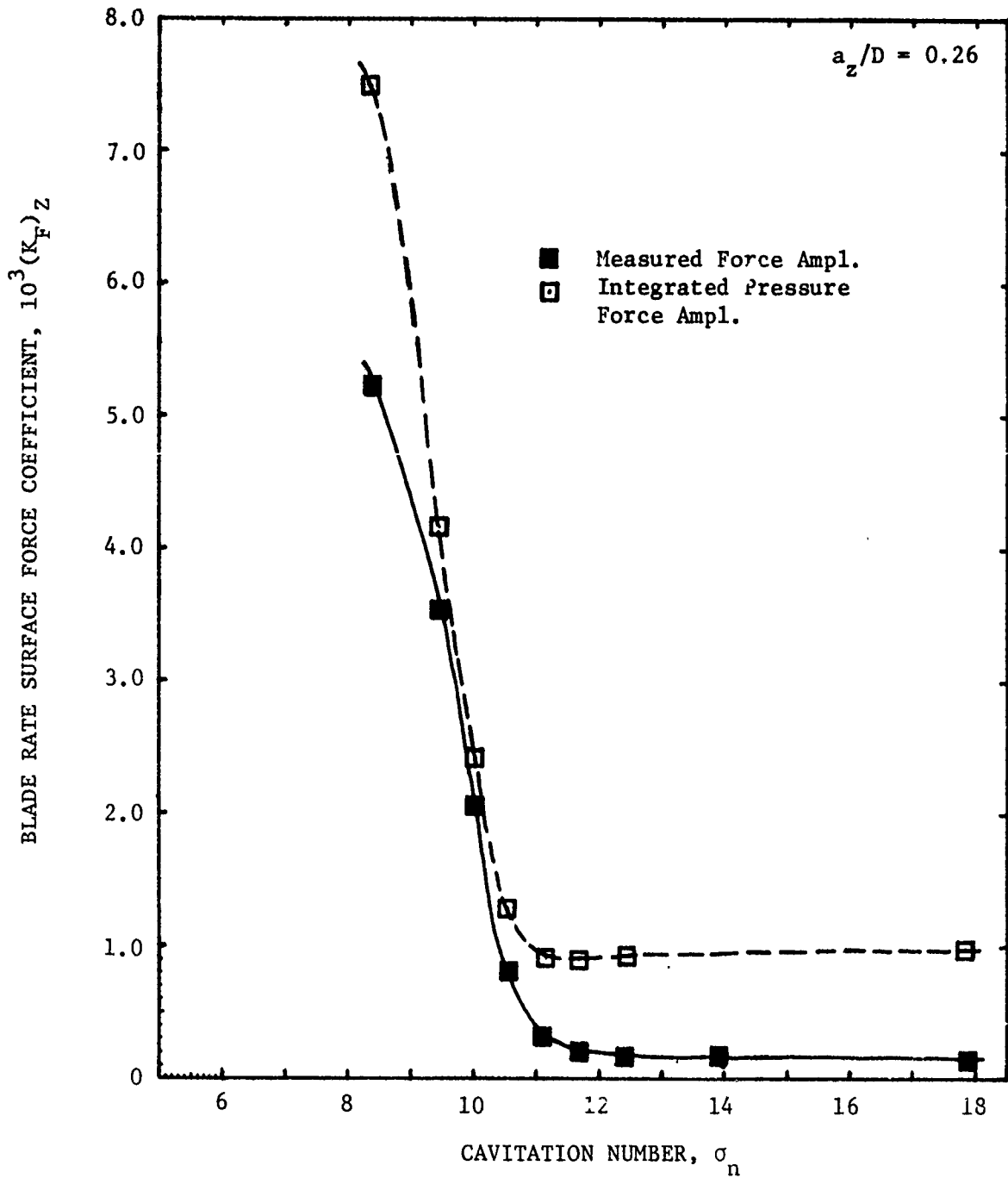


Figure 27 - Blade Rate Harmonic of Disc Force Coefficient versus Cavitation Number, Comparison Between Measured Force and Integrated Pressure, with $a_z/D = 0.26$

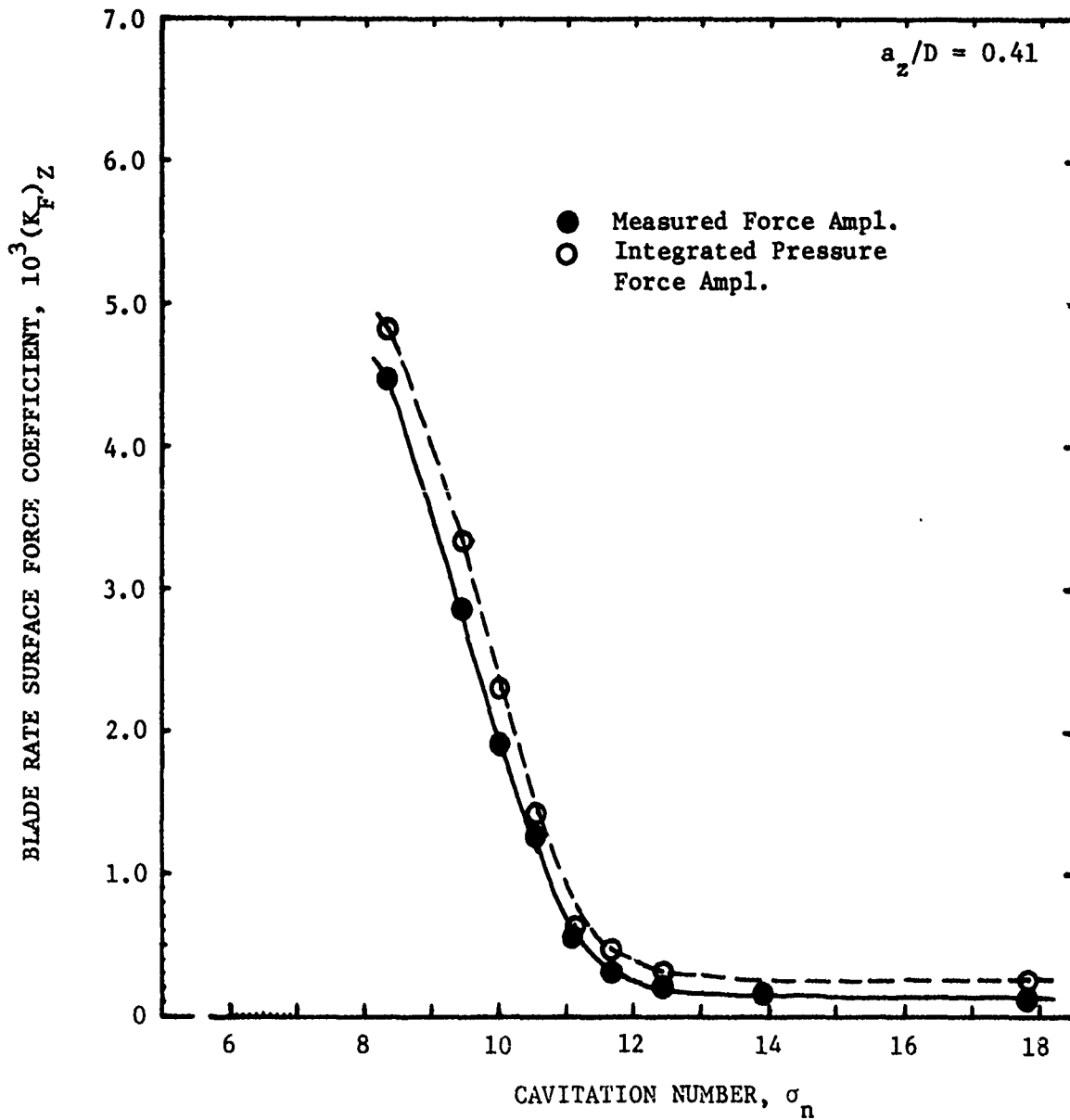


Figure 28 - Blade Rate Harmonic of Disc Force Coefficient versus Cavitation Number, Comparison Between Measured Force and Integrated Pressure, with $a_z/D = 0.41$

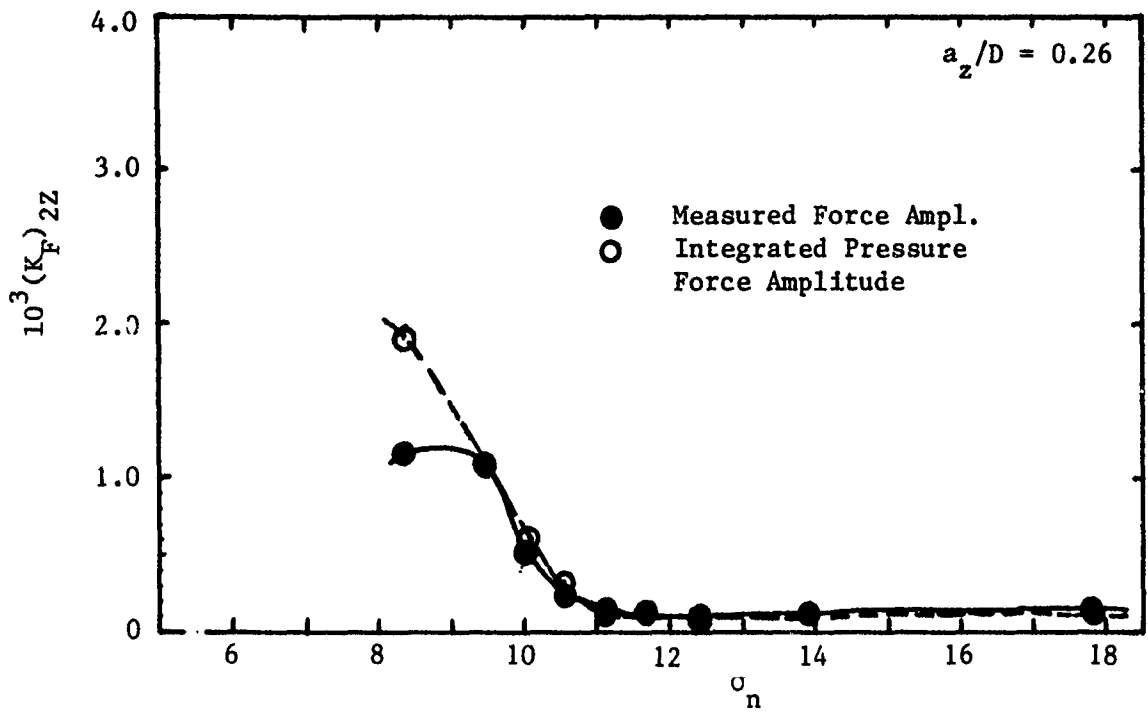


Figure 29 - Twice Blade Rate Harmonic of Disc Force Coefficient versus Cavitation Number, with $a_z/D = 0.26$

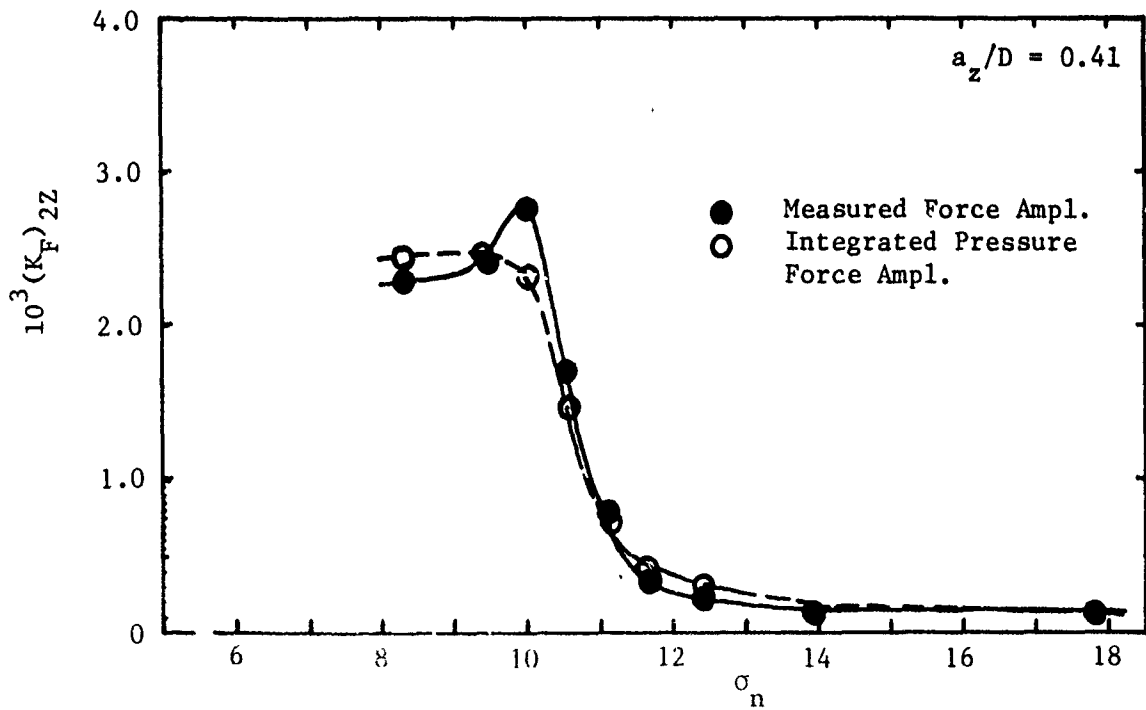


Figure 30 - Twice Blade Rate Harmonic of Disc Force Coefficient versus Cavitation Number, with $a_z/D = 0.41$

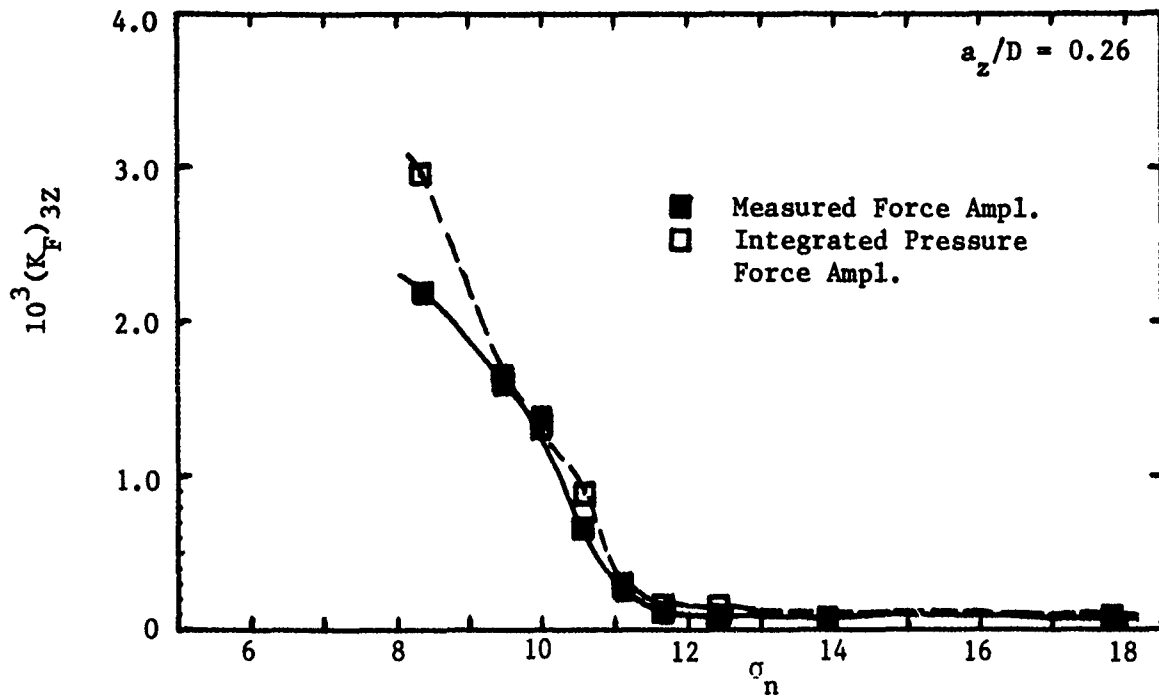


Figure 31 - Thrice Blade Rate Harmonic of Disc Force Coefficient versus Cavitation Number, with $a_z/D = 0.26$

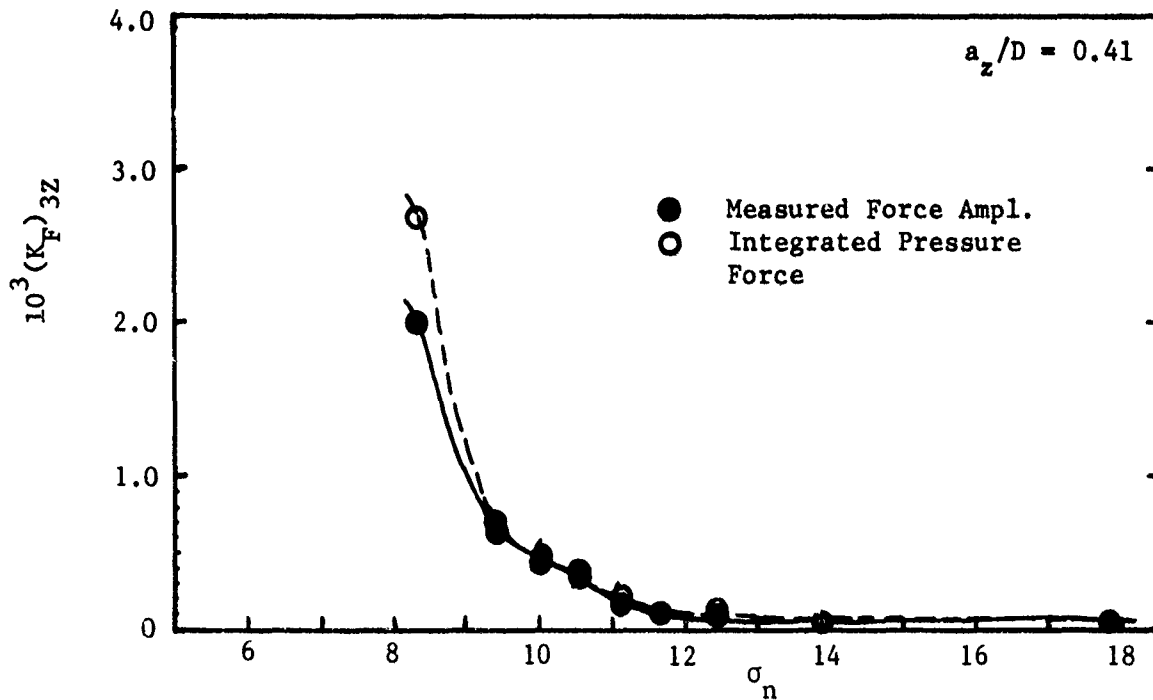


Figure 32 - Thrice Blade Rate Harmonic of Disc Force Coefficient versus Cavitation Number, with $a_z/D = 0.41$

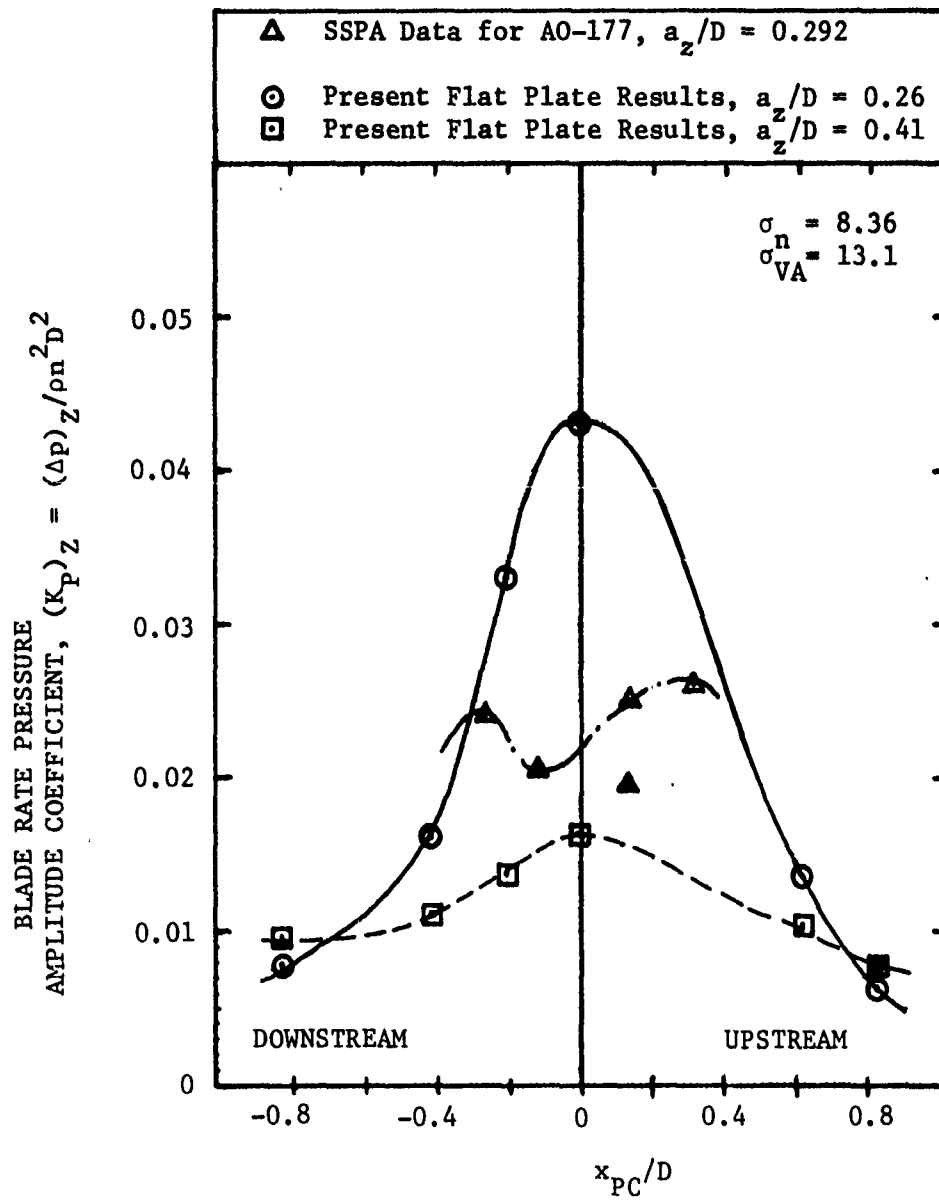


Figure 33 - Comparison of Measured Blade Rate Pressure Amplitude Longitudinal Distribution

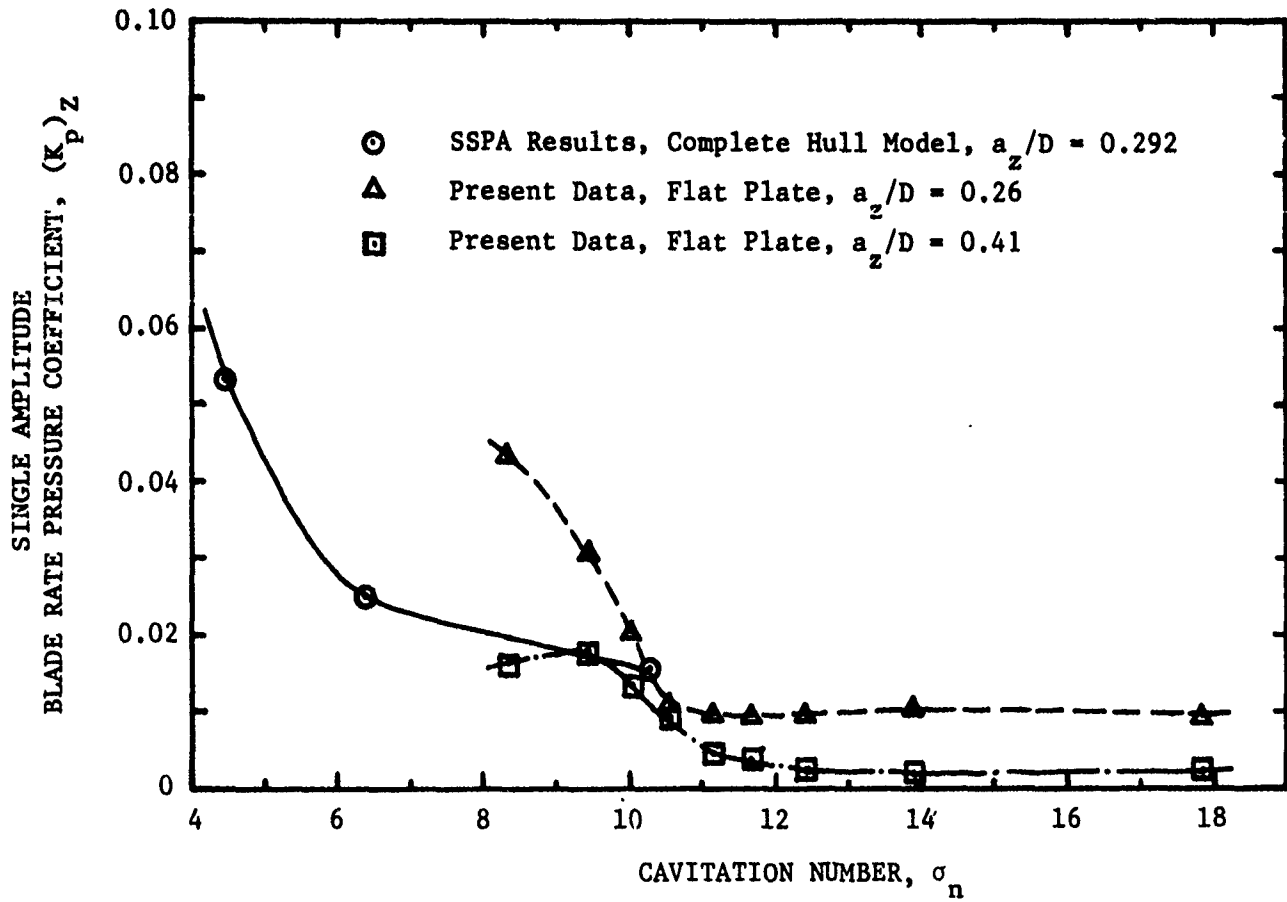
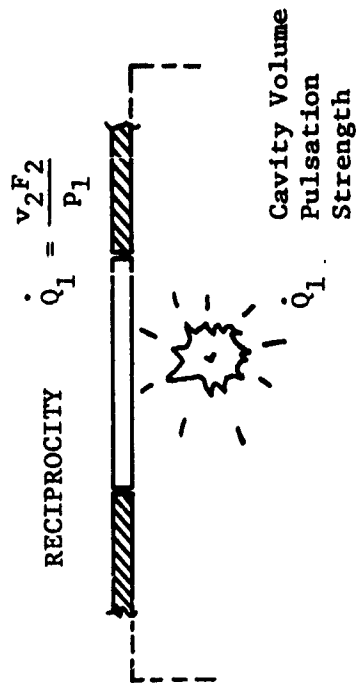
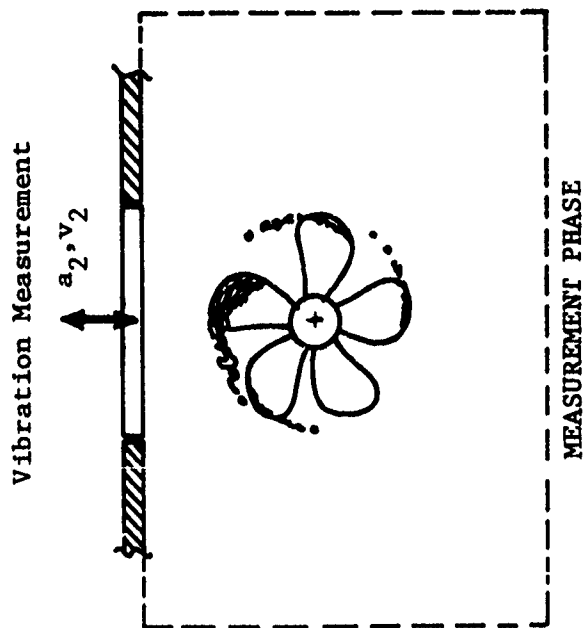
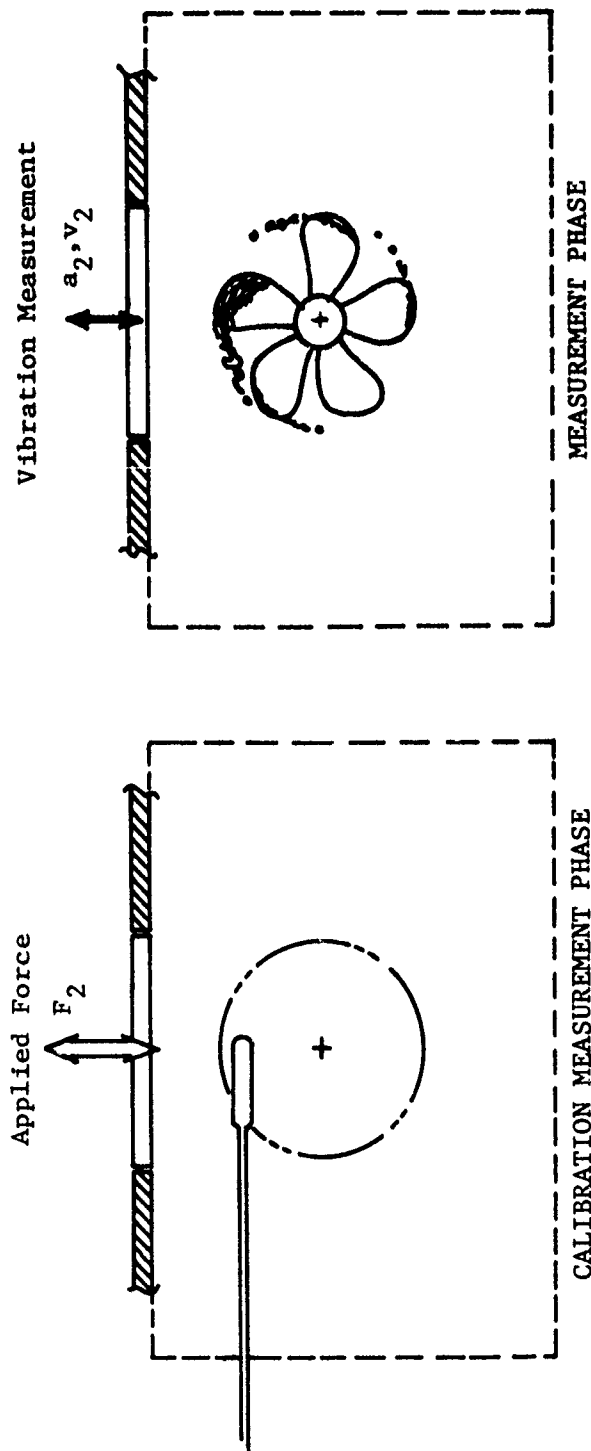


Figure 34 - Comparison of Blade Rate Pressure Amplitude Coefficient Above the Propeller versus Cavitation Number



$$\dot{Q}_1 = \frac{v_2 F_2}{P_1}$$

Figure 35 - Schematic of the Measurement of Cavity Volume Velocity by Reciprocal Method

TABLE 1 - SUMMARY OF INSTRUMENTATION CHARACTERISTICS

	Force Gauges	Accelerometer	Pressure Gauges	
Make/Type	Wilcoxon Model L10 Piezoelectric	Edevco Model 2217E	CEC Type 4-312 Strain gauged diaphragm	Kulite XTM-190 Strain gauged
Range	down to 10^{-4} lb	to 250g	to 25 psi (172 kPa)	to 10 psi (69 kPa)
Signal Conditioning	Gilmore Zero Drive	Gilmore Zero Drive Model N400	Vishay	Vishay
Filter	1000 Hz	5 kHz	1000 Hz	

v_2 is made at point 2 in the same direction as the calibration drive force, with the cavitating propeller running as the system excitation. The volume velocity of the cavity at point 1 is thus obtained as

$$\dot{v}_1 = \left(\frac{F_2}{p_1} \right) \quad (\text{A.4})$$

For harmonic oscillations of the system, the acceleration at point 2 in the same direction as the velocity v_2 is

$$a_2 = i\omega v_2 \quad (\text{A.5})$$

Thus, another version of the basic reciprocity relationship is expressed as

$$\dot{v}_1 = \frac{F_2 a_2}{i\omega p_1} \quad (\text{A.6})$$

Note that the variables measured for the calibration and final measurement phases can be rearranged for convenience. For example, suppose that during the calibration phase the acceleration a_2 at the drive point is measured as well the corresponding fluid pressure p_1 . In this case, the appropriate transfer function is the ratio (p_1/a_2) . Then the run measurement of F_2 (in the same direction as the calibrating drive acceleration) leads to the determination of the cavity volume velocity \dot{v}_1 from Equation (A.6). In either of the forms, the calibrated transfer function is a complex function of the real-valued frequency ω . The other measured quantities involved must also be treated as complex.

The basic form of the simplified reciprocity relationship of Equation (A.4) or (A.6) can be derived in a formal way using the second Green theorem following concepts discussed by Chertock.⁷⁷

APPENDIX A

RECIPROCITY CONCEPT AND APPLICATION

The reciprocity principle states that for a linear system, there is a reciprocal relationship between the force applied and the system response at any two points. That is, the system vibration velocity response v , say, at point 1 due to a force applied at point 2 is the same as the response at point 2 due to a force at point 1. Thus,

$$\frac{v_1}{F_2} = \frac{v_2}{F_1} \quad (\text{A.1})$$

or

$$v_1 F_1 = v_2 F_2 \quad (\text{A.2})$$

For the assumed linear system, the resulting flow of power monitored at the check points can be expressed in terms of other conjugate variables, for example, volume velocity \dot{v} times fluid acoustic pressure p .

Then

$$\dot{v}_1 p_1 = F_2 v_2 \quad (\text{A.3})$$

Figure 35 provides a definition sketch and outline for the experiments needed to make the reciprocity calibration and to provide one of several interpretations of the expression given above.

For the calibration phase, a mechanical shaker can be used to provide an input force at point 2 on a body surface element (or within the hull of a complete body). The fluid pressure is measured simultaneously, at point 1 in the propeller plane where the center of the unsteady cavitation volume is expected to occur. A transfer function is formed from the ratio (F_2/p_1) and this remains as a property of the system. Then the measurement of vibration velocity

TABLE 2 - GEOMETRIC CHARACTERISTICS OF AO-177 CLASS AUXILIARY
OILER HIGHLY SKEWED PROPELLER DESIGN

	<u>blade chord</u> diameter	<u>pitch</u> diameter	<u>skew</u> angle	<u>thickness</u> chord	<u>camber</u> chord	<u>rake</u> diameter
r/R	c/D	P/D	θ_s (deg)	t_m/c	f_m/c	total
0.2	0.207	1.125	0.0	0.20	0.0490	0.0
0.3	0.2456	1.223	2.2	0.1625	0.0444	0.0058
0.4	0.2722	1.288	7.1	0.1325	0.0367	0.021
0.5	0.2817	1.318	13.1	0.1080	0.0314	0.041
0.6	0.2684	1.309	20.0	0.0880	0.030	0.065
0.7	0.2320	1.250	27.7	0.0715	0.0295	0.0913
0.8	0.1815	1.140	34.5	0.0590	0.0281	0.109
0.9	0.1180	0.970	40.3	0.0500	0.0263	0.1168
1.0	0.0	0.722	45.0	0.045	0.0240	0.1148

Number of blades 7
 Section meanline $a=0.8$
 Section thickness distribution NACA 66 Modified
 Expanded area ratio 0.77
 Mean width ratio 0.216
 Blade thickness fraction 0.062
 Projected skew at tip 45 deg
 Model diameter 9.812 in. (24.92 cm)
 Full scale diameter 21 ft (6.401 m)

APPENDIX B

CAVITY VOLUME VELOCITY MEASUREMENTS AND COMPARISONS

Disc force measurements obtained with excitation from the operating propeller, together with the calibrated transfer function (p/a) shown in Figure 5 have been used to make estimates of the cavity volume velocity harmonic from the expression in Equation (2). The unsteady disc force due to the effect of cavity volume variation must be isolated from the measured total force variation by vectorially subtracting away the noncavitating or reference force, taking proper account of amplitude and phase. At the blade rate frequency of 98 Hz for the seven-bladed propeller, an average value of the pressure-to-acceleration transfer function was determined to be

$$(p/a) = 0.6747 \text{ slug/ft}^2 \text{ (105.99 kg/m}^2\text{)}$$

This is for the case of $a_z/D = 0.26$, for which the calibrated transfer function of Figure 5 applies.

The blade rate disc force amplitude coefficient and phase angle for the noncavitating propeller at $a_z/D = 0.26$ were found to be $(10^3)K_{FNC} = 0.1622$ and $\phi_{nc} = 1.90^\circ$. Then Table B.1 provides the amplitude and phase data for the disc force characteristics used to obtain the inferred blade rate harmonic of cavity volume velocity given in nondimensional form.

Measured and computed blade rate results for volume velocity coefficient versus cavitation number are compared in Figure B.1, where calculated values from two versions of the propeller analysis scheme PUF-3 are displayed. The original M.I.T. cavitating propeller analysis program developed by Lee⁷⁸ is designated here as PUF-3(OLD). Improvements and non-linear leading edge corrections to the linear cavitating blade section analysis have been incorporated into the original computation scheme, as outlined in the paper by Kerwin, Kinnas, Wilson, and McHugh.⁷⁹ Results of the improved analysis are denoted by PUF-3(NEW). It can be seen that the revised theory predicts smaller sheet cavity volumes than does the original calculation. This coincides with the prediction of shorter cavity lengths as well. The measured values of cavity volume also include the effect of substantial fluctuating tip vortex cavitation, a contribution not included in the analytical result. Considering the various approximations and experimental uncertainties involved, the comparison shown in Figure B.1 is reasonable.

TABLE B.1 - ESTIMATE OF BLADE RATE CAVITY VOLUME VELOCITY
USING RECIPROCAL MEASUREMENTS

σ_n	Total Force		Cavitating Force		Cavity Volume Velocity Coeff. $(\dot{V}_c)_Z/nR^3$
	Coeff (10^3) K_{FT}	Phase $\phi_T(\text{deg})$	Coeff (10^3) K_{Fc}	Phase $\phi_c(\text{deg})$	
10.03	2.052	-16.37	1.899	17.91	0.00081
9.47	3.538	40.6	3.414	42.3	0.00146
8.36	5.22	-4.3	5.06	4.46	0.00216

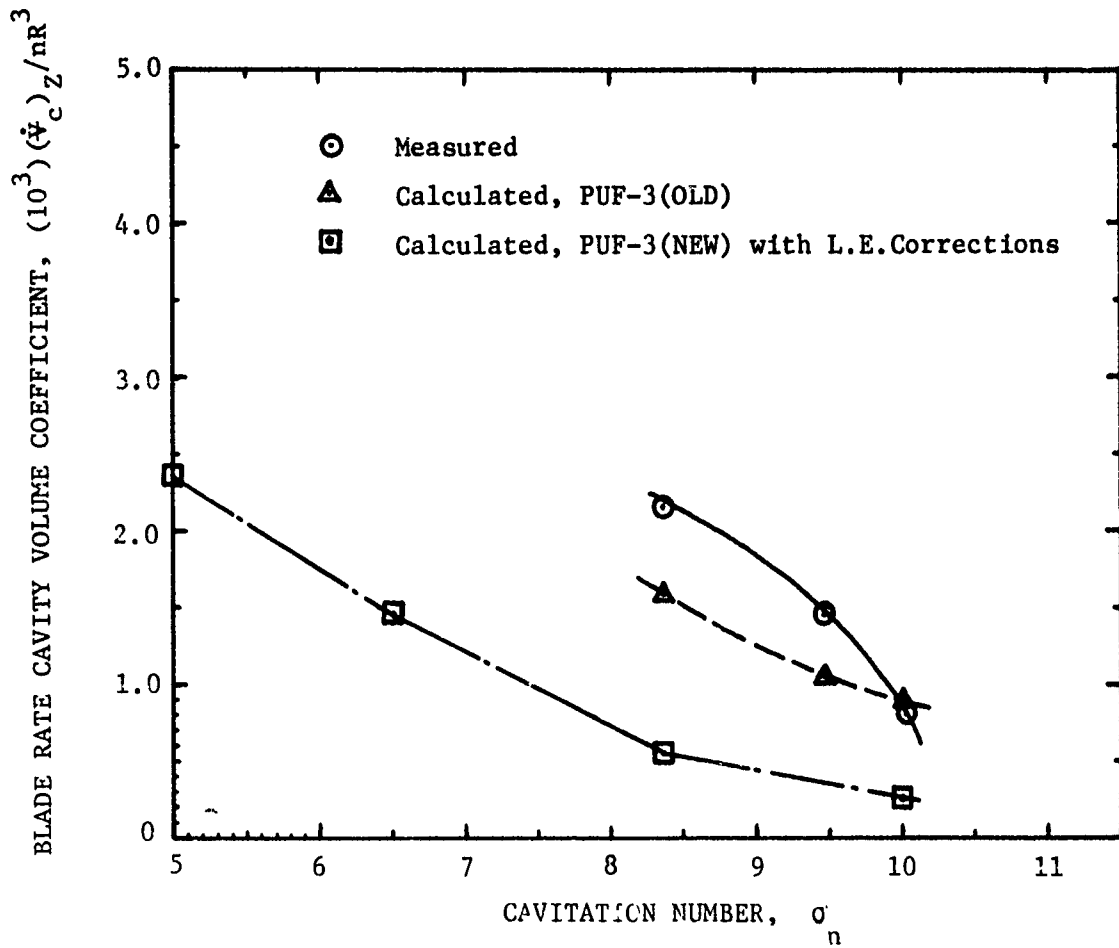


Figure B.1 - Comparison of Measured and Calculated Blade Rate Cavity Volume Velocity versus Cavitation Number

DTNSRDC ISSUES THREE TYPES OF REPORTS:

1. **DTNSRDC reports, a formal series,** contain information of permanent technical value. They carry a consecutive numerical identification regardless of their classification or the originating department.
2. **Departmental reports, a semiformal series,** contain information of a preliminary, temporary, or proprietary nature or of limited interest or significance. They carry a departmental alphanumerical identification.
3. **Technical memoranda, an informal series,** contain technical documentation of limited use and interest. They are primarily working papers intended for internal use. They carry an identifying number which indicates their type and the numerical code of the originating department. Any distribution outside DTNSRDC must be approved by the head of the originating department on a case-by-case basis.